

**Established and Emerging Techniques of  
Cardiovascular Magnetic Resonance Imaging in  
Coronary Artery Disease**

Pankaj Garg

Submitted in accordance with the requirements for the degree of Doctor of  
Philosophy (PhD)

The University of Leeds

Division of Cardiovascular and Diabetes Research

Leeds Institute of Cardiovascular and Metabolic Medicine

School of Medicine

February 2017

## **Intellectual property and publication statements**

The candidate confirms that the work submitted is his own, except where work which has formed part of jointly-authored publications has been included. The contribution of the candidate and the other authors to this work has been explicitly indicated below. The candidate confirms that appropriate credit has been given within the thesis where reference has been made to the work of others.

This copy has been supplied on the understanding that it is copyright material and that no quotation from the thesis may be published without proper acknowledgement.

© 2017 The University of Leeds and Pankaj Garg.

Chapter 1 includes content from the following peer-reviewed publication:

**Garg P, Underwood SR, Senior R, Greenwood JP, Plein S. Noninvasive cardiac imaging in suspected acute coronary syndrome. *Nat Rev Cardiol* 2016;13:266–275.**

Author contributions: Literature research, PG; Guarantors of integrity of entire study PPS, SP; manuscript drafting or manuscript revision for important intellectual content, PG, SRU, RS, JPG, SP; approval of final version of submitted manuscript, PG, SRU, RS, JPG, SP.

## **Publications arising from this work**

### **Review papers**

**Garg P**, Underwood SR, Senior R, Greenwood JP, Plein S. Noninvasive cardiac imaging in suspected acute coronary syndrome. *Nat Rev Cardiol* 2016;13:266–275.

**Garg P**, Greenwood JP, Plein S. Multiparametric relaxometry by cardiac magnetic resonance imaging in Takotsubo cardiomyopathy. *Eur Heart J Cardiovasc Imaging* 2015;16:1174.

### **Original research papers**

**Garg P**, Kidambi A, Foley JRJ, Musa T Al, Ripley DP, Swoboda PP, Erhayiem B, Dobson LE, McDiarmid AK, Greenwood JP, Plein S. Ventricular longitudinal function is associated with microvascular obstruction and intramyocardial haemorrhage. *Open Heart*. 2016 May 2;3(1):e000337.

**Garg P**, Kidambi A, Swoboda PP, Foley JRJ, Musa TA, Ripley DP, Erhayiem B, Dobson LE, McDiarmid AK, Fent GJ, Haaf P, Greenwood JP, Plein S. The role of left ventricular deformation in the assessment of microvascular obstruction and intramyocardial haemorrhage. *Int J Cardiovasc Imaging*. 2017 Mar;33(3):361-370.

### **Oral abstracts**

**Garg P**, Hassell M, Foley JRJ, Ripley DP, Dobson L, Swoboda PP, Fent GJ, Musa TA, Erhayiem B, Haaf P, Greenwood JP, Nijveldt R, Westenberg J, Geest R van der, Plein S. 1373 Reliability and reproducibility of trans-valvular flow measurement by 4D flow magnetic resonance imaging in acute myocardial infarct patients: two centre study. *Eur Heart J Cardiovasc Imaging*. 2016. p. Volume 17, Issue suppl 1.

**Garg P**, Aziz R, Foley J, Fent G, Musa T, Haaf P, Dobson L, Swoboda P, Greenwood JP, Plein S, Geest R van der, Westenberg J. 1423 Head-to-head comparison of acceleration algorithms in 4-dimensional flow CMR. *Eur Heart J Cardiovasc Imaging*. 2016. p. SUP i1–100.

## **Acknowledgements**

This research work was carried out between August 2014 till January 2017 and was predominantly funded by British Heart Foundation.

This research has been carried out by a team which has included Adam McDiarmid, Bara Erhayiem, Ananth Kidambi, David Ripley, Tarique al Musa, Laura Dobson, Graham Fent, Philip Haaf, Peter Swoboda, James Foley, Gavin Bainbridge, Stephen Mhiribidi, Margaret Saysell, Caroline Richmond, Petra Bijsterveld, Fiona Richards, Annabel Nixon and Lisa Clarke. My own contributions, fully and explicitly indicated in the thesis, have been study design, ethical approval, patient recruitment, scanning and data collection, data analysis and manuscript preparation. The other members of the group and their contributions have been as follows:

Recruitment- Jos Westenberg, Rahoz Aziz, David Ripley, Graham Fent, James Foley

Scan Acquisition- Gavin Bainbridge, Stephen Mhiribidi, Margaret Saysell and Caroline Richmond

Phantom Studies- Jos Westenberg

Data analysis- Rob van der Geest, Jos Westenberg, Mohammed El-Baz

Statistical analysis- Philip Haaf, Peter Swoboda

I would like to thank my supervisors Professors Plein and Greenwood for the support and opportunity to explore areas of research that I have found interesting.

I would like to thank my wife Svetlana and my family for their enduring patience and support.

I dedicate this work to my parents, Dr Mahesh Chandra Garg and Mrs Manju Garg. My mother taught me the value of hard work and my father the importance of reverie and aspiration.

## **Abstract**

### **Background**

In patients with coronary artery disease (CAD), multi-parametric cardiovascular magnetic resonance (CMR) provides detailed information about the myocardial tissue composition and its function. This thesis aims to investigate how myocardial tissue composition characteristics influence its function. Additionally, this thesis aims to develop methods for time-resolved, three-dimensional flow imaging *in-vitro* and in health.

### **Methods**

We have prospectively recruited and conducted multi-parametric CMR in 76 patients with ST-elevation myocardial infarction (STEMI), 44 patients with stable chest pain and 35 healthy volunteers.

### **Results**

Study 1 and 2 evaluated if CMR derived function parameters are associated with the presence of microvascular obstruction (MVO) or intramyocardial haemorrhage (IMH) in STEMI patients. Study 1 demonstrated the diagnostic accuracy of mitral annular plane systolic excursion (MAPSE) to detect MVO/IMH. Study 2 demonstrated that peak global longitudinal strain (GLS) is most strongly associated with MVO/IMH when compared to other myocardial deformation parameters. Study 3 demonstrated that during first-pass perfusion stress CMR, at peak hyperemic stress, GLS is reduced in the presence of a perfusion defect in patients being investigated for CAD. Study 4 demonstrated that acute ECV-maps can reliably quantify area at risk and final infarct size (at 3-month follow) in reperfused STEMI patients. Study 5 investigated 3 main acceleration methods for 4-dimensional flow (4D Flow) in phantoms and healthy volunteers. In phantoms, all 4D Flow methods underestimated peak velocity but their mean errors were within reasonable limits for clinical applications. In volunteers, 4D echo planer imaging (EPI) method had the shortest acquisition time, best agreement with 2-dimensional phase contrast, best internal consistency between mitral and aortic valve flows.

## **Conclusions**

CMR derived longitudinal functional parameters of the left ventricle are associated with pathologies predominantly in the sub-endocardium and could be used as a surrogate imaging markers. ECV-maps offer an alternative to IS quantification. 4D EPI is the most robust acceleration method for whole-heart flow assessment.

## Table of contents

Intellectual property and publication statements .....	2 -
Publications arising from this work.....	3 -
Acknowledgements.....	4 -
Abstract.....	5 -
Background .....	5 -
Methods.....	5 -
Results.....	5 -
Conclusions .....	6 -
Table of contents.....	7 -
Figures.....	14 -
Tables.....	15 -
Abbreviations .....	16 -
1 Introduction .....	19 -
1.1 Established role of CMR in the assessment of ACS.....	20 -
1.2 CMR Techniques used in the assessment of patients with ACS .....	22 -
1.3 Left ventricular functional assessment.....	23 -
1.3.1 Volumetric analysis .....	23 -
1.3.2 Myocardial deformation analysis .....	25 -
1.4 Multi-parametric tissue characterization .....	26 -
1.4.1 Myocardial oedema and area at risk analysis .....	26 -
1.4.2 Infarct size and viability analysis .....	27 -
1.4.3 Microvascular obstruction and intra-myocardial haemorrhage ...	28 -
1.4.4 Left ventricular thrombus assessment .....	30 -

1.4.5	Extracellular volume quantification .....	- 30 -
1.5	Role of haemodynamic assessment post MI .....	- 33 -
1.6	Aims of thesis.....	- 34 -
2	Methods .....	- 35 -
2.1	Study Populations .....	- 35 -
2.1.1	Patient population for Chapter 3, 4, 6 and 7 .....	- 35 -
2.1.2	Patient population for Chapter 5 .....	- 36 -
2.2	Ethics and approvals .....	- 36 -
2.3	MRI Scanner Hardware .....	- 36 -
2.4	Common CMR Protocol .....	- 36 -
2.4.1	Cine imaging .....	- 37 -
2.4.2	Early gadolinium enhancement imaging (EGE) .....	- 37 -
2.4.3	Late gadolinium enhancement imaging (LGE).....	- 38 -
2.5	Common CMR analysis .....	- 39 -
2.5.1	LV Ejection fraction analysis .....	- 39 -
2.6	Statistical analysis .....	- 39 -
2.6.1	Generic sample size estimations .....	- 40 -
3	Study 1- Ventricular Longitudinal Function is Associated with Microvascular Obstruction and Intramyocardial Haemorrhage .....	- 41 -
3.1	Abstract .....	- 41 -
3.1.1	Background.....	- 41 -
3.1.2	Methods .....	- 41 -
3.1.3	Results .....	- 41 -
3.1.4	Conclusions.....	- 42 -
3.2	Introduction .....	- 43 -
3.3	Study specific methods.....	- 45 -

3.3.1	CMR protocol.....	- 45 -
3.3.2	CMR interpretation .....	- 45 -
3.3.3	Statistical analysis.....	- 47 -
3.4	Results .....	- 47 -
3.5	Discussion .....	- 54 -
3.5.1	Clinical Implications.....	- 55 -
3.5.2	Study limitations.....	- 55 -
3.6	Conclusions.....	- 56 -
4	Study 2- The Role of Left Ventricular Deformation in the Assessment of Microvascular Obstruction and Intramyocardial Haemorrhage .....	- 57 -
4.1	Abstract .....	- 57 -
4.1.1	Introduction.....	- 57 -
4.1.2	Methods .....	- 57 -
4.1.3	Results .....	- 57 -
4.1.4	Conclusion .....	- 58 -
4.2	Introduction.....	- 59 -
4.3	Study specific methods.....	- 60 -
4.3.1	Cardiac catheterization .....	- 60 -
4.3.2	CMR examination .....	- 60 -
4.3.3	CMR interpretation .....	- 60 -
4.3.4	Follow-up scans .....	- 63 -
4.3.5	Statistical analysis.....	- 63 -
4.4	Results .....	- 63 -
4.4.1	Baseline data .....	- 66 -
4.4.2	Follow-up data.....	- 71 -
4.4.3	Adverse LV Remodelling.....	- 71 -

4.5	Discussion .....	- 73 -
4.5.1	Role of Echocardiography.....	- 74 -
4.5.2	MAPSE or FT – which one to use? .....	- 74 -
4.5.3	Clinical Implications.....	- 75 -
4.5.4	Study limitations.....	- 75 -
4.6	Conclusions.....	- 76 -
5	Study 3- Effects of hyperaemia on left ventricular longitudinal strain: A first-pass stress perfusion cardiovascular magnetic resonance imaging study. ....	- 77 -
5.1	Abstract .....	- 77 -
5.1.1	Background.....	- 77 -
5.1.2	Methods .....	- 77 -
5.1.3	Results .....	- 77 -
5.1.4	Conclusions.....	- 78 -
5.2	Introduction .....	- 79 -
5.3	Study specific methods.....	- 81 -
5.3.1	Cardiac Magnetic Resonance Protocol.....	- 81 -
5.3.2	Image Analysis.....	- 82 -
5.3.3	Statistical Analysis .....	- 84 -
5.4	Results .....	- 85 -
5.4.1	Study demographics and characteristics .....	- 85 -
5.4.2	Feature tracking analysis.....	- 87 -
5.4.3	Influence of previous Myocardial Infarction .....	- 90 -
5.4.4	Receiver operator characteristics (ROC) analysis.....	- 90 -
5.4.5	Regression analysis.....	- 93 -
5.5	Discussion .....	- 93 -
5.5.1	Practical implications.....	- 95 -

5.5.2	Study limitations.....	- 96 -
5.6	Conclusion .....	- 96 -
6	Study 4- Acute Infarct Extracellular Volume Mapping to Quantify Myocardial Area at Risk and Chronic Infarct Size on Cardiovascular Magnetic Resonance Imaging	
	- 97 -	
6.1	Abstract .....	- 97 -
6.1.1	Background.....	- 97 -
6.1.2	Methods .....	- 97 -
6.1.3	Results .....	- 97 -
6.1.4	Conclusions.....	- 98 -
6.2	Introduction .....	- 99 -
6.3	Methods .....	- 100 -
6.3.2	CMR protocol.....	- 100 -
6.3.3	Image Analysis.....	- 100 -
6.3.4	Extracellular volume mapping analysis .....	- 101 -
6.3.5	Validation of ECV thresholds .....	- 101 -
6.3.6	Follow-up scans .....	- 104 -
6.3.7	Statistical analysis.....	- 104 -
6.4	Results .....	- 104 -
6.4.1	Patient characteristics .....	- 104 -
6.4.2	Validation of ECV thresholds .....	- 109 -
6.4.3	Myocardial area at risk (AAR) characteristics .....	- 110 -
6.4.4	Infarct Size (IS) characteristics.....	- 112 -
6.4.5	Per segment viability characteristics .....	- 113 -
6.4.6	Regression analysis.....	- 115 -
6.5	Discussion .....	- 117 -

6.5.1	Multi-parametric tissue characterisation .....	- 117 -
6.5.2	ECV-mapping in acute and chronic myocardial infarction.....	- 117 -
6.5.3	Limitations .....	- 120 -
6.6	Conclusion .....	- 120 -
7	Study 5– Comparison of Acceleration Algorithms in Whole-Heart Four-Dimensional Flow for Cardiovascular Applications: Two-centre, 1.5T, Phantom and In-vivo Validation Study. ....	- 121 -
7.1	Abstract .....	- 121 -
7.1.1	Aims.....	- 121 -
7.1.2	Methods .....	- 121 -
7.1.3	Results .....	- 121 -
7.1.4	Conclusions.....	- 122 -
7.2	Introduction .....	- 123 -
7.3	Acceleration methods.....	- 124 -
7.4	Methods .....	- 124 -
7.4.1	Static and pulsatile phantom.....	- 124 -
7.4.2	Cardiac Magnetic Resonance Imaging.....	- 127 -
7.4.3	Image analysis .....	- 129 -
7.4.4	Statistical analysis.....	- 130 -
7.5	Results .....	- 130 -
7.5.1	Phantom Experiments .....	- 130 -
7.5.2	Healthy Volunteers.....	- 130 -
7.5.3	Acquisition time and image quality assessments .....	- 131 -
7.5.4	Intra-cardiac peak velocity assessment.....	- 134 -
7.5.5	Consistency of flow volume assessment .....	- 136 -
7.5.6	Diastolic flow assessment.....	- 138 -

7.6	Discussion .....	- 139 -
7.6.1	Limitations .....	- 141 -
7.7	Conclusion .....	- 142 -
8	Final Conclusions .....	- 143 -
8.1	Effect of MVO/ IMH on Myocardial Deformation.....	- 143 -
8.2	Effect of Myocardial Hyperaemia on Myocardial deformation .....	- 144 -
8.3	Quantification of AAR and IS by ECV-maps.....	- 144 -
8.4	Validation of whole-heart 4D Flow CMR acceleration methods.....	- 144 -
8.5	Future directions .....	- 145 -
8.5.1	Myocardial deformation in coronary artery disease .....	- 145 -
8.5.2	ECV-maps in acute myocardial infarction.....	- 145 -
8.5.3	Whole heart 4D flow .....	- 146 -
	References.....	- 147 -
9	Appendix .....	- 185 -
9.1	Ethical approval for chapter 3, 4 and 6 .....	- 185 -
9.2	Ethical approval for chapter 5 and 7 .....	- 187 -

## Figures

<b>Figure 1.1</b> Ischaemic myocardium and applied imaging techniques. ....	- 19 -
<b>Figure 1.2</b> Multi-parametric CMR in suspected ACS .....	- 21 -
<b>Figure 1.3</b> Tissue characterization in STEMI.....	- 29 -
<b>Figure 3.1</b> Illustration of orientation of Myocardial fibres.....	- 44 -
<b>Figure 3.2</b> Multi-parametric CMR examination of two STEMI cases.....	- 46 -
<b>Figure 3.3</b> Box-plot of averaged MAPSE.....	- 50 -
<b>Figure 3.4</b> ROC for the detection of MVO/IMH by averaged MAPSE.....	- 51 -
<b>Figure 4.1</b> Multi-parametric CMR examination.....	- 62 -
<b>Figure 4.2</b> Study design .....	- 64 -
<b>Figure 4.3</b> Multiple comparison bars of myocardial strain .....	- 68 -
<b>Figure 5.1</b> Illustration demonstrating myocardial fiber orientation .....	- 80 -
<b>Figure 5.2</b> Two cases of first pass perfusion CMR.....	- 83 -
<b>Figure 5.3</b> Multiple comparison bars .....	- 88 -
<b>Figure 5.4</b> ROC analysis of different strain models. ....	- 92 -
<b>Figure 6.1</b> AAR and IS quantification by multiple methods.....	- 104 -
<b>Figure 6.2</b> Recruitment flowchart. ....	- 105 -
<b>Figure 6.3</b> Comparison of established quantification methods and ECV-map..	- 111 -
<b>Figure 6.4</b> Statistical results. ....	- 114 -
<b>Figure 6.5</b> Short-axis illustration of the LV post acute STEMI .....	- 118 -
<b>Figure 7.1</b> Phantom illustrations.. .....	- 126 -
<b>Figure 7.2</b> Image quality of mitral and aortic valve flow acquisitions.....	- 132 -
<b>Figure 7.3</b> Bland Altman and scatter plots analysis .....	- 133 -
<b>Figure 7.4</b> Scatter plots analysis.....	- 138 -

## Tables

<b>Table 2.1</b> List of exclusion criteria.....	- 35 -
<b>Table 2.2</b> Pulse sequence parameters for EGE-imaging.....	- 37 -
<b>Table 2.3</b> Pulse sequence parameters for LGE-imaging.....	- 38 -
<b>Table 3.1</b> Study population characteristics.....	- 48 -
<b>Table 3.2</b> Infarct characteristics at baseline.....	- 49 -
<b>Table 3.3</b> Univariate and multivariate analysis.....	- 52 -
<b>Table 4.1</b> Study demographics.....	- 65 -
<b>Table 4.2</b> Imaging parameters at baseline CMR study.....	- 66 -
<b>Table 4.3</b> Regression analysis.....	- 69 -
<b>Table 4.4</b> Association of volumetric and strain parameters to size of MVO.....	- 70 -
<b>Table 4.5</b> Association of parameters to adverse LV remodelling.....	- 72 -
<b>Table 5.1</b> Study demographics and baseline CMR parameters.....	- 87 -
<b>Table 5.2</b> Myocardial deformation parameters.....	- 89 -
<b>Table 5.3</b> C-statistics for myocardial strains.....	- 91 -
<b>Table 5.4</b> Logistic regression analysis.....	- 93 -
<b>Table 6.1</b> Clinical and angiographic characteristics.....	- 108 -
<b>Table 6.2</b> Validation of ECV thresholding.....	- 110 -
<b>Table 6.3</b> Baseline infarct characteristics at 1.5T and 3T.....	- 112 -
<b>Table 6.4</b> Regression analysis.....	- 116 -
<b>Table 7.1</b> CMR Protocol in healthy volunteers.....	- 128 -
<b>Table 7.2</b> Demographics and CMR scan parameters.....	- 131 -
<b>Table 7.3</b> Consistency and variability of flow measurements.....	- 135 -
<b>Table 7.4</b> Diastolic flow assessment using all acceleration methods.....	- 137 -

## Abbreviations

2D	Two-dimensional
3D	Three-dimensional
4D	Four-dimensional
4D flow CMR	Four-dimensional flow cardiovascular magnetic resonance
4D-EPI	Four-dimensional echo planar imaging
4D-k-t BLAST	Four-dimensional <i>k-t</i> Broad-use Linear Acquisition Speed-up Technique
4D-TFE	Four-dimensional turbo field echo
5SD	5-standard deviation
A'	Myocardial late diastolic velocity
AAR	Area at risk
ACS	Acute coronary syndrome
AMI	Acute myocardial infarction
AUC	Area under the curve
AV	Aortic valve
BLAST	Broad-use Linear Acquisition Speed-up Technique
bSSFP	balanced steady-state free precession
CAD	Coronary artery disease
CMR	Cardiovascular magnetic resonance
CoV/CV	Coefficient of variability
E'	Myocardial early diastolic velocity
ECG	Electrocardiogram
ECM	Extracellular matrix
ECV	Extra-cellular volume
EDV	End-diastolic volume
EF	Ejection fraction
EGE	Early gadolinium enhancement
EPI	Echo planar imaging
ESC	European Society of Cardiology
ESV	End-systolic volume

FFR	Fractional flow reserve
FOV	Field of view
FT	Feature tracking
FWHM	Full width half maximum
GCS	Peak global circumferential strain
GCSR	Peak global circumferential strain rate
GLS	Peak global longitudinal strain
GLSR	Peak global longitudinal strain rate
GRAPPA	Generalised auto-calibrating partially parallel acquisitions
GRS	Peak global radial strain
GRSR	Peak global radial strain rate
HLA	Horizontal long axis
IMH	Intramyocardial haemorrhage
IS	Infarct size
LGE	Late gadolinium enhancement
LV	Left ventricular
LV	Left ventricle
LVEDV	Left ventricular end diastolic volume
LVEDVi	Left ventricular end diastolic volume indexed
LVESV	Left ventricular end systolic volume
LVESVi	Left ventricular end systolic volume indexed
MAPSE	Mitral annular plane systolic excursion
MBF	Myocardial blood flow
MI	Myocardial infarction
MR	Magnetic resonance
MRI	Magnetic resonance imaging
MV	Mitral valve
MVO	Microvascular obstruction
NFF	Net forward flow
NT-proBNP	N-terminal pro b-type natriuretic peptide
PC	Phase contrast
PCI	Percutaneous coronary intervention

PEFR	Peak early filling rate
PLFR	Peak late filling rate
PPCI	Primary percutaneous coronary intervention
RF	Radiofrequency
ROC	Receiver-operator characteristic
ROI	Region of interest
RV	Right ventricular
SD	Standard deviation
STEMI	ST-elevation myocardial infarction
SV	Stroke volume
T2*	T2-star-weighted imaging
T2W	T2-weighted
TIMI	Thrombolysis in Myocardial Infarction
VENC	Velocity encoding
VLA	Vertical long axis

# 1 Introduction

Coronary artery disease (CAD) is now the largest cause of death worldwide (Mortality and Causes of Death, 2015). Acute chest pain remains one of the main symptoms of presentation and admission to hospital. It contributes about 20-40% of all medical admissions. Even though contemporary biomarkers of myocardial injury are very sensitive in detecting acute coronary syndrome (ACS), they can suffer from low specificity.

Cardiac imaging can contribute to the diagnosis of ACS, in particular when combined with the clinical history, 12-lead electrocardiogram (ECG) findings and cardiac biomarkers. When cardiac imaging is used appropriately in this setting, it can reduce the number of missed ACS, filter out those who were wrongly diagnosed as ACS and guide the management of those with confirmed ACS. Different time points in the ischaemic cascade can be imaged by various imaging modalities depending on the patho-physiological changes in the coronary arteries and the ischaemic myocardium (Figure 1.1).

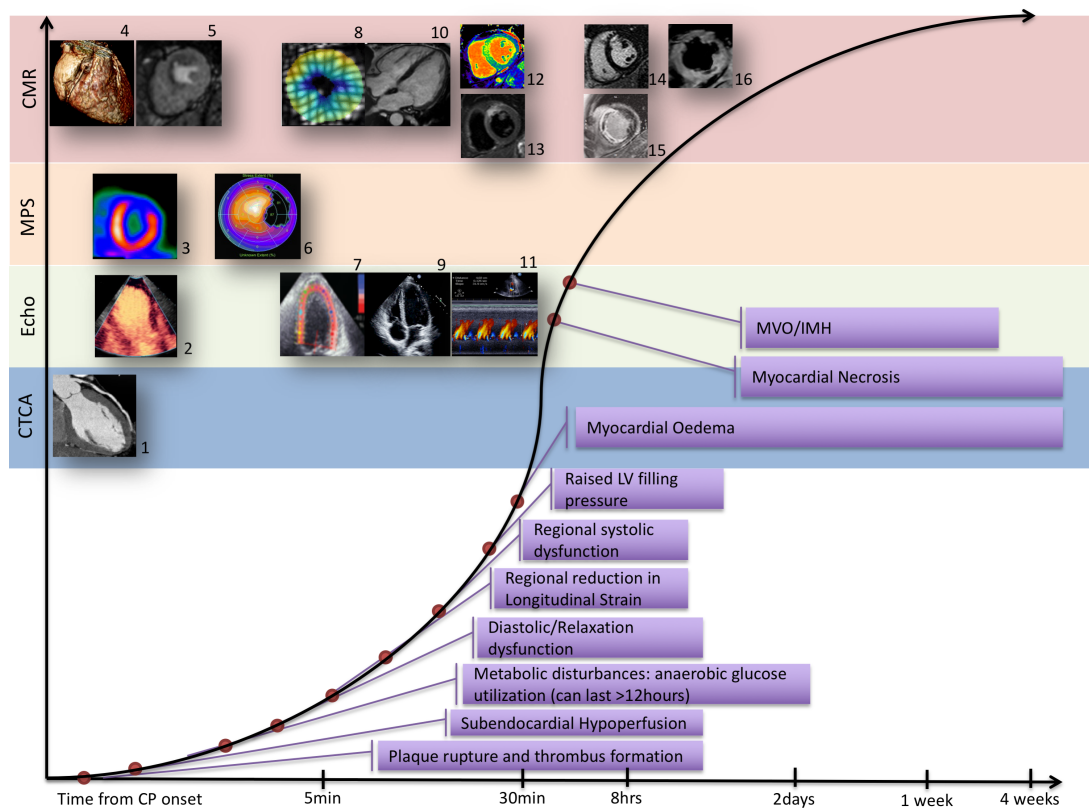


Figure 1.1 Timeline of patho-physiological changes in ischaemic myocardium and applied imaging techniques.

*1 Computed tomography coronary angiography; 2 Myocardial contrast echocardiography for the assessment of perfusion defects; 3 Rest myocardial perfusion scintigraphy; 4 Contrast enhanced magnetic resonance angiography for detection of proximal coronary anomaly; 5 Stress cardiac magnetic resonance; 6 Myocardial ischaemic memory imaging with  $\beta$ -methyl-p-iodophenylpentadecanoic acid; 7 Strain imaging on echocardiography for heterogeneity of strain curves; 8 Myocardial tagging with cardiac magnetic resonance for regional strain variations in ischaemic myocardium; 9 Echocardiography to detect regional wall motion abnormality; 10 Cine cardiac magnetic resonance imaging to detect regional wall motion abnormality; 11 Ratio of peak mitral inflow velocity (E) and mitral valve propagation velocity (Vp) for estimating LA pressure (E/Vp); 12 Native T1-Maps on cardiac magnetic resonance imaging for quantification of myocardial oedema; 13 T2-weighted cardiac magnetic resonance imaging for myocardial oedema; 14 Late gadolinium enhancement imaging on cardiac magnetic resonance for scarred myocardium; 15 late gadolinium enhancement (LGE) imaging for microvascular obstruction; 16 T2\*-imaging on cardiac magnetic resonance for intra-myocardial haemorrhage.*

### ***1.1 Established role of CMR in the assessment of ACS***

Cardiac Magnetic Resonance (CMR) has an emerging role in the assessment and management of patients with ACS, in particular those who are clinically stable. It provides structural and functional assessment of regional myocardial motion and thickening, rest and stress perfusion, myocardial oedema, microvascular obstruction and intramyocardial haemorrhage (Lockie et al., 2009).

The 2006 American Appropriateness Criteria for Cardiac Computed Tomography and Cardiac Magnetic Resonance Imaging recommends stress CMR as appropriate for the evaluation of intermediate likelihood patients when the ECG is uninterpretable or the patient is unable to exercise (Hendel et al., 2006). MR coronary angiography, where available, may be appropriate to detect coronary anomalies. Current European Society of Cardiology (ESC) guidelines highlight in particular the ability of CMR to detect myocarditis, assess viability and perfusion defects in suspected ACS patients (Hamm et al., 2011) (Figure 1.2). Additionally, the ESC guidelines on the

management of suspected non-ST elevation MI also recommend stress CMR (Class I, Level A evidence) in patients without recurrent pain, normal ECG, negative troponin and a low ( $\leq 108$ ) 'Global Registry of Acute Coronary Events' (GRACE) risk score.

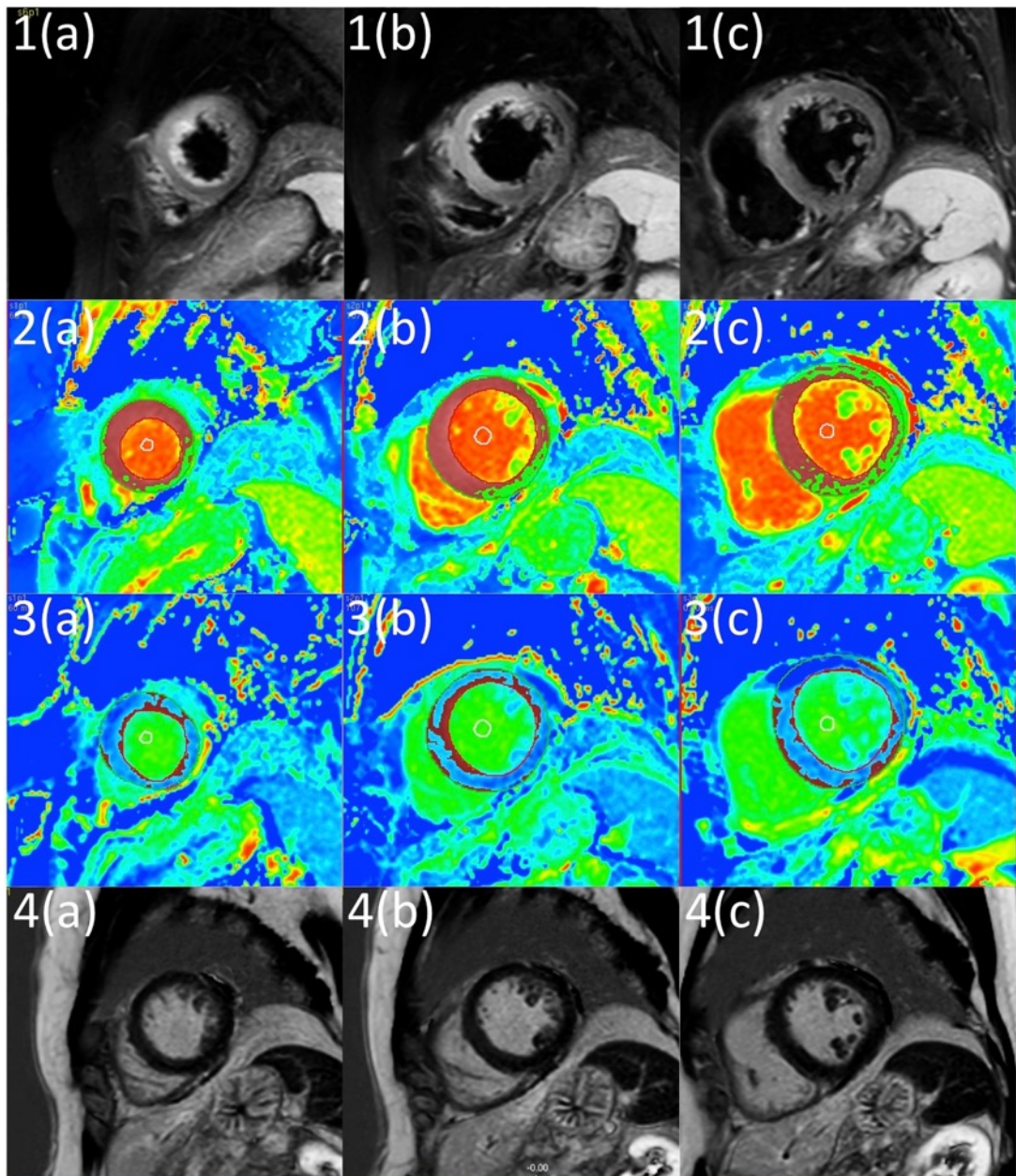


*Figure 1.2 Multi-parametric CMR in suspected ACS*

*This is a case of a 67-year-old female with takotsubo cardiomyopathy (Garg, John P Greenwood and Plein, 2015). T2-weighted imaging demonstrated corresponding high signal suggestive of myocardial oedema (Panel 1a-c). Native-T1 maps (Panel 2a-c, using cut-off of 1000msec) and extra-cellular volume (ECV) maps (Panel 3a-c, using*

*cut-off of 29%) demonstrated high native-T1 and mildly raised ECV in the same segments. LGE imaging (Panel 4a-c) showed no evidence of infarction.*

CMR imaging is feasible, robust and safe in patients with recent non-ST elevation MI (Plein et al., 2004). In the same study, Plein et al demonstrated that CMR imaging within 3 days of the acute event had sensitivity 96% and specificity 83% for significant CAD defined by invasive angiography. It was also more accurate than the Thrombolysis in Myocardial Infarction (TIMI) risk score ( $P < 0.001$ ). In a study of 161 patients presenting to the emergency department within 12 hours of symptoms suggestive of ACS but without ST elevation on initial ECG, total imaging time was 38 minutes and patients were absent from the emergency department for less than 1 hour (Kwong et al., 2003). Although the sensitivity and specificity for the diagnosis of ACS as defined by troponin-I and invasive angiography for this CMR protocol was only 84% and 85%, respectively, CMR added incremental value over clinical parameters. A study of 135 low-risk patients presenting to the emergency department with chest pain showed that no patients with a normal adenosine CMR study had a subsequent diagnosis of CAD or an adverse outcome after one year (Ingkanisorn et al., 2006). In the same study, the sensitivity of stress-CMR was 100% with a specificity of 93% for predicting adverse outcomes during a one-year follow-up period. In two similar separate studies evaluating 192 patients who received adenosine stress and rest CMR, none of the patients with normal CMR had clinical events during 9-months of follow-up (Lerakis et al., 2009; Hartlage et al., 2012). Lastly, in a randomised trial evaluating cost-effectiveness of stress CMR in 110 intermediate- and high-risk ACS patients, stress CMR led to a cost saving of over 20% compared with standard inpatient care (\$3101 vs \$4742;  $P = 0.004$ ) due to reduced coronary artery revascularization, readmissions and further cardiac testing without an increase in post discharge ACS at 90-days (Miller et al., 2011).

## ***1.2 CMR Techniques used in the assessment of patients with ACS***

A typical CMR study takes between 30 and 60 minutes and typically includes T1 weighted black blood images for assessment of anatomy, cine images in multiple planes for assessment of left ventricular (LV) and right ventricular (RV) volumes as

well as LGE imaging for delineation of scar and fibrosis (Figure 1.2). This basic protocol can be complemented with stress perfusion for ischaemia detection, T2-weighted imaging to detect myocardial oedema or intra-myocardial haemorrhage. Additionally, pre-/post-contrast T1 mapping techniques can be used for assessment of the extracellular volume (ECV) fraction.

The basic principles of CMR assessment of cardiac structure, function and tissue composition are debated in detail before an appraisal of how each of these techniques can be applied to the research questions investigated in this thesis.

### ***1.3 Left ventricular functional assessment***

#### **1.3.1 Volumetric analysis**

Assessment of LV chamber volumes and ejection fraction (EF) forms the cornerstone of assessment of cardiac structure by CMR. Echocardiography is the most broadly available and utilised non-invasive imaging modality for the evaluation of ventricular volumes. When suboptimal imaging quality does not allow for assessment of EF or more accurate assessment of EF is required, both American (Yancy et al., 2013) and European (McMurray et al., 2012) guidelines recommend the use of CMR.

EF is usually measured by CMR with the acquisition of a two-dimensional continuous stack of short axis gradient-echo cine images covering the full length of the LV. The total number of slices, and subsequently the number of breath-holds, depends on the length of the left ventricle and the chosen imaging parameters, in particular slice thickness and gap. In patients with poor breath-hold capacity, the acquisition can be shortened close to real-time with acceleration techniques (such as sensitivity encoding [SENSE], simultaneous acquisition of spatial harmonics [SMASH] and generalized auto-calibrating partially parallel acquisitions [GRAPPA]), usually at the expense of signal-to-noise ratio, spatial or temporal resolution (Larkman and Nunes, 2007). The EF is typically calculated from these images by the “summation of discs” method (Utz et al., 1987). On each cine image within the stack, endocardial contours are drawn at end-systole and end-diastole. As the slice thickness is known, the volume of each disc can be calculated and by adding the volumes of each slice end-diastolic volume (EDV), end-systolic volume (ESV) and consequently EF can be

calculated. This technique has been shown to be highly reproducible with inter-study reproducibility that is significantly better than two-dimensional echocardiography (Grothues et al., 2002). It has been projected that to detect a 3% change in EF by echocardiography 87 patients are needed whereas only 11 patients are needed by CMR.

Measurement of EF by CMR inform diagnosis and prognosis. The degree of LV impairment is associated with adverse outcomes and increased mortality (Gradman et al., 1989). In the Candesartan in Heart Failure: Assessment of Reduction in Mortality and Morbidity (CHARM) study, every 10% decrease in the EF below 45% was accompanied with a 39% increase in all-cause mortality (Solomon et al., 2005). For a more comprehensive assessment of prognosis, EF can also be incorporated as one of several factors in a risk score (Ketchum and Levy, 2011).

Right ventricular (RV) volumes and RV EF can also be calculated by CMR using the summation of discs method described previously. In patients with previous myocardial infarction (MI), RV EF <40% was associated with adverse outcomes independently of other factors including LV EF (Larose et al., 2007). Impaired RV function is associated with adverse outcomes in diseases that primarily affect the RV such as pulmonary arterial hypertension and arrhythmogenic right ventricular cardiomyopathy and in patients with heart failure (Valsangiacomo Buechel and Mertens, 2012).

From the same continuous short axis LV stack used to measured EF; LV mass can also be computed. Contours are drawn on the endocardial and epicardial borders at one point in the cardiac cycle, usually end diastole and the LV mass calculated using the 'summation of discs' principle (Schulz-Menger et al., 2013).

Post ACS, adverse left ventricular remodelling is associated significant morbidity and mortality (Frangiannis, 2006). Animal studies have revealed that post-infarct remodeling is the consequence of an interplay between numerous mechanical, neuro-hormonal, microvascular, and macrovascular factors (Sutton and Sharpe, 2000). Post MI, European Society of Cardiology guidelines recommend CMR for viability assessment and in patients with poor echocardiographic windows (Steg et al., 2012). CMR derived LV volumetric measurements of left ventricular end-diastolic volume, EF and infarct size are increasingly used as surrogate endpoints in clinical

trials post-MI (Desch et al., 2011). The current standard criteria for adverse LV remodelling on follow-up CMR study is a 20% increase in LV end diastolic volume at follow-up (Carrick et al., 2015).

### **1.3.2 Myocardial deformation analysis**

Volume based assessment of EF is the most widely used and best validated measure of left ventricular function. However, this method doesn't inform us about 'myocardial' regional or global function and is extremely sensitive to loading conditions. Importantly, in several cardiomyopathies including hypertrophic cardiomyopathy, the EF remains preserved and if anything, the EF increases in mild to moderate concentric hypertrophy. However, in these patients left ventricular longitudinal function is markedly reduced (Young et al., 1994). Hence these limitations of volumetric assessment, have led to an interest in techniques that provide more objective measures of contractile function.

The LV myocardium simultaneously contracts in the longitudinal and circumferential planes and thickens in the radial plane in systole, with reciprocal changes in diastole. Myocardial deformation/strain imaging allows for more direct assessment of myocardial muscle shortening and lengthening throughout the cardiac cycle. Strain is defined as the change in length of a segment of myocardium relative to its resting length and is expressed as a percentage; strain rate is the rate of this deformation. Longitudinal and circumferential shortening results in negative strain values, whereas radial thickening results in a positive strain value (Shah and Solomon, 2012). Myocardial strain assessment by CMR provides important diagnostic and prognostic information and has been used to detect subclinical impairment of both regional and global cardiac function in a wide variety of conditions (Parsai et al., 2012).

Feature tracking is a new post processing technique which allows for tracking of myocardial features during the 30-60 phases of the cine imaging throughout the cardiac cycle. This technique is comparable and provides similar results to speckle tracking, which is a well validated echocardiography measure of strain (Onishi et al., 2015). Feature tracking allows for quantification of strain without the need for the acquisition of separate tagged cine imaging. Feature tracking derived strain has

demonstrated similar high reproducibility to strain measured by CMR tissue tagging (Khan et al., 2015).

## ***1.4 Multi-parametric tissue characterization***

### **1.4.1 Myocardial oedema and area at risk analysis**

Abrupt occlusion of coronary artery results in initiation of several structural, metabolic and functional pathways within the subtended myocardium which eventually results in myocardial necrosis. Necrosis is initiated from the sub-endocardium to the epicardium in a wave-front manner (Reimer and Jennings, 1979). Myocardial oedema develops before ischaemic necrosis or even troponin release (Abdel-Aty et al., 2009) and can persist even when ECG changes and myocardial dysfunction have resolved (h-Ici et al., 2014) (Figure 1.1). Post ischaemic injury, myocardial oedema can persist up to six month (Dall'Armellina et al., 2011). In CMR study, T2-weighted imaging (T2W-imaging) is the standard imaging technique for detecting acute myocardial edema. It is used for differentiation of acute from chronic MI (Abdel-Aty et al., 2004), assessment of the area at risk (AAR) (Payne et al., 2011), myocarditis (Friedrich et al., 2009) and increasingly as a surrogate end-point in clinical trials. T2W-imaging improves the overall accuracy of CMR protocol to diagnose ACS often before cardiac biomarkers were elevated (Cury et al., 2008).

Emerging CMR methods for ACS imaging include in particular parametric mapping techniques. T1-mapping can quantify the extent and severity of acute ischaemic injury. In an early study, non-contrast T1-maps had 96% sensitivity and 91% specificity for detecting acute MI (Messroghli et al., 2007). In a more recent study, T1-mapping was superior to T2W-imaging in detecting non-ST-elevation MI (area under the curve  $0.91 \pm 0.02$  versus  $0.81 \pm 0.04$ , respectively  $P=0.004$ ) (Dall'Armellina et al., 2012). T1-mapping is also superior to T2W and LGE-imaging in detecting acute myocarditis, which is one of the key differential diagnoses in acute chest pain patients (Ferreira et al., 2013; Garg, John P J.P. Greenwood and Plein, 2015).

Post ACS, area at risk (AAR) is defined as total area of the myocardium subtended by the culprit occluded vessel. If no reperfusion occurs in the occluded vessel, this

whole area potentially can necrose resulting into permanent transmural scar and also potentially leading to adverse LV remodeling. Urgent reperfusion therapy, reduces necrosis and limits the overall infarct burden. On CMR imaging post ACS, AAR is identified as total hyper-enhanced area on T2W imaging, which includes the infarcted myocardium. Salvaged myocardium is the area of myocardium which has been saved because of reperfusion therapy, that is, AAR minus the infarcted myocardium.

#### **1.4.2 Infarct size and viability analysis**

Gadolinium based CMR contrast agents are exclusively extracellular and can only passively enter damaged cells with a leaky cell membrane. These contrast agents therefore accumulate in areas with damaged cells and avascular extracellular regions. This phenomenon is exploited in LGE CMR imaging. LGE imaging involves administration of typically 0.1-0.2mmol/kg of a gadolinium based contrast agent. After a delay of 5-20 minutes the contrast agent is retained to a greater extent in areas of scar or fibrosis than in normal myocardium. An inversion recovery sequence with an inversion time specified to null “normal” myocardium then displays scarred myocardium as bright when compared to the reference. The pattern of hyper-enhancement on LGE can aid in the diagnosis of the aetiology of many cardiac pathologies. For example, sub-endocardial or transmural LGE is seen in ischemic cardiomyopathy, mid wall LGE in dilated and hypertrophic cardiomyopathies, epicardial LGE in myocarditis and global diffuse sub-endocardial LGE in amyloidosis. The presence of hyper-enhancement on LGE imaging is shown to match well with discrete fibrosis on histology and is associated with adverse prognosis in many cardiomyopathies (Ismail et al., 2012).

Post myocardial infarction, LGE imaging plays an important role in defining infarct size (IS) and the assessment of viability in the infarcted segments (Kwong and Korlakunta, 2008). IS and viability assessment are important measures of reperfusion success and predictors of remodeling and prognosis (Klem et al., 2011). Both IS and AAR are quantified with semi-automated thresholding methods applied on LGE imaging. For AAR, full width half maximum (FWHM) has been validated in histopathological study (Aletras et al., 2006). For acute IS, 5-standard deviation (5SD)

or FWHM thresholding methods have been shown to provide reliable results of quantification (Flett et al., 2011; Heiberg et al., 2008). These semi-quantitative methods have important limitations and manual contouring is still one of the best methods for quantification of IS and AAR (McAlindon et al., 2015).

### **1.4.3 Microvascular obstruction and intra-myocardial haemorrhage**

Microvascular obstruction (MVO) occurs post ST-elevation myocardial infarction (STEMI) in a certain group of patients who receive reperfusion therapy after prolonged myocardial ischaemia (Moens et al., 2005). It has been associated with 'no-reflow' on invasive coronary angiogram in the culprit vessel. No-reflow is characterized by the additional important contributing factors of micro-embolization and the resultant inflammation (Schwartz and Kloner, 2012). Rupture or erosion of epicardial coronary artery plaques, either spontaneously or induced mechanically by percutaneous coronary intervention, can result in distal showering of embolic debris, consisting of atherosclerotic plaque components and/or thrombotic material. Distal embolization may not only contribute to mechanical obstruction of the micro-vessels but also causes an inflammatory response with the elaboration of vasogenic and thrombogenic factors that further exacerbate existing microvascular dysfunction. Therefore, patho-physiologically, MVO is the result of the complex interplay of a number of related processes.

Reperfusion may also lead to intramyocardial haemorrhage (IMH) in the infarct core (Roberts et al., 1983) via extravasation of blood through damaged endothelium (Basso and Thiene, 2006). Both MVO and IMH are gradually being recognized as a poor prognostic marker and an indicator of subsequent adverse LV remodeling, independently of IS (Morishima et al., 2000; Wu et al., 1998; Mather et al., 2011).

In pre-clinical and human studies post-acute reperfused infarction (Judd et al., 1995; Lima et al., 1995), regions of myocardial hypo-enhancement within the first 2 minutes of contrast administration were observed within the infarct region that were characterized by significantly reduced regional blood flow and correlated in size with anatomic no-reflow zones measured by thioflavin-S. Subsequently, these hypo-enhanced areas seen on CMR were termed MVO. Therefore, MVO represents the hypo-intense core within the infarcted zone on LGE imaging. Volumes of MVO

can be calculated from manually planimetered areas through the whole short-axis LV LGE stack by the modified Simpson's method. The presence and extent of IMH is assessed by combined analysis of T2W and T2\* images (Figure 1.3). IMH can be visualized by T2-weighted (T2W) sequences because hemorrhage and the breakdown products of oxygenated hemoglobin influence magnetic properties of the surrounding tissue. On T2W images, areas with mean signal intensity less than 2 standard deviation below the periphery of the area at risk (AAR) is considered to be haemorrhage (Kidambi, Adam N Mather, et al., 2013). On the T2\* images, the presence of a dark core within the infarcted area by visual inspection of the images can confirm myocardial haemorrhage. The standardized imaging method or protocol for assessment of IMH is still debated. However, concordant results between T2w and T2\* are now used in research studies to confirm haemorrhage reliably (Kidambi et al., 2014).

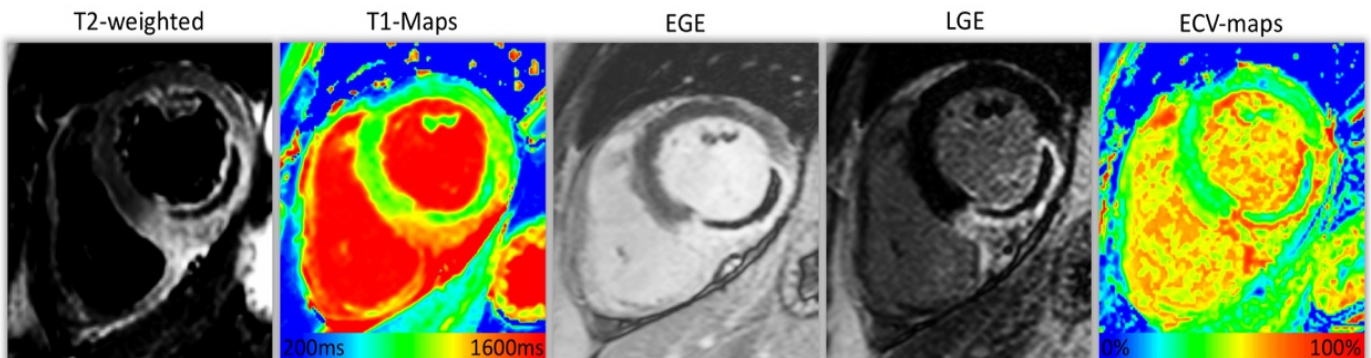


*Figure 1.3 Tissue characterization in STEMI.*

*This is a case of inferior STEMI patient who received urgent reperfusion therapy. T2W imaging demonstrates hyper-enhancement in the infero-lateral segments with a dark core within it. LGE imaging demonstrates extensive infero-lateral myocardial infarction. The dark core on T2W is located exactly in the dark core on the LGE imaging and is this would be consistent with a diagnosis of MVO with IMH. T1-maps and ECV-maps demonstrate pseudo-normalization of values within this 'dark' core.*

#### **1.4.4 Left ventricular thrombus assessment**

LV thrombus formation is one of the worst complications of myocardial infarction and can lead to fatal systemic embolization (Delewi et al., 2012). In current era of urgent reperfusion therapy, the incidence is around 5-7%. Early gadolinium enhancement (EGE) imaging is superior to transthoracic/transesophageal echocardiography for the detection of LV thrombus (Mollet et al., 2002). EGE imaging is done immediately post contrast administration in multiple planes to detect the presence of LV thrombus (Goyal and Weinsaft, 2013). On EGE imaging, thrombus is seen as a dark hypo-intense area with the left ventricle. Patients diagnosed with LV thrombus are routinely started on anti-coagulation with warfarin for at least 3-6 months.

#### **1.4.5 Extracellular volume quantification**

Extracellular fibrosis is a common pathological finding in many aetiologies of heart failure. As described in the preceding section, LGE imaging is a well-established method to assess and quantify the size and transmural extent of discrete areas of fibrosis/infarction. However, this process relies on nulling the healthy myocardium and on comparing the enhancement of healthy and diseased myocardium qualitatively. When the myocardium is more diffusely diseased, techniques that characterize the myocardium quantitatively provide incremental insights into myocardial disease.

There has been renewed recent interest in methods that quantify the inherent T1 (Messroghli et al., 2004) and T2 (Verhaert et al., 2011) signal of the myocardium and create an intuitive visual map of their values. Native tissue maps alone can be used for tissue characterization or can be combined with post contrast acquisitions. Native (non-contrast) T1-maps can detect pathology related to excess water in oedema, protein deposition, changes in lipid/iron content in the myocardium (Moon et al., 2013). However, native T1-maps do not inform us about the intra-/extra-cellular composition of the myocardium. Additionally, even though quantification of native T1 is highly reproducible, it varies with different field strengths, vendor platforms and mapping sequences (Dabir et al., 2014).

Gadolinium-based contrast agents shorten the T1 relaxation time and tissues with an expanded extracellular space due to fibrosis, infiltration or scar have a larger distribution volume for the extracellular contrast agent. In these tissues, the reduction in T1 relaxation time is therefore more pronounced than in normal tissue and is correlated with the extent of the extracellular space. Post-contrast myocardial T1 has been shown to significantly correlate with histological areas of fibrosis (Iles et al., 2008).

Post contrast T1 mapping makes assumptions about the kinetics of gadolinium contrast agents and the results can be influenced by renal function, haematocrit and body composition. These assumptions can be overcome by combining pre-/post-contrast T1 mapping of both myocardium and blood and correcting for the blood volume of distribution (1-haematocrit). From these data, maps of the extracellular volume (ECV) fraction can be calculated which show significant correlation with histological degree of fibrosis and volume of collagen in the myocardium (Flett et al., 2010). ECV is calculated using the formula:

$$ECV = (1 - Hct) \frac{R1(myo\ pre) - R1(myo\ post)}{R1(blood\ pre) - R1(blood\ post)} \quad \text{where } R1 = 1/T1$$

ECV is a promising measure of extracellular matrix (ECM) expansion, which is adversely related to mechanical, electrical and vasomotor dysfunction of the myocardium (Moon et al., 2013). Increased ECV have been reported in several cardiomyopathies including amyloidosis, dilated cardiomyopathy and hypertrophic cardiomyopathy (Dass et al., 2012; Puntmann et al., 2013; Sado et al., 2012). Hence, ECV-maps add incremental diagnostic value to quantify global/focal myocardial fibrosis, which is mainly a process in the ECM. ECV values are independent of the field strength of the CMR scanners.

In a recent study of 1172 subjects, Schelbert and Wong demonstrated that myocardial fibrosis quantified by ECV-maps is associated with subsequent hospitalization for heart failure (hazard ratio 1.77; 95% CI 1.32 to 2.36 for every 5% increase in ECV), death (hazard ratio 1.87 95% CI 1.45 to 2.40), or both, even after adjusting for age, sex, renal function, myocardial infarction size, ejection fraction,

hospitalization status, and heart failure stage (Schelbert et al., 2015). Another study which investigated the use of ECV quantification in diabetes, also demonstrated that higher ECV is associated with mortality and incidence of hospitalization for heart failure in diabetic individuals when adjusted for demographics, infarct size by LGE-imaging and other CMR parameters (T.C. Wong et al., 2014).

Recent studies have investigated ECV rise in different segments of myocardium post STEMI (Carberry et al., 2016; Bulluck et al., 2016). In these studies, the remote myocardium was defined as the AHA segment 180 degrees from the infarct territory with normal motion and no LGE. Carberry et al demonstrated that acute remote zone ECV post STEMI is associated with few baseline patient characteristics (male gender, body mass index and history of diabetes). Also, in their study they showed that the remote zone ECV is associated with baseline N-terminal pro b-type natriuretic peptide (NT-proBNP). Bulluck et al demonstrated that mean segmental ECV value in the remote myocardium is raised acutely post STEMI and also acute infarct segmental ECV predicted functional recovery.

### ***1.5 Role of haemodynamic assessment post MI***

Post myocardial infarction, haemodynamic assessment by routine echocardiography informs about LV filling pressures and the likelihood of heart failure (Hozumi et al., 1999). This non-invasive haemodynamic assessment can guide therapy and inform about prognosis (Iwahashi et al., 2012; Hillis et al., 2004).

Routine haemodynamic assessment by echocardiography is predominantly done by pulse-wave Doppler echocardiography (DE) technique. However, DE has several limitations due to 2D-planar assessment, through-plane motion, high intra-inter-operator variability and a recent meta-analysis queries the diagnostic accuracy of this method (Sharifov et al., 2016). Therefore, new quantitative measures of LV haemodynamics and flow are warranted post MI.

The development of four-dimensional flow cardiac magnetic resonance imaging (4D flow CMR) now allows mapping and quantification of intra-left ventricular flow and its kinetic energy (KE). This method is uniquely placed to provide new insight into the distribution of intra-left ventricular flow in health and disease. As this technology is less operator dependant, and allows to quantify intra-cardiac flow using three-dimensional plane, it has the potential to reduce intra-/inter-observer variability and importantly, measure flow indices, with higher accuracy and precision.

Hence, in this thesis, we take the first step in validating the best four-dimensional flow CMR imaging method for clinical applications on Philips 1.5 Tesla systems.

## ***1.6 Aims of thesis***

Myocardial deformation analysis using CMR feature tracking offers mechanistic insights into regional myocardial function. Additionally, it can discriminate and quantify the function of the three main different types of myofiber orientations: longitudinal, circumferential and radial orientation. In patients with ACS or CAD, there remains limited understanding on how the presence of MVO, IMH or perfusion defect on first-pass perfusion CMR influences the function of the three main myofiber orientations or myocardial deformation. Alteration in myocardial deformation could potentially be used clinically or as a surrogate end-point in research across other imaging modalities.

Quantification of ECV in acute infarct patients seems to add incremental information above LGE-imaging. Moreover, LGE imaging overestimates acute infarct size. Quantitative maps which offer more reliable assessment of IS and AAR are warranted. Additionally, there is a need for newer methods to assess and quantify intra-cardiac flow reliably, so that in future studies, a more comprehensive insight into adverse LV remodelling can be attained.

The subsequent chapters each have a specific aim with individual introduction, methods, results and discussion:

Study 1: To establish whether acute mitral annular plane systolic excursion (MAPSE) is associated with MVO or IMH

Study 2: To investigate the association of MVO, IMH and convalescent left ventricular (LV) remodelling with strain parameters measured by feature tracking CMR

Study 3: To investigate how first-pass adenosine stress perfusion CMR affects left ventricular longitudinal deformation

Study 4: To investigate if acute ECV-maps can reliably quantify myocardial area at risk (AAR) and final infarct size (IS)

Study 5: To investigate which is the most reliable and robust acceleration method in four-dimensional (4D) flow CMR in phantoms and in-vivo

## 2 Methods

### 2.1 Study Populations

Details of specific patients populations by chapter are listed in the individual sections below.

Exclusion criteria common to all patient groups are detailed in Table 2.1.

Number	Contraindications
1	Contraindication to CMR (e.g. non-CMR conditional permanent pacemaker or defibrillator, intra-orbital metal, claustrophobia etc.)
2	Pregnant or breastfeeding patients
3	Weight $\geq$ 120kg
4	Inability to lie flat for the duration of the CMR scan
5	Inability to give written, informed consent
6	Previous AMI or coronary artery bypass grafting

Table 2.1 List of exclusion criteria.

#### 2.1.1 Patient population for Chapter 3, 4, 6 and 7

Patients presenting with first ST-segment elevation AMI who were revascularized by primary percutaneous intervention (PCI) within 12 hours of onset of chest pain were prospectively recruited from a single tertiary centre between January 2011 to August 2014. AMI was defined as per current guidelines (Thygesen, Joseph S. Alpert, et al., 2012). After PPCI, patients received standard post-AMI secondary prevention therapy and were enrolled in a cardiac rehabilitation programme (Steg et al., 2012). For chapter 4, age and sex matched healthy volunteers serving as controls were recruited. Importantly, for chapter 6, patient population is different to patient population to Chapter 3 and 4. For chapter 7, healthy volunteers were recruited only from two sites: Leeds and Leiden. Healthy volunteers had no history or symptoms of cardiovascular disease, were on no cardiovascular or other relevant medication and had no contraindications to CMR.

### **2.1.2 Patient population for Chapter 5**

Patients presenting to the rapid access chest pain clinic and who were referred for a stress CMR study for the evaluation of coronary artery disease in a single tertiary cardiology centre were prospectively recruited in this prospective cohort study.

## ***2.2 Ethics and approvals***

For chapter 3,4 and 6, the study protocol was approved by the National Research Ethics Service (12/YH/0169). For chapter 5 and 7, the study protocol was approved by the National Research Ethics Service (12/YH/0551). For chapter 7, at Leiden, the institutional Medical Ethical Committee (P11.136) approved the study. All patients and health volunteers gave written informed consent to participate in all studies. Research studies complied with the Declaration of Helsinki.

## ***2.3 MRI Scanner Hardware***

All scans at 1.5T were conducted using the same 1.5T system (Ingenia, Philips, Best, The Netherlands) using the same 32-channel coil, vectorcardiographic triggering and multi-transmit technology (Philips, Best, The Netherlands). Chapter 5, 6 and 7 were done on 1.5T system.

All scans at 3.0T were conducted using the same 3.0T system (Achieva, Philips, Best, The Netherlands) using the same 32-channel coil, vectorcardiographic triggering and multi-transmit technology (Philips, Best, The Netherlands). Chapter 3, 4 and 6 were done on 3T system.

## ***2.4 Common CMR Protocol***

Key components of common CMR protocol all described in this section. At the start of any CMR protocol, free breathing low-resolution survey scan of the chest were done to mark anatomical landmarks. For each pulse sequence, images with artefact were repeated until any artefact was removed or minimized. The highest quality images were used for analysis.

### 2.4.1 Cine imaging

Long-axis cines: Vertical long axis (VLA or 2-chamber), horizontal long axis (HLA or 4-chamber) acquired with a balanced steady-state free precession (bSSFP), single-slice breath-hold sequence. Typical parameters for bSSFP cine were as follows: echo time 1.3 milliseconds, repetition time 2.6 milliseconds, flip angle 40°, field of view 320-420 mm according to patient size, SENSE acceleration, slice thickness 10 mm, and 30 phases per cardiac cycle.

Short-axis LV cine stack: Resting wall motion and left ventricular function were assessed with a contiguous stack of multiphase ventricular short-axis bSSFP cines (10-12 slices, 30 phases, 10-mm slice thickness, 0-mm gap and pulse sequence parameters were same as the long-axis cines).

### 2.4.2 Early gadolinium enhancement imaging (EGE)

EGE-imaging was done immediately post gadolinium based contrast administration. EGE was done by inversion recovery spoiled gradient echo pulse sequence. Comprehensive information on pulse sequence parameters are detailed in Table 2.2.

EGE-imaging	1.5 Tesla	3 Tesla
Short-axis contiguous slices, 2-chamber and 4-chamber	IR spoiled GE SENSE factor 1.7 Typical TE/TR = 2.8/5.7 ms Flip angle = 25° Typical BW = 300 Hz/pix Typical in-plane resolution = 1.5 mm acq/0.8 mm recon Look-Locker scout determined TI Slice thickness = 8 mm	IR spoiled GE SENSE factor 1.5 Typical TE/TR = 2.0/3.8 ms Flip angle = 25° Typical BW = 700 Hz/pix Typical in-plane resolution = 1.5 mm acq/0.7 mm recon Look-Locker scout determined TI Slice thickness = 10 mm

Table 2.2 Pulse sequence parameters for EGE-imaging.

### 2.4.3 Late gadolinium enhancement imaging (LGE)

LGE-imaging was performed 10-15 minutes after the bolus contrast injection (0.1 mmol/kg gadolinium-DTPA: gadopentetate dimeglumine; Magnevist, Bayer, Berlin, Germany) was then administered using a power injector (Spectris, Solaris, PA).using phase-sensitive inversion recovery (PSIR) or inversion recovery (IR) prepared gradient echo. A modified Look-Locker (MOLLI) approach was used to determine the optimal inversion time (ms) required to adequately null the LV myocardium.

LGE-imaging	1.5 Tesla	3 Tesla
Short-axis contiguous slices, 2-chamber and 4-chamber	PSIR spoiled GE SENSE factor 1.7 Typical TE/TR = 3.0/6.1 ms Flip angle = 25° Typical BW = 250 Hz/pix Typical in-plane resolution = 1.6 mm acq/0.8 mm recon Look-Locker scout determined TI Slice thickness = 10 mm	IR spoiled GE SENSE factor 1.5 Typical TE/TR = 2.0/3.7 ms Flip angle = 25° Typical BW = 800 Hz/pix Typical in-plane resolution = 1.6 mm acq/0.7 mm recon Look-Locker scout determined TI Slice thickness = 10 mm

Table 2.3 Pulse sequence parameters for LGE-imaging.

## ***2.5 Common CMR analysis***

Images were evaluated offline using the following software's: 1) Commercially available software (cvi42 v4.1.5, Circle Cardiovascular Imaging Inc., Calgary, Canada): Chapter 3,4 and 5. 2) In-house research software developed with collaborators: MASS (Version 2016EXP, Leiden University Medical Center, Leiden, The Netherlands): Chapter 6 and 7.

### **2.5.1 LV Ejection fraction analysis**

Left ventricular endocardial and epicardial borders were manually contoured from the short axis LV cine stack at both end systole and end diastole in order to generate LV end systolic and end diastolic volumes according to the summation of discs methodology (Vogel-Claussen et al., 2006). LV ejection fraction was derived from the equation:  $LVEF (\%) = ((LVEDV - LVESV) / LVEDV) \times 100$ . Both trabeculation and papillary muscles were excluded. LV mass values were calculated from the end diastolic myocardial volume according to established methods (Myerson et al., 2002).

## ***2.6 Statistical analysis***

All statistical analysis was performed using the PASW software package (V21, SPSS, IBM, Chicago, Illinois, USA). Data are presented as mean $\pm$ SD, median (interquartile range, IQR) or frequency (percentage). Data were tested for normality using the Shapiro-Wilks test. For normally distributed data, two-tailed unpaired Student's t tests were used for comparisons between groups, and paired Student's t tests were used for intragroup comparisons. For non-normally distributed data, the Related-Samples Wilcoxon Signed Rank Test and independent samples Mann-Whitney U test were used. To compare between groups an analysis of variance (ANOVA) and Tukey post-hoc tests were used. The Chi-squared test was used for comparing categorical variables. Pearson's correlation coefficients were used to assess the correlation of dependent and independent variables. P values <0.05 were considered statistically significant.

### **2.6.1 Generic sample size estimations**

Based on the published data (Bellenger et al., 2000), the group size required to detect a 10ml change in LVEDV is 12 patients, 10 patients to detect a 10ml change in LVESV, 15 to detect a 3% change in LVEF and 9 to detect a 10g change in LV mass. Therefore, on the assumption that around 25% patient post-STEMI will develop adverse LV remodelling, we need to recruit a minimum of 40-44 patients, to investigate adverse remodelling in chapter 3,4 and 6. Chapter 5 and 7 were mainly mechanistic and validation studies investigating mean error or correlation on continuous datasets. They did not investigate any hard end-points and hence sample size estimations were not made. However, the total recruitment size was informed by previous studies in similar study populations to demonstrate changes (Zaman et al., 2015; Kidambi, Adam N. Mather, et al., 2013).

### **3 Study 1- Ventricular Longitudinal Function is Associated with Microvascular Obstruction and Intramyocardial Haemorrhage**

#### ***3.1 Abstract***

##### **3.1.1 Background**

Microvascular obstruction (MVO) and intramyocardial haemorrhage (IMH) are associated with adverse prognosis, independently of infarct size after reperfused ST-elevation myocardial infarction (STEMI). Mitral annular plane systolic excursion (MAPSE) is a well-established parameter of longitudinal function on echocardiography. We aimed to investigate how acute MAPSE, assessed by a 4-chamber cine-cardiovascular magnetic resonance (CMR), is associated with MVO, IMH and convalescent left ventricular (LV) remodelling.

##### **3.1.2 Methods**

54 consecutive patients underwent CMR at 3T (Intera CV, Philips Healthcare, Best, The Netherlands) within 3 days of reperfused STEMI. Cine, T2-weighted, T2\* and late gadolinium enhancement (LGE) imaging were performed. Infarct and MVO extent were measured from LGE images. The presence of IMH was investigated by combined analysis of T2w and T2\* images. Averaged MAPSE (medial-MAPSE + lateral-MAPSE/2) was calculated from 4-chamber cine imaging.

##### **3.1.3 Results**

44 patients completed baseline scan and 38 patients completed 3-month scans. 26 (59%) patients had MVO and 25 (57%) patients had IMH. Presence of MVO and IMH were associated with lower averaged-MAPSE (11.7±0.4mm versus 9.3±0.3mm;  $p<0.001$  and 11.8±0.4mm versus 9.2±0.3mm;  $p<0.001$ , respectively). IMH (beta=-0.655,  $p<0.001$ ) and MVO (beta=-0.567,  $p<0.001$ ) demonstrated a stronger correlation to MAPSE than other demographic and infarct characteristics. MAPSE  $\leq$  10.6mm demonstrated 89% sensitivity and 72% specificity for the detection of MVO

and 92% sensitivity and 74% specificity for IMH. LV remodelling in convalescence was not associated with MAPSE (AUC 0.62, 95% CI 0.44-0.77, p=0.22).

### **3.1.4 Conclusions**

Post reperfused STEMI, LV longitudinal function assessed by MAPSE can independently predict the presence of MVO and IMH.

### ***3.2 Introduction***

Following reperfused acute myocardial infarction (AMI), the left ventricle (LV) undergoes structural adaptations both within and outside of the infarct zone, referred to as LV remodelling. In approximately 50% of patients, coronary reperfusion is associated with microvascular obstruction (MVO) (Moens et al., 2005). Reperfusion may also lead to intramyocardial haemorrhage (IMH) in the infarct core (Roberts et al., 1983) associated with extravasation of blood (Basso and Thiene, 2006). Both MVO and IMH are associated with adverse prognosis and adverse LV remodelling, independently of infarct size (Morishima et al., 2000; Wu et al., 1998; Mather et al., 2011).

Acute myocardial ischaemia initially affects the subendocardium and progresses to the subepicardial layers in a 'wave front' manner (Ambrosio et al., 1989; Judd et al., 1995). Similarly, MVO and IMH predominantly affect the subendocardial layer. Endocardial fibres are structurally longitudinal fibres (Greenbaum et al., 1981) and therefore predominantly contribute to longitudinal contractile function of the LV (Birkeland et al., 1992). MVO and IMH are therefore likely to affect predominantly longitudinal function (Reimer et al., 1977) (Figure 3.1).

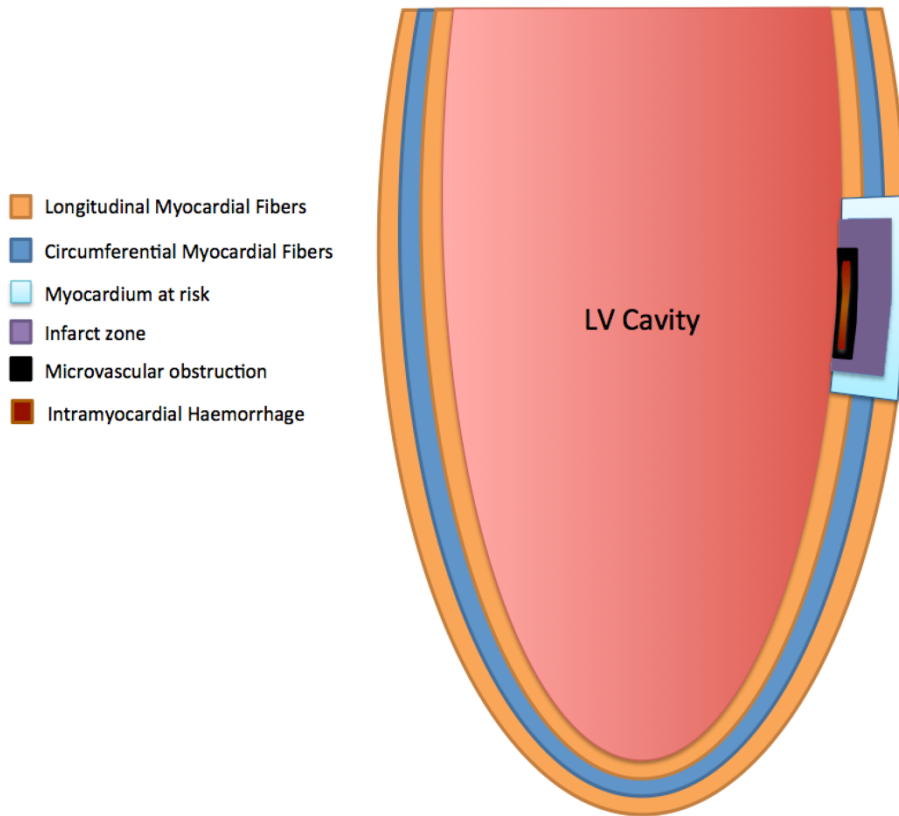


*Figure 3.1 Illustration of orientation of myocardial fibres with corresponding representation of infarct related zones.*

Mitral annular plane systolic excursion (MAPSE) is a well-established and easily obtained echocardiographic parameter for the assessment of longitudinal function and has been shown to correlate with LV systolic function (Hu et al., 2013). Post AMI, MAPSE has prognostic importance in the risk stratification of patients, for example a MAPSE of <8mm is associated with a >3x higher incidence of hospitalization and mortality ( $p=0.0001$ ) (Brand et al., 2002).

Traditionally, longitudinal functional assessment using MAPSE has been based on M-mode transthoracic echocardiography. It can also be evaluated from a standard four-chamber cardiovascular magnetic resonance (CMR) cine image. CMR based MAPSE is easily measured, reproducible and strongly correlates with the echocardiographic equivalent (Bulluck et al., 2014; Abdel-Aty et al., 2012).

We sought to investigate the effect of MVO and IMH on MAPSE in patients with acute STEMI and to determine correlations of CMR derived MAPSE with other markers of adverse outcome.

### **3.3 Study specific methods**

#### **3.3.1 CMR protocol**

T2w, T2\* and late gadolinium enhancement (LGE) imaging were performed using the '3-of-5' approach by acquiring the central 3 slices of 5 parallel short-axis slices spaced equally from mitral valve annulus to LV apical cap (Messroghli et al., 2005).

#### **3.3.2 CMR interpretation**

Cine, T2w, T2\* and LGE images were evaluated offline using commercially available software (cvi42 v4.1.5, Circle Cardiovascular Imaging Inc., Calgary, Canada). Infarct location was determined by LGE imaging, according to standard guidelines (Cerqueira et al., 2002). The presence and size of infarction and MVO were measured from LGE images. Infarct was defined as an area of LGE  $\geq 2$  standard deviations (SD) above remote myocardium, and infarct volume estimation included any hypointense core. We used the 2 SD method over the full-width half maximum (FWHM) method as there are more prognostic data for the 2 SD infarct size estimation (Kwon et al., 2014). The 2 SD cut-off was chosen for consistency with analysis of T2w images. MVO was defined visually as a hypointense core within the infarcted zone on LGE images and planimeted manually. Volumes of infarct and MVO were calculated from planimeted areas across the whole LV stack by the modified Simpson's method. The presence and extent of myocardial haemorrhage was assessed by combined analysis of T2w and T2\* sequences [8]. On T2w images, areas with mean signal intensity more than 2 SD below the periphery of the area at risk (AAR) were considered to represent haemorrhage (Kidambi, Adam N Mather, et al., 2013). On the T2\* images, the presence of a dark core within the infarcted area by visual inspection of the images was used as confirmation of myocardial haemorrhage. Only when T2w and T2\* images showed concordant findings was an area considered to represent haemorrhage. Presence of both MVO and IMH were scored in a binominal mode.

For longitudinal functional assessment, the 4-chamber cine images were used (Figure 3.2). A region-of-interest (ROI) line was drawn across both the medial and lateral mitral annulus as a reference point in end-diastole (just after closure of mitral

valve). A second of ROI line was drawn across the same plane on an image taken just after closure of the aortic valve, assessed from the LV outflow tract cine. The longitudinal distance between the two lines parallel to the left ventricular walls was measured for both medial and lateral walls.

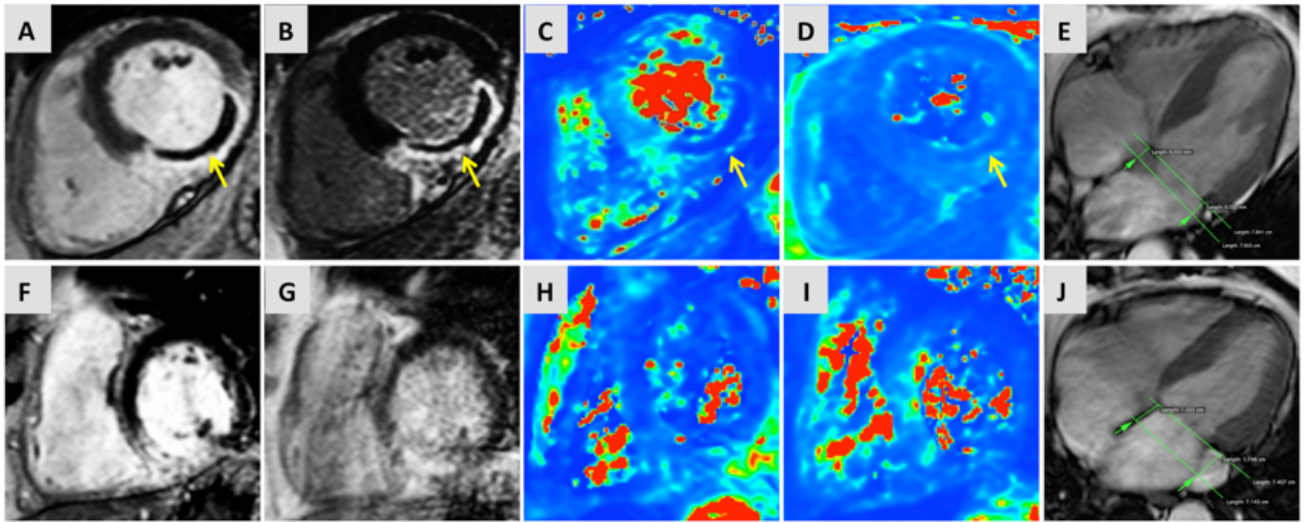


*Figure 3.2 Multi-parametric CMR examination of two cases of ST-elevation myocardial infarction.*

*Case 1 (top row): Case of inferior-lateral MI with presence of MVO on EGE (A) and LGE (B). IMH within MVO was confirmed on T2-weighted maps (C) and T2\*-maps (D). 4-chamber cine imaging (E) confirmed reduced averaged MAPSE (overlay of systolic and diastolic annular position shown in green). Case 2: Case of inferior MI without the presence of MVO (F, G) or IMH (H, I) and comparatively better longitudinal displacement than Case 1 (J).*

For MAPSE, three parameters were assessed – septal wall MAPSE; lateral wall MAPSE and averaged MAPSE (medial MAPSE + lateral MAPSE)/2). It takes approximately 1-2 minutes to measure MAPSE on 4-chamber cine.

Longitudinal functional assessment was carried out independently by two physicians experienced in both echocardiography and CMR imaging (PG, five-year experience; JRJF, four-year experience). For intra-observer variability assessment, one observer (PG) repeated the analysis after 90-days, blinded to the original results. Patients with sub-optimal 4-chamber cine images were excluded from analysis.

Follow-up scans were planned at 3 months following the indexed event. For analysis, patients were divided into 2 groups based on the presence of LV remodelling, defined by the following: a) an increase of LV end-diastolic volume > 20% at 3 months' follow-up scan or b) as increase of LV end-systolic volume > 20% at 3 months' follow-up scan.

### **3.3.3 Statistical analysis**

Multivariate linear regression was used for variables with statistical significance from univariate analysis ( $p < 0.1$ ). The accuracy of averaged-MAPSE in predicting presence of MVO and IMH was examined using receiver-operator characteristic (ROC) curve analyses, using Medcalc (v14.12.0). Intra-/inter-observer variability was tested using coefficient of variation (CoV).

## **3.4 Results**

54 patients met the inclusion criteria. In 5 patients the infarct size was too small for accurate analysis; in another 5 patients the 4-chamber cine was of insufficient quality for longitudinal functional analysis due to breathing artefact. Therefore 44 patients were included in the statistical analysis. Patient characteristics are shown in Table 3.1. Infarct characteristics on CMR are listed in Table 3.2. No gender-based differences in characteristics were present ( $p > 0.1$  for all).

<b>Patient characteristic</b>	
n	44
Age, years	58.3 ± 11.4
Male	37 (84%)
Body mass index, kg/m <sup>2</sup>	28.2 ± 3.5
Current smoker	24 (55%)
Hypertension	11 (25%)
Hypercholesterolemia	13 (30%)
Diabetes mellitus	6 (14%)
Pain to balloon time, min (median (IQR <sup>*</sup> ))	213 (268)
TIMI flow grade 0 or 1 pre-PCI	40 (91%)
TIMI flow grade 3 post PCI	42 (95%)
Peak troponin I, ng/L (median)	>50000
Peak CK <sup>†</sup> , iu/L (median (IQR))	615 (1510)
Infarct territory	
Anterior	20 (45%)
Inferior	18 (41%)
Lateral	6 (14%)

*Table 3.1 Study population characteristics. Data as mean ± SD or n (%) unless indicated. \* IQR interquartile range, † CK creatine kinase.*

### 3.4.1.1 Baseline Data

The mean ejection fraction of the study cohort was 48±10%, septal MAPSE was 9.6±2.9mm, lateral MAPSE 11±2.3mm and averaged MAPSE of 10.3±2.1mm (Table 3.2).

Twenty-six (59%) patients had MVO and 25 (57%) had IMH. No patient had IMH without MVO. Averaged MAPSE for patients with MVO was significantly lower than for patients without MVO (9.3±0.3mm versus 11.7±0.4mm; p<0.001). Similarly, in patients with IMH, MAPSE was significantly lower than in those without IMH (9.2±0.3mm versus 11.8±0.4mm; p<0.001) (Figure 3.3).

Characteristic	First Scan
Ejection fraction,%	48 ± 10
LV EDVi <sup>*</sup> , ml/m <sup>2</sup>	82 ± 16
LV ESVi <sup>†</sup> , ml/m <sup>2</sup>	42 ± 12
LV indexed mass, g/m <sup>2</sup>	65 ± 14
LGE infarct volume, ml	15 ± 12
LGE MVO volume, ml	3 ± 5
MAPSE (septal), mm	9.6 ± 2.9
MAPSE (lateral), mm	11 ± 2.3
MAPSE (averaged), mm	10.3 ± 2.1
MVO present	26 (59%)

*Table 3.2 Infarct characteristics at baseline.*

*Data as mean ± SD. LV measurements are indexed to body surface area, infarct volumes are unindexed. <sup>\*</sup>LV EDVi Left ventricular end diastolic volume (indexed), <sup>†</sup>LV ESVi Left ventricular end systolic volume (indexed).*

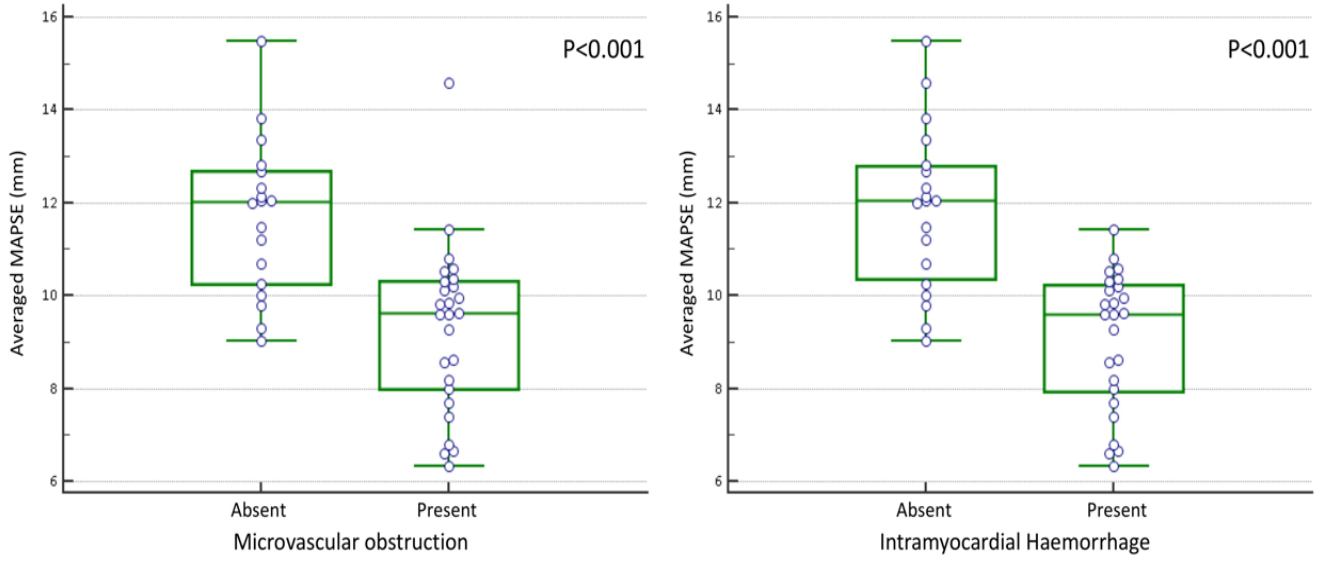


Figure 3.3 Box-plot of averaged MAPSE with or without the presence of (a) MVO or (b) IMH.

On linear regression analysis, using the variables in Table 3.3, the presence of IMH (beta= -0.65,  $p < 0.001$ ) and MVO (beta=-0.57,  $p < 0.001$ ) demonstrated the strongest association with averaged-MAPSE. The size of MVO correlated negatively with averaged MAPSE ( $r = -0.420$ ,  $p = 0.03$ ). Infarct location did not influence medial MAPSE ( $p = 0.316$ ), lateral MAPSE ( $p = 0.770$ ) or averaged MAPSE ( $p = 0.391$ ). The area under the curve (AUC) for determining the presence of MVO by averaged MAPSE was 0.84 (95% CI: 0.70 to 0.93;  $p < 0.001$ ) and for IMH was 0.88 (95% CI: 0.77 to 0.96;  $p < 0.001$ ) (Figure 3.4). The optimal cut-off value determined by the Youden index for averaged-MAPSE was 10.6mm for the detection of MVO (sensitivity 88.5% and specificity 72.2%) and IMH (sensitivity 92.0% and specificity 73.7%) (Ruopp et al., 2008).

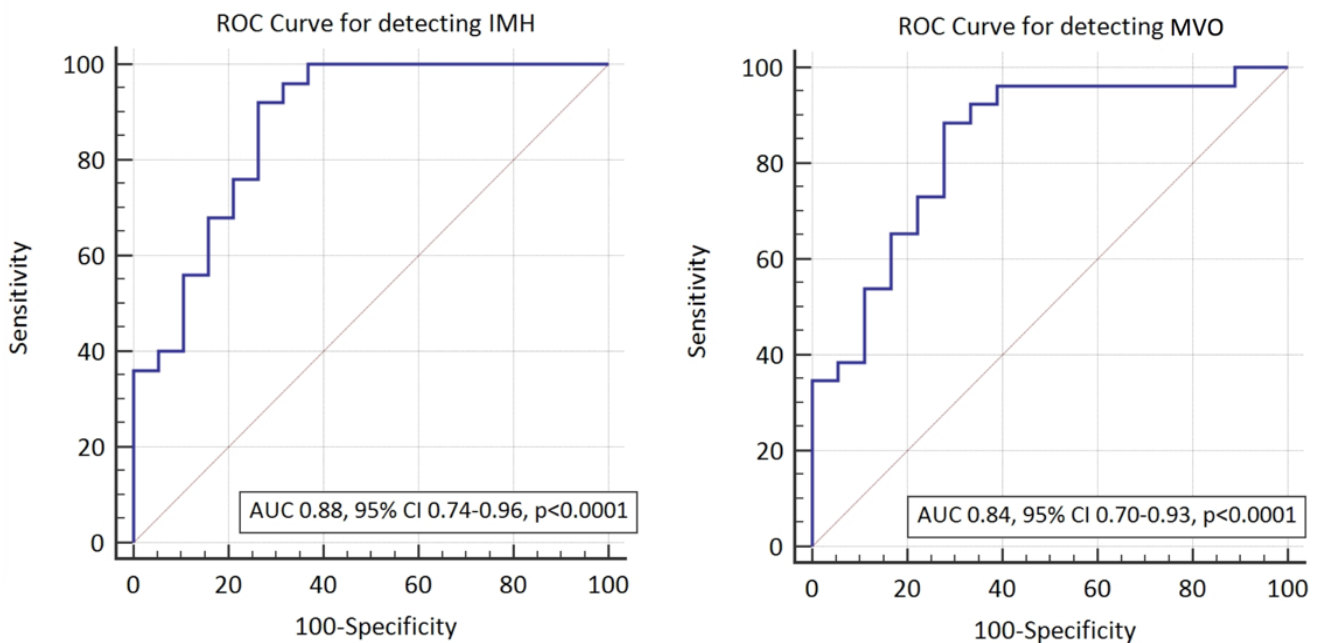


Figure 3.4 Receiver operator characteristics curve for the detection of (A) IMH, (B) MVO using averaged MAPSE.

		MAPSE (Septal) p-value		MAPSE (Lateral) p-value		MAPSE (Averaged) p-value (beta)	
		UV	MV	UV	MV	UV	MV
<b>Demographics</b>	Diabetes Mellitus	0.002	0.006	0.60		0.01	0.05
	Age	0.36		0.11		0.13	
	CK	0.26		0.72		0.33	
	Pain-Balloon Time	0.0	0.004	0.26		0.45	
	Sex	0.27		0.44		0.74	
	Smoking History	0.79		0.86		0.77	
	Hypertension	0.64		0.65		0.94	
	Hypercholesterolemia	0.81		0.69		0.95	
<b>Imaging biomarkers</b>	MVO	0.002	0.415	0.001	0.36	<0.01 (-0.57)	0.229
	IMH	<0.01	<0.01	<0.01	<0.01	<0.01 (-0.65)	<0.001
	Ejection Fraction	0.02	0.246	0.09	0.82	0.01	0.293
	SVi	0.06	0.187	0.27		0.06	0.207
	Infarct Volume	0.69		0.23		0.35	
	Infarct Mass	0.11		0.49		0.48	
	Anterior Infarct	0.33		0.91		0.54	
	LVEDVi	0.95		0.97		0.98	
Abbreviations: UN, univariate; MV, multivariate							

*Table 3.3 Univariate and multivariate analysis of longitudinal parameters of LV function to CMR derived clinical and prognostic markers*

### **3.4.1.2 Follow-up data**

Thirty-eight of 44 patients underwent day-90 CMR, while 6 patients refused follow-up scans. All 38 patients scans were of good quality and could be analysed. All patients had complete resolution of MVO and IMH on 90-day scans. Infarct volume reduced from  $14.1 \pm 11.8$ mls at baseline to  $8.2 \pm 6.7$ mls ( $p < 0.001$ ) at follow up. As compared to baseline, EF improved by  $21 \pm 22\%$  and averaged-MAPSE improved by  $28 \pm 22\%$  ( $p < 0.001$  for each). On linear regression analysis taking into account day-2 CMR parameters (LVEDV, LVESV, averaged-MAPSE, MVO, IMH), LVESV at day-2 showed the strongest correlation with day-90 EF ( $r = 0.717$ ,  $p < 0.001$ ).

Out of 38 patients with follow-up data, nine patients (24%) demonstrated adverse left ventricular remodelling. LV remodelling showed no significant association with day-2 averaged-MAPSE (AUC 0.62, 95% CI 0.44-0.77,  $p = 0.22$ ).

### **3.4.1.3 Observer variability**

On intra observer analysis, the means of septal MAPSE ( $8.52 \pm 2.2$ mm versus  $8.54 \pm 2.1$ mm;  $p = 0.87$ , CoV 4%), lateral MAPSE ( $9.97 \pm 2.2$ mm versus  $9.99 \pm 1.9$ mm;  $p = 0.92$ , CoV 5.9%) and septal MAPSE ( $9.24 \pm 1.8$ mm versus  $9.27 \pm 1.8$ mm;  $p = 0.88$ , CoV 4.1%) were similar.

On inter observer analysis, the means of septal MAPSE were ( $9.1 \pm 2.4$ mm versus  $9.3 \pm 2.2$ mm;  $p = 0.49$ , CoV of 8.3%), lateral MAPSE ( $11.1 \pm 2.4$ mm versus  $11.5 \pm 2$ mm;  $p = 0.37$ , CoV 8.4%) and averaged MAPSE ( $10.4 \pm 1.8$ mm versus  $10.1 \pm 1.8$ mm;  $p = 0.25$ , CoV 5.9%).

### ***3.5 Discussion***

This study demonstrates that longitudinal LV function measured by averaged MAPSE on CMR is strongly associated with the presence of MVO and IMH. Moreover, the size of MVO adversely affects averaged MAPSE.

MAPSE is a well-established and endorsed parameter of global LV longitudinal function in echocardiography. A lower absolute value of MAPSE in post AMI is a poor prognostic marker (Hu et al., 2013). Previous studies using speckle tracking echocardiography in AMI patients have shown that MVO determined on CMR adversely affects global longitudinal strain (GLS) on echocardiography (Bergerot et al., 2014; Bière et al., 2014). However, with current technology, there remains marked variability in GLS depending on the measurement algorithms on the vendor's software and also on the sample volume definition. Therefore, no specific vendor independent normal ranges are provided in current American and European guidelines (Thomas and Badano, 2013). MAPSE, on the contrary, is a vendor independent parameter of global longitudinal function, which can also be measured from standard cine CMR images [18,33]. Limited data are available in the literature on the association of MAPSE assessed by CMR to microvascular obstruction and none for IMH. This study demonstrated that reduced averaged-MAPSE is associated the presence of MVO/IMH.

Myocardial deformation, including global longitudinal function (GLS), can also be studied on CMR using strain measurements derived from tissue tagging or feature tracking (FT). Tagging derived strain requires longer scanning time and both methods need dedicated post-processing software to analyse the data. In a post AMI study comparing tagging to FT-derived strain, FT-derived strain was quicker to analyse, tracked myocardium better, had better inter-observer variability and stronger correlations with infarct and oedema (Khan et al., 2015). Furthermore, similar to echocardiography, there remains significant inter-vendor and inter-software variability in FT-derived strain (Almutairi et al., 2015). Hence, MAPSE remains the quickest, vendor-software independent and reproducible method to assess global longitudinal function from routinely acquired cine images.

Our data confirm previous observations of a weak association of LV remodelling with LV global longitudinal function (Bochenek et al., 2011; Buss et al., 2015), due to the fact that longitudinal function of the left ventricle is driven mainly by the endocardial fibres (Figure 3.1). Also, longitudinal fibres contribute only 19% to the total stroke volume of the left ventricle versus circumferential fibres which contribute 43% (Maciver, 2012). Hence, even though MAPSE may be more adversely affected in patients with MVO or IMH, MAPSE does not necessarily result in LV remodelling. LV remodelling is directly proportional to the infarct transmural extent and hence more related to strain parameters, which involve more mid, and epicardial fibres, for example, circumferential strain.

### **3.5.1 Clinical Implications**

Our findings have potential clinical implications and suggest that MAPSE can be performed easily on standard cine CMR images, without the need for additional MR tissue characterisation techniques (T2W and T2\*) and analysis methods. As shown, MAPSE can potentially predict the presence of MVO/IMH early after primary PCI for STEMI. MVO and IMH are independent histo-pathological and cardiac imaging markers of adverse prognosis and their early detection from routinely acquired CMR images by MAPSE may help tailor appropriate pharmacological interventions. Patients with previous history of allergy to gadolinium-based contrast or patients with end-stage renal failure may also benefit from this technique to predict the likelihood of presence of MVO or IMH. MAPSE can also be evaluated by bedside M-Mode echocardiography in post infarct patients and it could potentially act as a gatekeeper for further assessment by CMR.

### **3.5.2 Study limitations**

The study sample size is relatively small and the results are therefore mainly hypothesis generating. In this study, we also excluded patients who were unstable post PPCI (higher Killip class, not able to lie flat because of shortness of breath and use of invasive monitoring). These patients are more likely to represent a higher risk group with more adverse prognosis. In our study population, the majority of patients with MVO had IMH and only one patient with MVO had no IMH. Hence, it was not

possible to investigate whether there remains an incremental value of using averaged-MAPSE for the detection of IMH. Additionally, the absolute measure of MAPSE does not take the total length of the LV into account, which is potentially a better measure of LV longitudinal function as it measures absolute change in longitudinal parameters. In some diseases, like apical pericardial effusion, the apex may be mobile and this may influence the longitudinal function independently.

### ***3.6 Conclusions***

Averaged-MAPSE, evaluated using cine CMR is strongly associated with the presence of MVO and IMH when compared to advanced MR relaxometry techniques (T2w and T2\*), in patients with recent reperfused AMI. Global left ventricular longitudinal function, assessed by averaged MAPSE, is feasible and shows high reproducibility. In this study, the size of MVO adversely affected averaged MAPSE. However, averaged MAPSE did not show any significant correlation with left ventricular remodelling.

## **4 Study 2- The Role of Left Ventricular Deformation in the Assessment of Microvascular Obstruction and Intramyocardial Haemorrhage**

### **4.1 Abstract**

#### **4.1.1 Introduction**

In the setting of STEMI, it remains unclear which strain parameter most strongly correlates with MVO or IMH. Therefore, the objective of this study was to investigate the association of MVO, IMH and convalescent left ventricular (LV) remodelling with strain parameters measured with cardiovascular magnetic resonance (CMR).

#### **4.1.2 Methods**

43 patients with reperfused STEMI underwent CMR within 3-days and at 3-months following reperfused STEMI. 10 age and gender matched healthy controls were recruited and received baseline CMR only. Cine, T2-weighted, T2\*-imaging and late gadolinium enhancement (LGE) imaging were performed. Infarct size, MVO and IMH were quantified. Peak global longitudinal strain (GLS), global radial strain (GRS), global circumferential strain (GCS) and their strain rates were derived by feature tracking analysis of LV short-axis, 4-chamber and 2-chamber cines.

#### **4.1.3 Results**

All 43 patients and 10 controls completed the baseline scan and 34 patients completed 3-month scans. In multivariate regression, GLS demonstrated the strongest association with MVO or IMH (beta=0.53, P<0.001). The optimal cut-off value for GLS was -13.7% for the detection of MVO or IMH (sensitivity 76% and specificity 77.8%). At follow up, 17% (n=6) patients had adverse LV remodeling (defined as an absolute increase of LV end-diastolic/end-systolic volumes >20%). Baseline GLS also demonstrated the strongest diagnostic performance in predicting adverse LV remodelling (AUC=0.79; 95% CI 0.60 – 0.98; p=0.03).

#### **4.1.4 Conclusion**

Post-reperfused STEMI, baseline GLS was most closely associated with the presence of MVO or IMH. Baseline GLS was more strongly associated with adverse LV remodelling than other CMR parameters.

## **4.2 Introduction**

Microvascular obstruction (MVO) and intra-myocardial haemorrhage (IMH) as detected by cardiovascular magnetic resonance (CMR) are established independent adverse prognostic markers following reperfused ST-elevation myocardial infarction (STEMI). The presence of MVO has been associated with 'no re-flow' on coronary angiography after revascularisation (Jaffe et al., 2008). IMH is invariably associated with MVO and is caused by endothelial dysfunction following prolonged ischaemia/reperfusion injury with disruption of inter-endothelial junctions and extravasation of erythrocytes (Betgem et al., 2015).

Myocardial systolic function after STEMI is conventionally assessed by calculating left ventricular ejection fraction (EF) from left ventricular volumes (Burns et al., 2002; Gibbons et al., 2004; Møller et al., 2006). However, global EF is load-dependent and neglects regional function (Vartdal et al., 2007). Myocardial deformation may be a more accurate parameter of LV function, but its assessment is more challenging, due in part to the complex spatial orientation and distribution of muscle fibres in the longitudinal and circumferential direction (Greenbaum et al., 1981). Emerging technologies have made it possible to study myocardial deformation by CMR using myocardial tagging and feature tracking (FT) derived strain (Hor et al., 2011; Ibrahim, 2011). Strain (S) and strain rate (SR) are already established as more accurate measures of both regional and the global left ventricular function when compared to ejection fraction and allow quantitative assessment of myocardial deformation (Shah and Solomon, 2012). From strain analysis, several parameters can be derived and it is currently not known which of these, if any, are associated with the presence of MVO, IMH and adverse LV remodelling.

This study aimed to investigate the association of FT derived peak global longitudinal strain (GLS), peak global circumferential strain (GCS), peak global radial strain (GRS), peak global longitudinal strain rate (GLSR), peak global circumferential strain rate (GCSR) and peak global radial strain rate (GRSR) with the presence of MVO, IMH and adverse LV remodelling in acute reperfused STEMI.

### **4.3 Study specific methods**

#### **4.3.1 Cardiac catheterization**

Coronary angiography and revascularisation were performed in a standard fashion as per current best practice guidelines (Windecker et al., 2014). TIMI flow grades were assessed visually as described previously after coronary angioplasty.

#### **4.3.2 CMR examination**

T2 weighted (T2w) and T2\* imaging were performed using the '3-of-5' approach by acquiring the central 3 slices (base, mid and apical) of 5 parallel short-axis slices (Messroghli et al., 2005).

#### **4.3.3 CMR interpretation**

Cine, T2w, T2\* and LGE images were evaluated offline. Infarct location was determined by LGE imaging, according to standard guidelines (Cerqueira et al., 2002). The presence and size of infarction and MVO were measured from LGE images. Infarcted myocardium was defined as an area of LGE  $\geq 2$  standard deviations (SD) above remote myocardium, and infarct volume estimation included any hypointense core. We used the 2SD method as there are prognostic data for the 2SD infarct size estimation in similar populations (Kwon et al., 2014), and for consistency with analysis of T2w images. MVO was defined visually as the hypointense core within the infarcted zone and planimeted manually. Volumes of infarct and MVO were calculated from planimeted areas through the whole short-axis LV LGE stack by the modified Simpson's method. The presence and extent of intra-myocardial haemorrhage was assessed by combined analysis of T2w and T2\* sequences [8]. On T2w images, areas with mean signal intensity less than 2 SD below the periphery of the area at risk (AAR) were considered to be haemorrhage (Kidambi, Adam N Mather, et al., 2013). On the T2\* images, the presence of a dark core within the infarcted area by visual inspection of the images was used as confirmation of myocardial haemorrhage. Concordant results between T2w and T2\* were needed to confirm haemorrhage. If there was inconsistency between them, agreement between two

experts informed the results. Presence/absence of both MVO and IMH were scored in a binary manner.

#### **4.3.3.1 Strain Analysis**

Strain analysis was performed in a semi-automated manner using cvi42 v5.1 (Figure 4.1). The observer (PG) performing the strain analysis was blinded to the baseline CMR parameters and advanced tissue characterization. Left ventricular endocardial and epicardial borders were manually contoured in end-diastole from both long-axis cines (4-chamber and 2 chamber). Endocardial borders, epicardial borders and reference points at both RV insertion points (anterior/inferior) were contoured manually for each slice at end-diastole from the short axis LV cine stack. GLS and GLSR were derived from the long-axis images and GRS, GRSR, GCS and GCSR were derived from the short-axis LV cine stack using published methods (Swoboda, McDiarmid, et al., 2016; Swoboda, Erhayiem, et al., 2016). Peak GLS, peak GLSR, GRS, peak GRSR, peak GCS and peak GCSR were quantified.

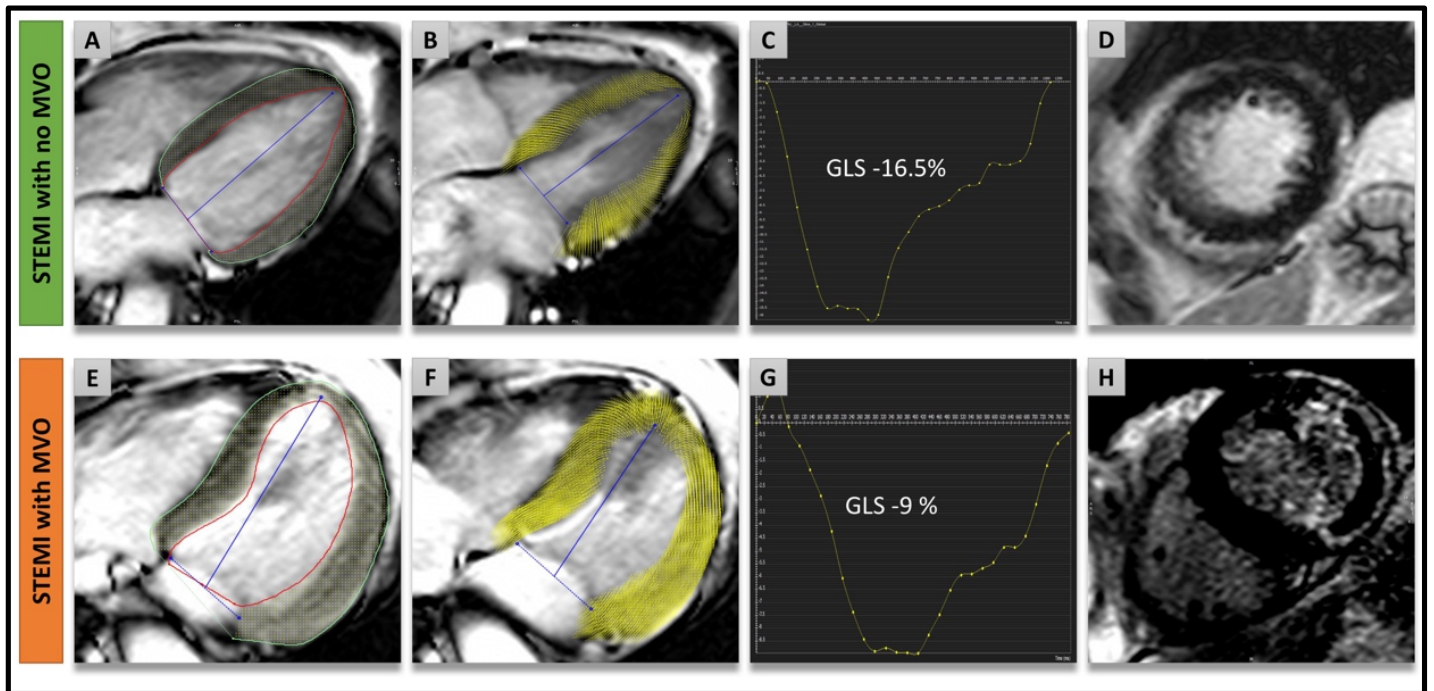


Figure 4.1 Multi-parametric CMR examination.

Two case studies with STEMI: Case 1 (A to D): Anterior MI without MVO. (A) Epicardial (green) and endocardial (red) contours on a 4-chamber cine. (B) Voxel derived feature tracking (FT) of the myocardium at end-systole. (C) Global longitudinal strain (GLS) curve demonstrating a GLS of -16.5% (D) LGE short-axis demonstrating infarct in anterior wall. Case 2 (E to H): (E) demonstrates the contours and (F) shows the end-systolic FT-derived strain myocardial points in a case of lateral infarction with MVO. (G) demonstrates a significantly lower GLS, -9%. (H) demonstrates infarct and presence of MVO on LGE-images.

#### **4.3.4 Follow-up scans**

Follow-up scans were planned at 3 months following the index event. Patients were divided into 2 groups based on the presence of LV remodelling. Adverse LV remodelling was defined as an absolute increase of LV end-diastolic or end-systolic volumes >20% at 3 months follow-up (Korosoglou et al., 2008; Warren et al., 1988; Pfeffer and Braunwald, 1990). Analysis of all follow-up data was performed blinded to acute scans.

#### **4.3.5 Statistical analysis**

Step-wise multivariate linear regression was used for parameters with statistical significance from one-way analysis ( $p < 0.1$ ). The accuracy of myocardial deformation parameters in predicting presence of MVO or IMH was examined using receiver-operator characteristic (ROC) curve analyses, using Medcalc (v15.8). To reduce transfer bias, baseline demographics and CMR parameters of the followed-up patients were compared to patients who did not receive follow-up CMR by ANOVA.

### **4.4 Results**

43 acute STEMI patients met the inclusion criteria (Figure 4.2). Demographics of patients and 10 healthy volunteers are shown in Table 4.1. Infarct characteristics on CMR are listed in Table 4.2. No gender and age based differences in characteristics were present between patient groups ( $p > 0.1$ ).

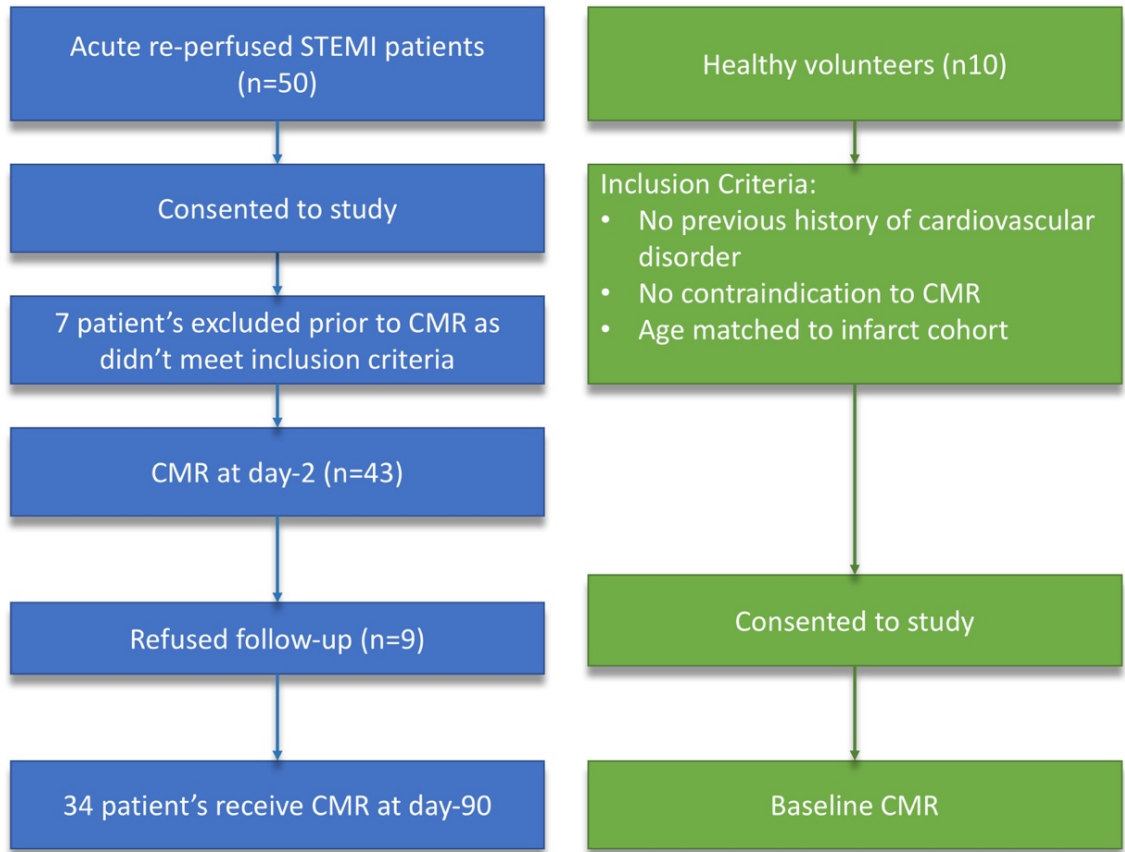


Figure 4.2 Study design

	STEMI WITH MVO or IMH	STEMI WITHOUT MVO or IMH	HV	P-VALUE
N	25	18	10	-
AGE, YEARS	59±12	57±10	62±9	0.86* / 0.30 †
MALE	22	14	3	0.69* / 0.35 †
BODY MASS INDEX, KG/M <sup>2</sup>	29±3	27±3	27±5	0.03* / 0.28 †
CURRENT SMOKER	14	9	0	0.90*
HYPERTENSION	7	4	0	0.88*
HYPERCHOLESTEROLEMIA	8	5	0	0.94*
DIABETES MELLITUS	5	1	0	0.30*
PAIN TO BALLOON TIME, MIN	286±211	376±386	NA	0.33*
TIMI FLOW GRADE 0/1 PRE-PCI	22	17	NA	0.78*
TIMI FLOW GRADE 3 POST PCI	23	18	NA	0.28*
PEAK TROPONIN I NG/L	45699±10455	26895±19586	NA	<0.01*
ANTERIOR INFARCT	12	8	NA	0.82*
INFERIOR INFARCT	10	7	NA	0.94*
LATERAL INFARCT	3	3	NA	0.67*

Table 4.1 Study demographics (\*P-value between STEMI with MVO and without; † P-value between STEMI without MVO and HV)

Characteristic	MI (n=43)	Healthy Volunteers (n=10)	P value
Ejection fraction,%	48 ± 10	63 ± 4	<0.001
LV EDVi <sup>*</sup> , ml/m <sup>2</sup>	82 ± 16	78 ± 20	0.47
LV ESVi <sup>†</sup> , ml/m <sup>2</sup>	42 ± 12	28 ± 8	<0.001
LV stroke volume indexed, ml	40 ± 11	49 ± 12	0.023
LGE infarct volume, ml	15 ± 12	NA	NA
LGE MVO volume, ml	3 ± 5	NA	NA
GRS, %	25 ± 8	38 ± 7	<0.001
GRSR, %/sec	164 ± 50	268 ± 125	<0.001
GCS, %	-13 ± 4	-20 ± 2	<0.001
GCSR, %/sec	-106 ± 132	-107 ± 12	0.99
GLS, %	-13 ± 4	-20 ± 2	<0.001
GLSR %/sec	-128 ± 314	-88 ± 13	0.68

*Table 4.2 Imaging parameters at baseline CMR study. Data as mean ± SD. LV measurements are indexed to body surface area; infarct volumes are unindexed. <sup>\*</sup> LV EDVi; Left ventricular end diastolic volume (indexed), <sup>†</sup> LV ESVi; Left ventricular end systolic volume (indexed), GCS; peak global circumferential strain, GCSR; peak global circumferential strain rate, GLS; peak global longitudinal strain, GLSR; peak global longitudinal strain rate, GRS; peak global radial strain, GRSR; peak global radial strain rate.*

#### **4.4.1 Baseline data**

Left ventricular EF, left ventricular end-systolic volume (LVESV), GLS, GCS, GRS and GRSR were significantly altered in infarct patients versus healthy volunteers (p<0.001 for all parameters individually) (Table 4.2).

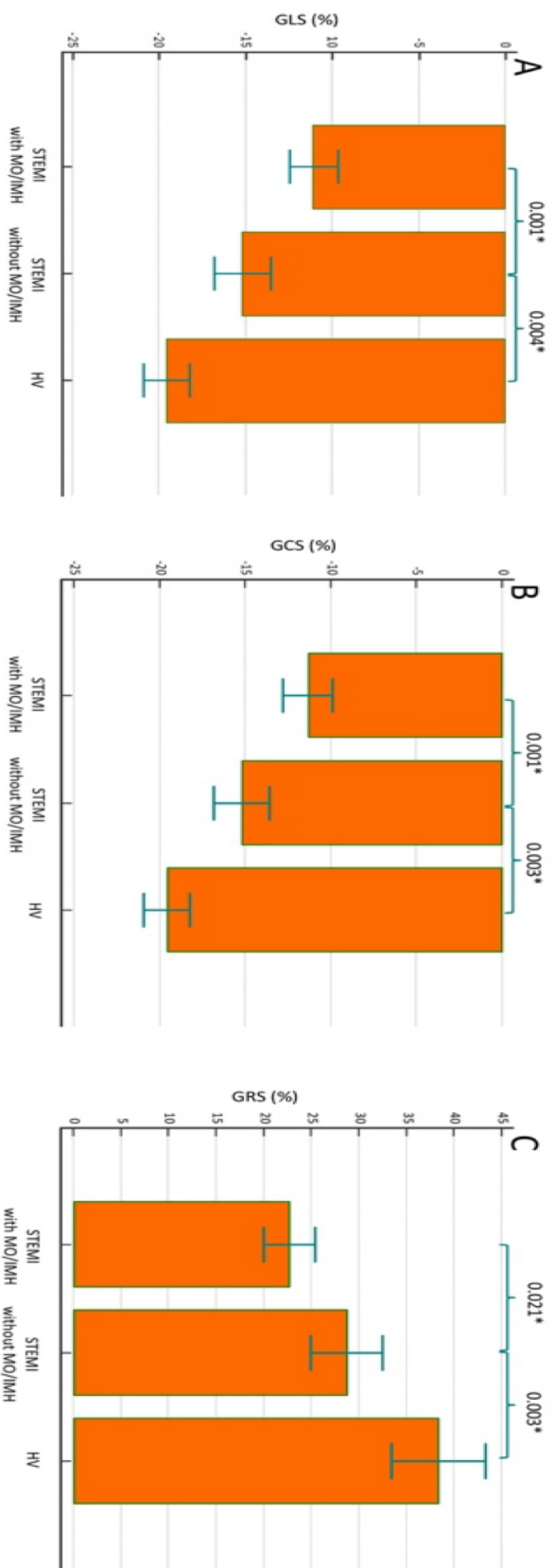
Stroke volume was also reduced in the infarct subjects (p=0.023 versus controls). Among the 43 infarct patients, 25 patients (58%) had MVO and 24 patients (56%) had confirmed IMH. GRS was significantly lower in patients with MVO or IMH than those without (22.7±7% versus 29±7%; p=0.02). Additionally, both GCS and GLS were

significantly lower in patients with compared with those without MVO or IMH (GCS:  $-11.6\pm 3\%$  versus  $-15.6\pm 3\%$ ,  $p<0.001$ ; GLS:  $-11\pm 3\%$  versus  $-15.2\pm 3.3\%$ ,  $p<0.001$ ) (Figure 4.3).

On linear regression analysis, using all the demographics and imaging variables including infarct size, GLS demonstrated the strongest association with presence of MVO or IMH (beta =0.53,  $p<0.001$ ) (Table 4.3).

Additionally, GCS demonstrated stronger correlation to the volume of MVO than GLS ( $r= 0.57$ ,  $P<0.001$  versus  $r= 0.46$ ,  $P=0.002$ ) (Table 4.4). The area under the curve (AUC) for the diagnostic performance of determining the presence of MVO or IMH by GLS was 0.82 (95% CI: 0.69 to 0.94;  $p<0.001$ ). The optimal cut-off value determined by Youden index for GLS was -13.7% for the presence of MVO or IMH (sensitivity 76% and specificity 78%) (Ruopp et al., 2008).

Figure 4.3 Multiple comparison bars of myocardial strain in the study population  
(whiskers: standard deviations; SD)



Microvascular Obstruction and Intra-myocardial haemorrhage

		Univariate		Multi-variate (Stepwise)	
		beta	p-value	beta	p-value
Demographics	Age	0.07	0.62		
	Sex	0.13	0.38		
	Smoking	0.06	0.70		
	Hypertension	0.07	0.67		
	Hypercholesterolemia	0.05	0.77		
	Diabetes Mellitus	0.21	0.19		
	Pain-Balloon Time	-0.15	0.33		
CMR parameters					
	LVEDVi	0.09	0.57		
	LVESVi	0.38	0.01*	0.17	0.26
	EF	-0.50	0.001*	-0.27	0.13
	GRS	-0.39	0.01*	-0.07	0.67
	Infarct size	0.50	0.001*	0.36	0.01*
	GCS	0.52	<0.001*	0.29	0.16
	GLS	0.53	<0.001*	0.53	<0.001**
	GRSR	-0.24	0.122		
	GCSR	-0.12	0.44		
	GLSR	0.18	0.26		

Abbreviations: EF; ejection fraction, LVEDVi; left ventricular end-diastolic volume indexed, LVESVi; left ventricular end-systolic volume indexed, GCS; peak global circumferential strain, GCSR; peak global circumferential strain rate, GLS; peak global longitudinal strain, GLSR; peak global longitudinal strain rate, GRS; peak global radial strain, GRSR; peak global radial strain rate.

*Table 4.3 Uni-/multi-variate analysis of strain parameters to CMR derived clinical and prognostic markers*

	LOCATION OF INFARCT		INFARCT VOLUME (%)		MICROVASCULAR OBSTRUCTION VOLUME (%)	
	r	P-value	r	P-value	r	P-value
<b>EF</b>	0.29	0.06	-0.37	0.01	-0.37	0.02
<b>LVEDVI</b>	-0.18	0.24	0.20	0.20	0.08	0.60
<b>LVESVI</b>	-0.24	0.12	0.41	0.01	0.30	0.05
<b>SVI</b>	0.03	0.87	-0.19	0.23	-0.24	0.13
<b>GRS</b>	0.19	0.21	-0.32	0.03	-0.39	0.01
<b>GRSR</b>	0.04	0.79	-0.24	0.13	-0.13	0.41
<b>GCS</b>	-0.18	0.25	0.54	<0.001	0.57	<0.001
<b>GCSR</b>	0.21	0.18	-0.01	0.94	-0.30	0.06
<b>GLS</b>	-0.33	0.03	0.34	0.02	0.46	0.002
<b>GLSR</b>	0.12	0.44	0.20	0.20	0.10	0.52

Abbreviations: EF; ejection fraction, GCS; peak global circumferential strain, GCSR; peak global circumferential strain rate, GLS; peak global longitudinal strain, GLSR; peak global longitudinal strain rate, GRS; peak global radial strain, GRSR; peak global radial strain rate, LVEDVi; left ventricular end-diastolic volume indexed, LVESVi; left ventricular end-systolic volume indexed; r, Pearson correlation coefficient.

*Table 4.4 Association of baseline CMR volumetric and strain parameters to size of microvascular obstruction*

#### **4.4.2 Follow-up data**

Thirty-four of the 43 patients underwent 3 month follow up CMR; 6 patients declined further follow-up and in 3 patients the scan quality of cines on follow up was not suitable for FT analysis. Demographics parameters (age, gender, hypertension, hypercholesterolaemia, smoking history, diabetes mellitus) and baseline CMR parameters (presence of MVO or IMH, LVEDVi, LVESVi and all strain parameters) were not significantly different in the 9 patients who did not attend for follow-up scans compared with the overall study population ( $p>0.1$ ). All 34 follow up scans showed complete resolution of MVO and IMH. As compared to baseline, relative improvement in EF was  $19\pm 24.5\%$ . Of all the baseline CMR parameters (LVEDVi, LVESVi, GLS, GCS, GRS, MVO, IMH), LVESVi ( $r=0.99$ ,  $p<0.002$ ) and GLS ( $r=0.97$ ,  $p<0.006$ ) demonstrated the strongest correlation with improvement in EF at follow-up scan. GCS ( $r=0.95$ ,  $p=0.01$ ) and GRS ( $r=0.91$ ,  $p=0.02$ ) also demonstrated good correlations with improvement in EF at follow-up.

#### **4.4.3 Adverse LV Remodelling**

Out of 34 patients with follow-up data, 6(17%) patients demonstrated adverse left ventricular remodelling. From all CMR baseline parameters, GLS demonstrated the strongest diagnostic performance in predicting adverse LV remodelling (AUC=0.79; 95% CI 0.60 – 0.98;  $p=0.03$ ) (Table 4.5).

**ADVERSE LV REMODELLING**

<b>LVEDVI</b>	AUC=0.60; 95% CI 0.34 – 0.86; p=0.44
<b>LVESVI</b>	AUC=0.60; 95% CI 0.32 – 0.87; p=0.47
<b>LV EF</b>	AUC=0.26; 95% CI 0.00 – 0.52; p=0.07
<b>GLS</b>	AUC=0.79; 95% CI 0.60 – 0.98; p=0.03*
<b>GLSR</b>	AUC=0.68; 95% CI 0.42 – 0.95; p=0.16
<b>GRS</b>	AUC=0.32; 95% CI 0.11 – 0.54; p=0.18
<b>GRSR</b>	AUC=0.34; 95% CI 0.16 – 0.52; p=0.22
<b>GCS</b>	AUC=0.71; 95% CI 0.48 – 0.87; p=0.11
<b>GCSR</b>	AUC=0.57; 95% CI 0.35 – 0.78; p=0.62

Abbreviations: AUC; area under the curve, CI; confidence interval, EF; ejection fraction, GCS; peak global circumferential strain, GCSR; peak global circumferential strain rate, GLS; peak global longitudinal strain, GLSR; peak global longitudinal strain rate, GRS; peak global radial strain, GRSR; peak global radial strain rate, LV; left ventricle, LVEDVI; left ventricular end-diastolic volume indexed, LVESVI; left ventricular end-systolic volume indexed; r, Pearson correlation coefficient.

*Table 4.5 Association of baseline CMR parameters to adverse LV remodelling at follow-up visit.*

## **4.5 Discussion**

The main findings of this study are as follows: first, myocardial deformation imaging by CMR reliably detects changes in acute infarct patients versus healthy controls. Second, the presence of MVO or IMH in acute reperfused STEMI is most strongly associated with GLS. Third, GLS showed modest association with adverse LV remodelling.

Our data complement the results of several previous investigations of the role of CMR-derived strain imaging in reperfused STEMI patients (Kidambi, Adam N Mather, et al., 2013; Kidambi, Adam N. Mather, et al., 2013; Khan et al., 2015; Buss et al., 2015). Kidambi et al studied the role of myocardial deformation using tissue tagging derived strain in an acute reperfused infarct population (Kidambi, Adam N Mather, et al., 2013). They demonstrated that regional functional recovery is poor in myocardial segments with MVO and IMH. Wong et al demonstrated that circumferential strain (CS) using tissue tagging correlates better than circumferential strain rate with regional functional recovery (D.T.L. Wong et al., 2014). Both of these studies used tissue tagging, which has a relatively low temporal resolution (<30 frames/s), potentially limiting its accuracy, especially in patients with higher heart rates. Moreover, acquisition of tissue tagged images often requires long series of breath holds, and tag fading during diastole limits the assessment of myocardial relaxation. FT analysis of cine loops may overcome these limitations. A study by Khan et al compared tissue tagging to FT-derived strain in 24 acute reperfused STEMI patients. FT-derived strain was quicker to analyse, tracked the myocardium better, had better inter-observer variability and stronger correlations with infarct and oedema (Khan et al., 2015).

In a study of 74 patients, Buss et al demonstrated that FT-derived GCS is strongly associated with infarct size and trans-murality of scar on LGE imaging (Buss et al., 2015). This study also demonstrated that FT-derived GCS was more accurate than GLS for predicting preserved LV function at follow-up. Notably, this study did not evaluate LV remodelling, presence of MVO, presence of IMH or functional recovery of LV defined by improvement in EF. Additionally, in this study, the FT-derived strain analysis algorithm tracked only the endo-/epi-myocardium to compute strain, and

did not track pixels within the myocardium (Garg, Kidambi and Plein, 2015). Tracking pixels within the myocardium is important, especially in the setting of acute reperfused infarct where each layer of myocardium (endo-, mid- and epi-) is going through different pathophysiological processes.

Our study adds to the growing body of literature on the ability of CMR to quantify left ventricular deformation with FT. We have shown that FT-derived myocardial deformation parameters (GCS, GRS and GLS) are altered significantly in patients with MVO or IMH ( $p < 0.05$ ). MVO and IMH affect predominantly the sub-endocardium, where most of the longitudinal myocardial fibres are located. It is thus plausible that GLS is the strongest predictor of MVO and IMH as shown in our study. GLS also demonstrated modest diagnostic performance to predict adverse LV remodelling at follow-up more than any other deformation parameter. In this study, the volume of MVO and infarct size were more strongly associated with GCS than GLS (Table 4.4). These results are not unexpected as larger infarcts with MVO will involve more myocardium transmurally.

#### **4.5.1 Role of Echocardiography**

It is acknowledged that strain examination is more readily available by echocardiography than CMR. All modern echocardiographic systems come with strain packages (Sutherland et al., n.d.; Heimdal et al., 1998). Early changes of microvascular obstruction (MVO) after AMI have been demonstrated by contrast echocardiography (Rinkevich et al., 2005; Senior et al., 2013; Gibson et al., 2014). In patients with AMI, echocardiographic studies can be performed at the bedside and GLS assessment may be used as a 'gatekeeper' for further advanced imaging, for example, multi-parametric tissue characterization on CMR. Further studies are needed to explore how echocardiography derived strain parameters compare to CMR-FT derived strain.

#### **4.5.2 MAPSE or FT – which one to use?**

In this thesis, we demonstrate that longitudinal function of LV is associated with MVO or IMH. This has been demonstrated by two different methods: MAPSE and FT derived GLS. Both methods of assessment of LV longitudinal function have pros and

cons. For example, MAPSE is a manual method and hence prone to intra/inter-observer variations. On the other hand, different vendors use different algorithms to derive GLS, making it less translational. MAPSE remains a quick method which can be done on any imaging modality.

### **4.5.3 Clinical Implications**

Our findings have possible clinical implications as FT-strain analysis can be performed rapidly from standard cine CMR images and allows the detection of the functional effects of MVO and IMH without the need for additional CMR tissue characterisation techniques (T2W and T2\*) and analysis methods. From our single-center experience, the time for total left ventricular strain analysis by CMR FT is approximately 7 minutes. As demonstrated, a cut off value of -13.7% for GLS detects MVO or IMH with a sensitivity of 76% and specificity of 77.8%. GLS can potentially predict the presence of MVO or IMH early after PPCI for STEMI. MVO and IMH are independent histopathological and cardiac imaging markers of adverse prognosis and we speculate that their early detection from routinely acquired CMR cines may help tailor appropriate pharmacological interventions or guide stem cell therapy. Patients with known allergy to gadolinium-based contrast agents or patients with end-stage renal failure may also benefit from this technique.

### **4.5.4 Study limitations**

In this study, we excluded patients who were unstable post-PPCI (higher Killip class, not able to lie flat because of shortness of breath and use of invasive monitoring). These patients are more likely to represent a higher risk group with an adverse prognosis. In our study population, the majority of patients with MVO had IMH and only one patient with MVO had no IMH. Hence, the data on GCS for IMH detection should be interpreted with caution.

Another important limitation of our study was that 9 of 43 patients did not have follow-up CMR scans. This may have introduced transfer bias although the two groups were not different for demographic and standard CMR parameters.

In our study, at follow-up, only 6 (17%) patients had adverse LV remodelling and hence the demonstrated diagnostic performance of GLS to predict remodelling should be interpreted with caution. Females were more represented in the HVs.

In the present study, only global parameters of strain were investigated. Assessment of regional left ventricular strain parameters by CMR FT demonstrates regional variations and their clinical role remains very speculative (Pedrizzetti et al., 2016).

#### ***4.6 Conclusions***

Myocardial deformation changes adversely in patients with acute STEMI. Baseline GLS by FT-analysis of cine CMR is strongly associated with the presence of MVO or IMH and could be used as surrogate functional imaging marker of these acute myocardial pathological changes in patients with acute STEMI. Baseline GLS demonstrated stronger association with adverse LV remodelling than other CMR parameters.

## **5 Study 3- Effects of hyperaemia on left ventricular longitudinal strain: A first-pass stress perfusion cardiovascular magnetic resonance imaging study.**

### **5.1 Abstract**

#### **5.1.1 Background**

Myocardial perfusion imaging during hyperaemic stress is commonly used to detect coronary artery disease. Although hyperaemic stress is not thought to induce myocardial ischaemia per se, it has differential effects on the myocardial layers that may lead to local changes in contractility. The aim of this study was to investigate the relationship between left ventricular global longitudinal strain (GLS), strain rate (GLSR), myocardial early (E') and late diastolic velocities (A') with adenosine stress first-pass perfusion cardiovascular magnetic resonance imaging (CMR).

#### **5.1.2 Methods**

50 patients with stable chest pain were recruited out of which 44 patients met the inclusion criteria and underwent CMR imaging. The CMR protocol included: rest/stress 4-chamber cine, rest/stress first pass adenosine perfusion imaging and late gadolinium enhancement imaging. Rest and stress 4-chamber cine CMR images were analysed using feature-tracking software for the assessment of myocardial deformation. The presence of perfusion defects was scored on a binomial scale.

#### **5.1.3 Results**

In patients with hyperaemia induced perfusion defects, rest GLS (P-value=0.02), E' (P-value=0.02), GLSR (P-value=0.01) and stress GLS (P<0.001) were significantly reduced when compared to patients with no perfusion defects. The absolute change in rest versus stress GLS increased in patients without perfusion defect versus a drop in patients with perfusion defects (-1.6±3.1 versus 0.5±3.8, P-value=0.05). Stress GLS was the strongest independent predictor of perfusion defects (OR 1.43 95% CI 1.14-

1.78, P-value<0.001). A threshold of -19.8% for stress GLS demonstrated 78% sensitivity and 73% specificity for the presence of hyperaemia-induced perfusion defects.

#### **5.1.4 Conclusions**

At peak hyperemic stress, GLS is reduced in the presence of a perfusion defect. This reduction is most likely caused by reduced endocardial blood flow at maximal hyperaemia as a result of transmural redistribution of blood flow in the presence of significant coronary stenosis.

## ***5.2 Introduction***

Cardiovascular magnetic resonance (CMR) imaging can detect obstructive coronary artery disease (CAD) by imaging the left ventricular (LV) passage of a contrast bolus during pharmacologically induced myocardial hyperaemia (Wolff et al., 2004). Although hyperaemic stress does not usually induce myocardial ischaemia, myocardium supplied by a significantly stenosed coronary artery shows reduced contrast uptake compared to normal myocardium. Hyperaemia also leads to a redistribution of myocardial blood flow (MBF) between the endocardial and epicardial layers (Pan et al., 2015), contributing to the detection of functionally significant CAD by imaging tests with sufficient spatial resolution to differentiate the myocardial layers. An endo- to epicardial gradient of blood flow exists at rest, reflecting the higher metabolic activity of the endocardial layer (Muehling et al., 2004; Radjenovic et al., 2010). In health, pharmacologically induced maximal hyperaemia increases MBF in all myocardial layers although the endo to epicardial gradient diminishes as MBF maximizes in all myocardial layers. In the context of functionally significant epicardial CAD, hyperaemia leads to a redistribution of MBF from the endo- to the epicardium, leading to relative endocardial ischaemia – or transmural myocardial steal (Algranati et al., 2011) (Figure 5.1).

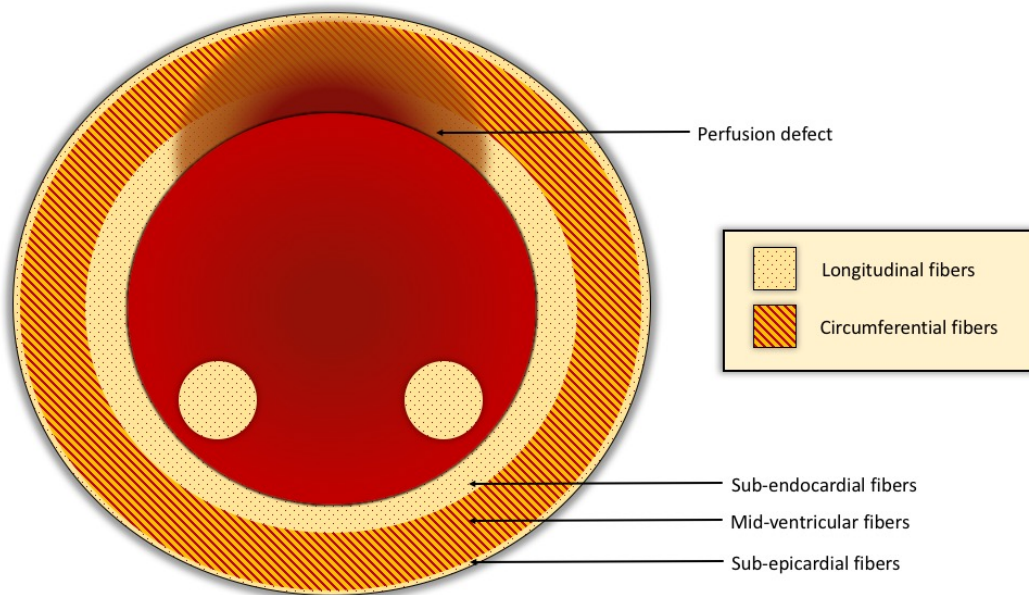


*Figure 5.1 Illustration demonstrating how fiber orientation of the left ventricle corresponds to perfusion defect gradient (high in sub-endocardium and lower in epicardium).*

Thanks to its high in-plane spatial resolution, this transmural perfusion gradient can be demonstrated *in vivo* with first pass myocardial perfusion CMR and a transmural perfusion gradient of 20% can accurately predict hemodynamically significant CAD as defined by fractional flow reserve (FFR) on invasive coronary angiography (Chiribiri et al., 2013).

Myocardial strain imaging allows quantification of subtle changes of left ventricular function that typically precede a reduction in left ventricular ejection fraction (EF) (Panaich et al., 2016). Myocardial deformation can be studied with CMR feature tracking (FT), in which strain is derived from routine cine acquisitions without the need for tagging (Hor et al., 2011; Swoboda, McDiarmid, et al., 2016). FT allows accurate and robust assessment of mainly left ventricular global longitudinal strain (Pedrizzetti et al., 2016). Because longitudinal myocardial fibers are predominantly located in the sub-endocardium, they may be preferentially affected in myocardial ischaemia and transmural steal during hyperaemia. The association of differential abnormalities in local left ventricular function assessed by myocardial strain and peak myocardial hyperaemia in the presence or absence of perfusion defect has not been established yet.

Therefore, the purpose of this study was to: 1) investigate the relationship between left ventricular global longitudinal strain (GLS), strain rate (GLSR), myocardial early (E') and late diastolic velocities (A') with adenosine stress first-pass perfusion CMR and 2) determine which strain parameter is most strongly associated with the presence of a perfusion defect.

### ***5.3 Study specific methods***

#### **5.3.1 Cardiac Magnetic Resonance Protocol**

CMR scan included usual cines described in Chapter 2 and the following:

1. Stress perfusion imaging: This was performed with adenosine administered initially at  $140 \mu\text{g kg}^{-1} \text{min}^{-1}$ . Adequate hemodynamic response was assessed by either  $\geq 10\%$  heart rate increase or  $\geq 10$  mm Hg decrease in systolic blood pressure. If there was an inadequate hemodynamic response, the dose was increased incrementally to  $170 \mu\text{g kg}^{-1} \text{min}^{-1}$  and then  $210 \mu\text{g kg}^{-1} \text{min}^{-1}$  for a further 2

minutes until hemodynamic response was achieved. Perfusion image acquisition used a 2-dimensional, T1-weighted saturation recovery–prepared gradient echo-pulse sequence in 3 short-axis slices, planned using the 3/5 technique, using parallel imaging acceleration (SENSE) (Messroghli et al., 2005). A bolus intravenous injection of 0.05 mmol/kg dimeglumine gadopentetate (Magnevist®, Schering AG, West Sussex, UK) followed by a 15 ml saline flush was delivered through an arm vein at 5 ml/s using a power injector (Spectris®, Medrad, Pittsburgh, Pennsylvania), during breath hold in end-expiration.

2. Stress HLA: First-pass perfusion imaging was immediately followed by repeat HLA cine (all parameters similar to the resting pre-stress HLA) while adenosine was still being infused.

3. Rest perfusion imaging: This study was done using identical pulse sequence, slice positioning, injection characteristics to the stress perfusion scan and was performed after waiting for 15 minutes.

4. LGE-imaging

### **5.3.2 Image Analysis**

Perfusion scan and LGE images were evaluated offline using commercially available software (cvi42 v5.1, Circle Cardiovascular Imaging Inc., Calgary, Canada). Infarct location was determined by LGE imaging, according to standard guidelines (Cerqueira et al., 2002).

#### **5.3.2.1 Feature Tracking Strain Analysis (Rest and Stress)**

Strain analysis was performed using a cvi42 (v5.1) feature tracking (FT) module in a semi-automated manner (Figure 5.2). For resting cines, left ventricular endocardial and epicardial borders were manually contoured in end-diastole from both long-axis cines (HLA and VLA). Stress global longitudinal strain parameters were derived from HLA cines only as no VLA images were acquired in order to minimize the duration of adenosine infusion. Peak GLS (peak LV shortening during systole), GLSR (LV shortening rate in systole), E' (peak early filling myocardial strain during diastole) and A' (peak late filling myocardial strain during diastole) were recorded per case.

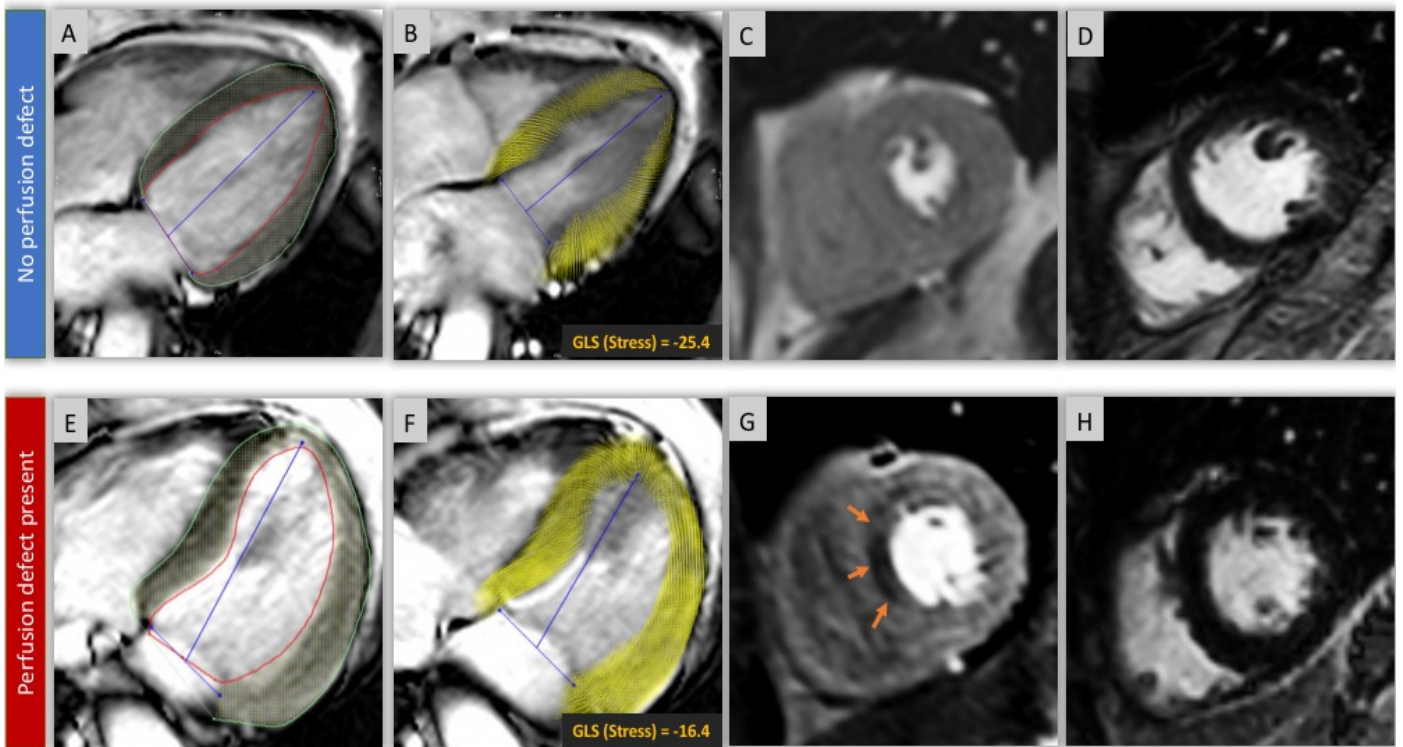


Figure 5.2 Two cases of first pass perfusion CMR.

Case 1(A – D). The top row shows CMR images of a 63-year-old female who presented with a history of chest pain. Panel A illustrates endo/epi contours on 4-chamber cine acquisition at peak stress. Panel B demonstrates the derived myocardial feature tracking and computed systolic GLS at peak stress. Panel C shows the corresponding stress perfusion image at the time of peak myocardial contrast enhancement, showing no inducible perfusion defects. Panel D shows that there is no infarction on late gadolinium enhancement (LGE) imaging. Case 2(E – H). The bottom row shows CMR images of a 59-year-old male who presented with a history of chest pain. This is a case with a perfusion defect in mid ventricular septum (orange arrows in panel G) on first-pass perfusion with no evidence of previous myocardial infarction on LGE imaging (Panel H). Notably, the peak stress GLS was significantly lower in this case.

### **5.3.2.2 Perfusion Analysis**

CMR images were anonymised, which included the removal of dates of acquisition and any identifiable data. The randomised images were independently analysed by two experts in perfusion analysis with greater than 3-years' experience each (TAM and DPR). Each expert reported on the presence of inducible stress perfusion defects that were not present on rest perfusion images and with no corresponding scar on LGE images. In case of disagreement between the two observers, a third independent expert analysed the images, and a discussion of the study commenced in order to reach a unanimous decision (PG). Studies in which a unanimous decision could not be reached were excluded. On stress perfusion imaging, an area of decreased signal intensity when compared to remote myocardium and the presence of an endocardial to epicardial perfusion gradient were classified as a perfusion defect (Plein et al., 2008).

### **5.3.3 Statistical Analysis**

The accuracy of myocardial deformation parameters in predicting the presence of a perfusion defect was examined using the receiver-operator characteristic (ROC) curve analyses described by Delong for comparison of the area under the curve (AUC), using Medcalc (v15.8). Forward (conditional) multivariable logistic regression was used for all strain parameters with statistical significance from one-way analysis ( $p < 0.1$ ). A linear regression model, comprising of the predictive values was generated for all the strain parameters which demonstrated significant association to the presence of perfusion defect in univariate analysis.

## ***5.4 Results***

### **5.4.1 Study demographics and characteristics**

A total of 50 patients were recruited. 4 patients had equivocal perfusion results, resulting in exclusion from the study and 2 patients were claustrophobic. From the rest 44 patients recruited, 22 patients had an inducible perfusion defect, and 22 patients had no inducible perfusion defects. The two independent graders agreed on the categorization of all cases with no arbitration required. The demographics, clinical data and baseline CMR results are shown in Table 5.1. No gender, age or characteristic based differences were present between the groups. Baseline CMR characteristics, including myocardial infarction, were not significantly different in both the groups.

<b>Characteristics</b>	<b>All patients</b>	<b>Perfusion defect</b>	<b>No perfusion defect</b>	<b>P-value</b>
<b>Demographics</b>	(n=44)	(n=22)	(n=22)	
Age (years)	64±12	64±12	63±13	0.53
Gender (male/female)	31/13	16/6	15/7	0.75
Current smoker [no. (%)]	13 (30)	7 (16)	6 (14)	0.75
Hypertension [no. (%)]	13 (30)	7 (16)	6 (14)	0.75
Diabetes Mellitus [no. (%)]	12 (27)	6 (14)	7 (16)	0.45
Dyslipidaemia [no. (%)]	7 (16)	3 (7)	4 (9)	0.69
Myocardial Infarction [no. (%)]	17 (39)	10 (23)	6 (14)	0.22
CABG [no. (%)]	6 (14)	4 (9)	1 (2)	0.13
Abnormal ECG [no. (%)]	13 (30)	8 (18)	5 (11)	0.33
<b>Baseline CMR parameters</b>				
LV EDV, (ml/m <sup>2</sup> )	143 ±45	151±46	133±43	0.19
LV ESV, (ml/m <sup>2</sup> )	55±32	63±39	45±21	0.06
LV SV, (ml/m <sup>2</sup> )	86±29	87.6±18	84.4±37	0.72
LV EF, (%)	64±13	61±13	67±12	0.07
LV Mass (grams)	111±35	112±26	109±43	0.76
Presence of Infarction (%)	25 (57%)	15 (34%)	10 (23%)	0.13
<b>Rest strain parameters</b>				
GLS (%)	-18±4	-16.9±3.7	-19.6±3.4	0.02
GLSR (s <sup>-1</sup> )	-98±11	-86±22	-109±38	0.02
E' (s <sup>-1</sup> )	80±39	69±31	93±38	0.04
A' (s <sup>-1</sup> )	80±29	74.5±25	86.7±33	0.18
<b>Stress strain parameters</b>				
GLS (%)	-19±4	-16.5±4	-21.2±3.1	<0.001
GLSR (s <sup>-1</sup> )	-104±54	-98±45	-112±60	0.36

E' (s-1)	97±41	90±50	106±32	0.21
A' (s-1)	93±50	88±43	113±81	0.20

*Table 5.1 Study demographics and baseline CMR parameters*

*Abbreviations: A', myocardial late diastolic velocity; CABG, coronary artery bypass grafting; E', myocardial early diastolic velocity; ECG, electrocardiogram EDV, end-diastolic volume; EF, ejection fraction; ESV, end-systolic volume; GLS, global longitudinal strain; GLSR, global longitudinal strain rate; SV, stroke volume. Data as mean ± SD or n(%) unless indicated. P-value <0.05 was taken as significant.*

#### **5.4.2 Feature tracking analysis**

All cine images were of adequate quality for FT analysis. Figure 5.2 demonstrates two cases from the study. Rest GLS, GLSR, E' and stress GLS were significantly lower in the group with perfusion defect compared to the no perfusion defect group (Table 4.1). Notably, rest GLS was not significantly different in patients without previous myocardial infarction and with/without ischaemia (Table 5.2) (Figure 5.3).

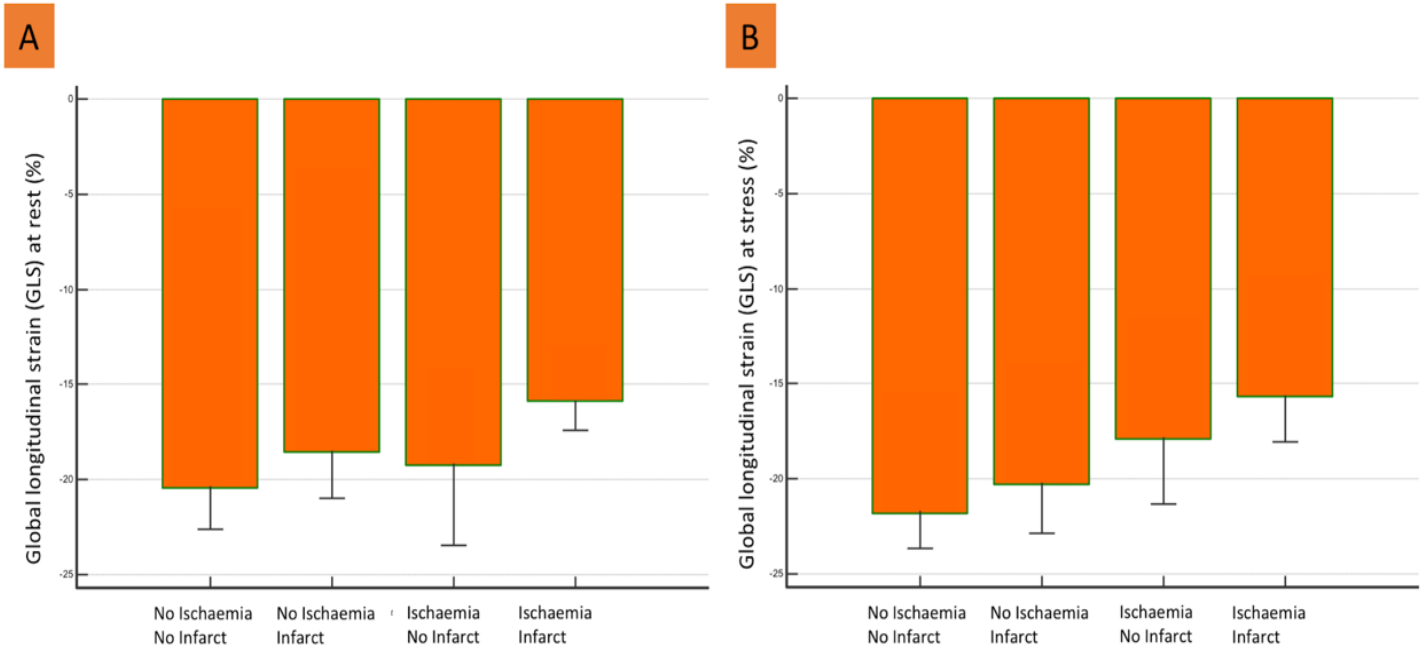


Figure 5.3 Multiple comparison bars. Multiple comparison bars of rest (Panel A) and stress (Panel B) global longitudinal function strain in patients with/without myocardial infarction and perfusion defect (whiskers: standard deviations; SD).

	Presence of MI	Strain parameters	With perfusion defect	Without perfusion defect	P-value
<b>Rest</b>	LGE -ve	GLS (%)	-19±5	-20±3	0.59
		GLSR (s <sup>-1</sup> )	-101±19	-119±53	0.41
		E' (s <sup>-1</sup> )	94±32	102±52	0.69
		A' (s <sup>-1</sup> )	93±15	97±36	0.75
	LGE +ve	GLS (%)	-16±3	-19±4	0.04
		GLSR (s <sup>-1</sup> )	-78±20	-99±13	0.01
		E' (s <sup>-1</sup> )	56±21	81±30	0.02
		A' (s <sup>-1</sup> )	66±24	74±25	0.45
<b>Stress</b>	LGE -ve	GLS (%)	-18±4	-22±3	0.02
		GLSR (s <sup>-1</sup> )	-136±55	-102±77	0.32
		E' (s <sup>-1</sup> )	128±62	111±24	0.39
		A' (s <sup>-1</sup> )	113±46	113±69	0.99
	LGE +ve	GLS (%)	-16±4	-20±3	0.01
		GLSR (s <sup>-1</sup> )	-80±27	-125±27	<0.001
		E' (s <sup>-1</sup> )	72±32	101±40	0.06
		A' (s <sup>-1</sup> )	76±36	114±97	0.18

*Table 5.2 Myocardial deformation parameters in the two groups of patients.*

*Data as mean ± SD or n (%) unless indicated. P-value <0.05 was taken as significant.*

The absolute change in rest versus stress GLS demonstrated an increase in GLS in patients without perfusion defects but a reduction in GLS at stress in patients with a perfusion defect (-1.6±3.1 versus 0.5±3.8, P-value=0.05). Other strain parameters, GLSR (-2.8±77 versus -12±31, P-value=0.60), E' (13±45 versus 22±40, P-value=0.45), A (27±65 versus 13±29, P-value=0.43) did not show significant changes between rest and stress.

### **5.4.3 Influence of previous Myocardial Infarction**

Patients with previous MI on LGE-imaging had lower rest GLS than patients with no MI ( $-16\pm 3\%$  vs.  $-20\pm 4\%$ , P-value = 0.007) and stress GLS ( $-17\pm 4\%$  vs.  $-20\pm 4\%$ , P-value = 0.02). However, patients with previous MI did not show more inducible perfusion defects than those without previous MI (OR 0.38, P-value=0.13).

### **5.4.4 Receiver operator characteristics (ROC) analysis**

Table 5.3 details the diagnostic performance for each of the parameters. Figure 5.4 displays the ROC plots. Stress GLS displayed a slightly better, though not statistically significant diagnostic performance compared to rest GLS (Table 5.3, Figure 5.4). A strain model comprising of rest GLS, GLSR, E' and stress GLS demonstrated significant superiority to rest GLS alone. The strain model displayed a sensitivity of 95% and specificity of 68% to detect perfusion defects.

		<b>Youden Cut-off</b>	<b>Sensitivity (%)</b>	<b>Specificity (%)</b>	<b>AUC</b>	<b>95% CI</b>		<b>P-value</b>
<b>Rest</b>	GLS (%)	>-18.55	77.27	68.18	0.72	0.56	0.87	0.006
	GLSR (s <sup>-1</sup> )	>-91.09	68.18	72.73	0.75	0.60	0.89	0.0008
	E' (s <sup>-1</sup> )	≤84.53	86.36	54.55	0.70	0.54	0.86	0.01
	A' (s <sup>-1</sup> )	≤108.8	100	32	0.59	0.42	0.77	0.28
6								
<b>Stress</b>	GLS (%)	>-19.80	77.3	72.7	0.82	0.70	0.94	<0.001
	GLSR (s <sup>-1</sup> )	>-99.7	63.6	86.4	0.74	0.58	0.89	0.003
	E' (s <sup>-1</sup> )	≤81.65	50	82	0.67	0.50	0.83	0.04
	A' (s <sup>-1</sup> )	≤58.65	36.36	86.36	0.58	0.41	0.76	0.34
1								
<b>Strain model<sup>@</sup></b>		---	96	68	0.87	0.76	0.97	<0.000

Table 5.3 C-statistics for myocardial strains at rest and stress CMR. Data as mean ± SD or n (%) unless indicated. P-value <0.05 was taken as significant.

<sup>@</sup> Model comprising of strain parameters associated to the presence of perfusion defect in univariate analysis: rest GLS, rest GLSR, rest E' and stress GLS

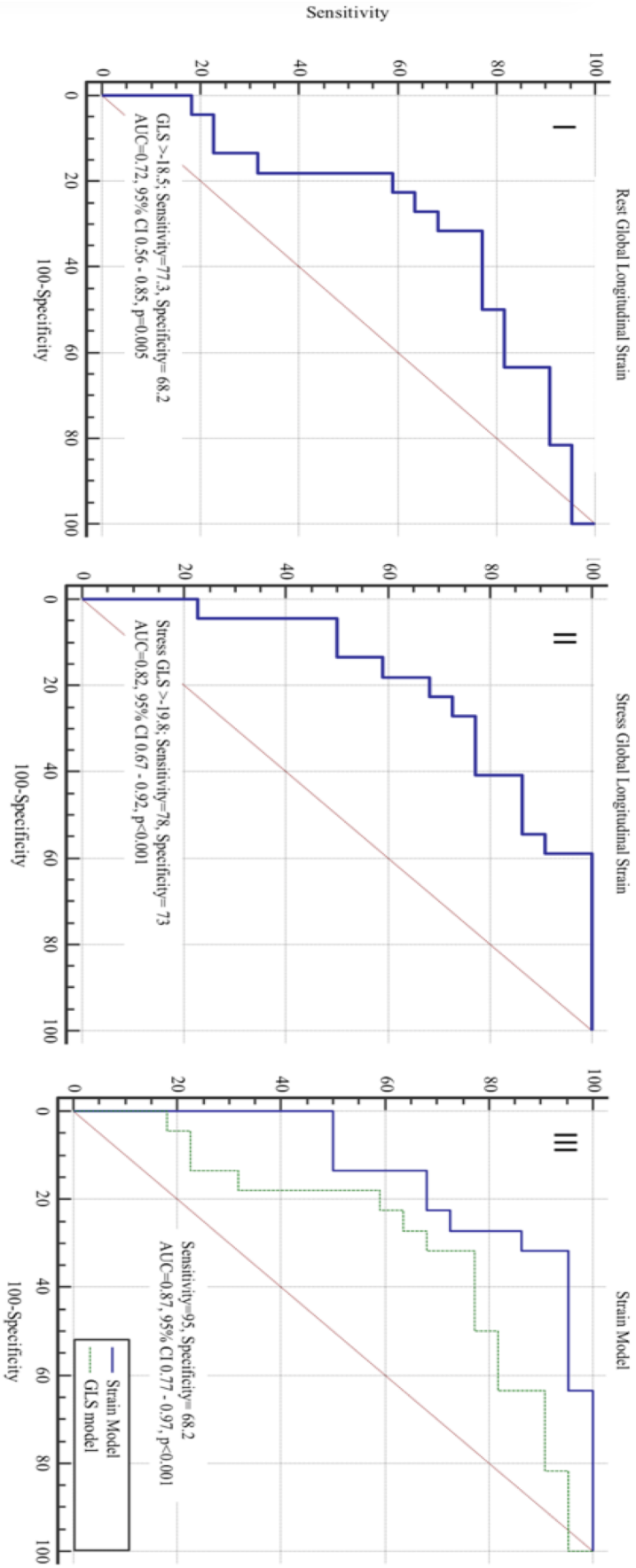


Figure 5.4 Receiver operator curves (ROC). ROC analysis of different strain models to predict the presence of myocardial perfusion defect: Resting global longitudinal strain (GLS) model (I), stress GLS (II) and strain model versus rest GLS (III).

	Variable	UV		MV (without model)		MV (with model)
		OR	95% CI	P-value	P-value	P-value
<b>Rest</b>	GLS	1.25	1.03 - 1.52	0.02	0.74	0.86
	GLSR	1.04	1.01 - 1.07	0.02	0.06	0.77
	E'	0.98	0.96 - 1.00	0.05	0.32	0.72
	A'	0.99	0.96 - 1.01	0.18	...	...
<b>Stress</b>	GLS	1.43	1.14 - 1.78	0.002	<0.001	0.68
	GLSR	1.01	0.99 - 1.02	0.37	...	...
	E'	0.99	0.97 - 1.01	0.21	...	...
	A'	0.99	0.98 - 1.00	0.22	...	...
<b>Strain Model<sup>@</sup></b>				<0.001	...	<0.0001

Table 5.4 Predictors of perfusion defect in univariable (UV) and multivariable (MV) logistic regression analysis. P-value <0.05 was taken as significant. CI, confidence interval; OR, odds ratio; UV, univariable; MV, @ Model comprising of strain parameters associated to the presence of perfusion defect in univariate analysis: rest GLS, rest GLSR, rest E' and stress GLS.

#### 5.4.5 Regression analysis

In the logistic regression analysis, stress GLS demonstrated the best independent association with the presence of a perfusion defect of the parameters tested (OR 1.43 95% CI 1.14 - 1.78, P-value<0.001) (Table 5.4). The logistic regression strain model was independently associated with presence of perfusion defect (P-value<0.001) when compared with other individual myocardial strain parameters.

### 5.5 Discussion

The main novel findings of this study are: 1) at peak myocardial hyperaemia GLS is reduced in patients with perfusion defects on simultaneously acquired first-pass

perfusion CMR 2) among several strain parameters tested, stress GLS is most strongly associated with the presence of a perfusion defect 3) a cut-off value of -19.8% for stress GLS demonstrates 77% sensitivity and 73% specificity for the presence of a perfusion defect.

Myocardial ischaemia initially affects the endocardium and progresses to the sub-epicardial layers in a 'wave front' manner. High resolution adenosine stress myocardial perfusion CMR can demonstrate a transmural gradient of myocardial perfusion in patients with flow limiting CAD, representing the redistribution of myocardial blood flow from the sub-endocardium to the sub-epicardium. Sub-endocardial fibers are structurally longitudinal fibers (Greenbaum et al., 1981) and therefore predominantly contribute to the longitudinal function of the LV (Birkeland et al., 1992). The main findings of the present study are consistent with these known concepts. We found that global longitudinal function assessed by GLS was adversely affected during adenosine stress in patients with perfusion defects while GLS in patients with no perfusion defects increased during hyperaemia. The most likely mechanism underpinning this observation is that relative ischaemia of the sub-endocardial myocardial layer ('transmural myocardial steal') affects longitudinal fibre function during hyperaemia and thus differentially reduces longitudinal LV function.

In patients with evidence of MI on LGE imaging, rest GLS, GLSR and  $E'$  were also correlated with the presence of perfusion defects, however these resting strain parameters did not discriminate between patients with and without perfusion defects in the absence of previous MI. Like ischaemia, MI predominantly affects the endocardial layer and thus longitudinal myocardial strain and a reduction in resting myocardial deformation can therefore be expected. The correlation with the presence of an inducible perfusion defect is likely to be caused by co-existing CAD in other territories or peri-infarct ischaemia, both of which were common in the present population in patients with prior MI. Resting strain parameters are however not reliable markers of inducible ischaemia as shown by the lack of correlation with perfusion defects in patients without MI.

A strain model, comprising of rest GLS, GLSR,  $E'$  and stress GLS performed slightly better than stress GLS alone in linear regression (Table 5.3) but was not statistically

superior to individual parameters in AUC analysis ( $P>0.05$ ). As the strain model required multiple strain analyses, the use of stress GLS alone may be a more practical approach for clinical studies.

Previous echocardiographic studies have reported findings that are consistent with our observations. Liang et al found that rest peak systolic strain rate (equivalent to GLSR in our study) and peak early diastolic strain rate ( $E'$  in our study) were significantly lower in patients with significant coronary artery disease ( $>70\%$  stenosis) than controls (Liang et al., 2006). Our study demonstrated similar global resting strain rate findings to Liang et al (Table 5.1). However, our study was able to accurately differentiate patients with previous MI on LGE-imaging and demonstrate the clear differences of strain rate at rest in patients with/without previous MI (Table 5.2). A pre-clinical porcine study by Reant et al also demonstrated that flow reduction in the coronary artery achieved by adenosine induced myocardial hyperaemia (flow reduction by 70%) adversely affected myocardial deformation parameters (mainly longitudinal and circumferential strain) at stress (Reant et al., 2008). In a multi-centre study of 102 patients who underwent concomitant dobutamine stress echocardiography and coronary angiography, longitudinal strain at peak stress demonstrated better diagnostic accuracy than wall motion score (Ng et al., 2009). In the same study, a dobutamine stress GLS cut-off of  $-20\%$  demonstrated 84% sensitivity and 87% specificity for significant CAD. The optimum cut-off for stress GLS in our study was very similar at  $-19.8\%$ .

### **5.5.1 Practical implications**

If confirmed in larger prospective populations, our data suggest that non-contrast adenosine stress cine imaging with FT analysis of GLS may be an alternative to first pass perfusion CMR for the detection of CAD in selected populations. Although the method cannot localize disease to a coronary territory, it may be useful in patients with contraindications to MR contrast agents such as those with advanced renal failure. Compared with dobutamine stress CMR, adenosine stress has a lower risk and imaging protocols are much faster as only one stress stage is required. The analysis time to compute GLS from one 4-chamber cine at stress is minimal and

provides valuable quantitative information which is less susceptible to subjectivity (McDonald et al., 2015).

### **5.5.2 Study limitations**

Our study has limitations. In this proof of concept study we investigated only a small study population. However, we found statistically significant differences on logistic regression, justifying larger studies to investigate this concept further. Secondly, for practical and conceptual reasons we did not use coronary stenosis on invasive angiography as the primary end-point (Chow et al., 2009). Nevertheless, contemporary CMR sequences for first-pass perfusion defect are highly accurate in the diagnosis of significant ischaemia (Greenwood et al., 2012). Thirdly, the present study did not evaluate regional myocardial function using standard quantitative methods including regional and global wall motion scores. Hence, we were not able to compare these with the strain parameters obtained. Fourthly, our results need to be used with caution in patients with infiltrative cardiomyopathies (hypertrophic cardiomyopathy, cardiac amyloidosis, sarcoidosis etc.), which are characterized by stiffening of the left ventricle, and may affect myocardial deformation (Seward and Casacang-verzosa, 2010). Several papers have demonstrated that the aforementioned infiltrative cardiomyopathies lead to reduced GLS and hence our results are not implacable in these disease states (Kristen et al., 2012; Afonso et al., 2012; Kul et al., 2014).

### **5.6 Conclusion**

At peak myocardial hyperaemic stress, GLS is reduced in the presence of a myocardial perfusion defect, most likely secondary to reduced endocardial blood flow as a result of hyperaemia induced redistribution of transmural perfusion in the presence of significant coronary stenosis. Additionally, this study demonstrates the feasibility of adenosine stress myocardial strain CMR in this demographic which may provide clinically relevant information and justifies further larger studies to investigate the accuracy of using CMR FT-derived strain to predict the presence of CAD.

## **6 Study 4- Acute Infarct Extracellular Volume Mapping to Quantify Myocardial Area at Risk and Chronic Infarct Size on Cardiovascular Magnetic Resonance Imaging**

### **6.1 Abstract**

#### **6.1.1 Background**

Late gadolinium enhancement (LGE) imaging overestimates acute infarct size. The main aim of this study was to investigate if acute ECV-maps can reliably quantify myocardial area at risk (AAR) and/or final infarct size (IS).

#### **6.1.2 Methods**

50 patients underwent cardiovascular magnetic resonance (CMR) imaging acutely (24hrs-72hrs) and at convalescence (3 months). The CMR protocol included: cines, T2-weighted (T2W) imaging, native T1-maps, 15-minute post-contrast T1-maps and LGE. Optimal AAR and IS ECV thresholds were derived in a validation group of 10 cases. 800 segments (16-per-patient) were analysed to quantify AAR/IS by ECV-maps (ECV thresholds for AAR: 33% and IS: 46%), T2W-imaging and acute LGE. Follow-up LGE-imaging was used as the reference standard for final IS and viability assessment.

#### **6.1.3 Results**

AAR quantified from ECV-maps demonstrated the best correlation and agreement with AAR by T2W-imaging at an ECV threshold of >33% (R=0.96, 95% CI 0.93-0.98; P<0.0001; bias on Bland-Altman (BA) analysis 0.18, 95% CI -1.6-1.3). ECV demonstrated the best linear correlation to final IS at a threshold of >46%, (R=0.92, 95% CI 0.86-0.95; P<0.0001). ECV-maps demonstrated better agreement with final IS than acute IS on LGE (ECV-maps: bias=1.9, 95% CI 0.4-3.4 versus LGE-imaging: bias=10, 95% CI 7.7-12.4). On multiple variable regression analysis, the number of non-viable segments was independently associated with IS by ECV-maps (beta=0.86, P<0.0001).

#### **6.1.4 Conclusions**

ECV-maps can reliably quantify AAR and final IS in reperfused AMI. Acute ECV-maps were superior to acute LGE in terms of agreement with final IS. IS quantified by ECV-maps are independently associated with viability at follow-up.

## **6.2 Introduction**

Infarct size (IS) and myocardial salvage are important determinants of clinical outcome after myocardial infarction and are most accurately assessed with cardiovascular magnetic resonance (CMR)(Schulz-Menger et al., 2013). The size and extent of myocardial infarction on late gadolinium enhancement (LGE) CMR has prognostic value in the chronic setting (Di Bella et al., 2013). Recent literature however suggests that infarct size on LGE-imaging has limited value in acute myocardial infarction (El Aidi et al., 2014) and overestimates actual IS compared to histopathology (Saeed et al., 2001; Hammer-Hansen et al., 2016; Jablonowski et al., 2015). Separately, T2-weighted (T2W) imaging can be used after acute myocardial infarction to quantify the myocardial area at risk (AAR) and together with LGE extent to compute the myocardial salvage index.

Commonly, IS and AAR are derived with semi-automated thresholding methods, but these methods have important limitations (McAlindon et al., 2015). Semi-automated thresholding is dependent on several factors including: 1) windowing by the operator to decide where the region of interest (ROI) is placed, 2) the variation of signal intensity within the ROI and 3) the size of ROI can also affect the signal intensity variations (Kwong and Farzaneh-Far, 2011). The cumulative effect of these factors can significantly influence quantification and intra-/inter-observer variation of the measurements.

Parametric mapping methods, in particular T1 mapping and the derived parameter of extracellular volume (ECV), allow an alternative method for quantification of IS and AAR on an absolute scale (0%-100%). ECV has previously been shown to be increased in the AAR and infarcted myocardium (Ugander, Oki, et al., 2012; Jablonowski et al., 2015; Hammer-Hansen et al., 2016), but thresholding to define cut-offs of ECV to quantify AAR and IS has not been investigated.

The purpose of this study was to: 1) determine ECV thresholds for AAR and IS 2) investigate if acute ECV-maps can be used to quantify the AAR (determined by T2W images during acute setting); 3) determine if acute ECV-maps perform better than LGE-imaging to predict actual IS at 3 months; 4) investigate the association of acute ECV-maps to viability at 3 months(Tarantini et al., 2006).

## **6.3 Methods**

### **6.3.1.1 Cardiac catheterization**

Coronary angiography and revascularisation were performed in a standard fashion according to current best practice guidelines (Steg et al., 2012). TIMI flow grades were assessed visually as described previously after coronary angioplasty (Anon, 1985).

### **6.3.2 CMR protocol**

All patients had CMR imaging at either 1.5 Tesla (Ingenia, Philips, Best, Netherlands) or 3.0 Tesla (Achieva TX, Philips, Best, Netherlands) within 72-hours (median 48-hours) of their index presentation and were invited to attend for a further CMR study at 3-months follow-up. A dedicated cardiac phased array receiver coil was used (1.5T: 24-channel; 3T: 32-channel).

Cine, T2W-imaging, LGE-imaging were performed using a contiguous stack of short-axis slices covering the whole left ventricle for each acquisition. The same slice geometry, position and 10mm slice thickness were used for all pulse sequences. Native T1-maps and post-contrast T1-maps were performed using the '3-of-5' approach by acquiring the central 3 slices of 5 parallel short-axis slices spaced equally from the mitral valve annulus to the LV apical cap (Messroghli et al., 2005). Post-contrast T1-maps were timed at 15 minutes after contrast administration and LGE-imaging was performed at 16-20 minutes. For each pulse sequence, images with artefact were repeated until any artefact was removed or minimized. The highest quality images were used for analysis.

### **6.3.3 Image Analysis**

Cine, T2W-images, and LGE-images were evaluated offline using Mass research software (Leiden University Medical Center, The Netherlands). Left ventricular volumes and EF were analysed from cine images using standard methods (Schulz-Menger et al., 2013).

Two validated methods were used to quantify the AAR on acute CMR scans: 1) for T2W-imaging, AAR was quantified using the previously published full-width at half maximum (FWHM) thresholding method (Aletras et al., 2006) and 2) for native-T1 maps we used 2 standard deviation (2SD) thresholding method validated by Ugander et al (Ugander, Bagi, et al., 2012). Infarct location was determined by LGE-imaging, according to standard guidelines (Cerqueira et al., 2002). Two validated methods were used to define acute infarct size (IS): 1) an area of LGE  $\geq 5$  standard deviations (SD) above remote myocardium (Bondarenko et al., 2005; Heiberg et al., 2008) and 2) the FWHM method (Flett et al., 2011; Amado et al., 2004). To decrease variability in the selection of the region of interest (ROI), ROI-contours were kept the same between two methods. For the FWHM, infarct core ROI was added as per the previously published techniques (Amado et al., 2004). IS and AAR estimation included any hypo-intense core (MVO with/without IMH). MVO was defined visually as the hypo-intense core within the infarcted zone and planimetered manually. IS, AAR and MVO were calculated from planimetered areas through the whole short-axis LV LGE stack by the summation of discs method.

#### **6.3.4 Extracellular volume mapping analysis**

ECV-maps were generated for the 3 slices (base, mid and apex) by super-imposing the pre-/post- contrast T1-maps and haematocrit values using standard techniques (Moon et al., 2013). The endo- and epi-cardial contours were then outlined to define myocardium for the three slices (Figure 6.1). Hypo-intense core of MVO/IMH was manually contoured to be included in the IS and AAR estimation.

#### **6.3.5 Validation of ECV thresholds**

Approximate ECV thresholds for AAR and IS were derived from previously published pre-clinical and clinical studies (Ugander, Oki, et al., 2012; Jablonowski et al., 2015). In a study by Jablonowski et al, the mean biopsy confirmed ECV value for AAR was 33% and for the 'border-zone' between AAR and infarct ECV was  $48.3\% \pm 4.4\%$  (7). AAR quantified by T2W imaging on acute CMR and IS quantified by LGE-imaging on follow-up scans were used as reference measures for validation in 10 cases. For the validation of AAR, thresholds between 32% and 34% were compared. For the

validation of IS, values of 44 to 52% were analysed, representing the mean and SD of the measurements in infarct border-zone in the study by Jablonowski. Thresholds were defined as the ECV value with the lowest minimal absolute error against the standard references. These thresholds were then prospectively applied to the entire population.

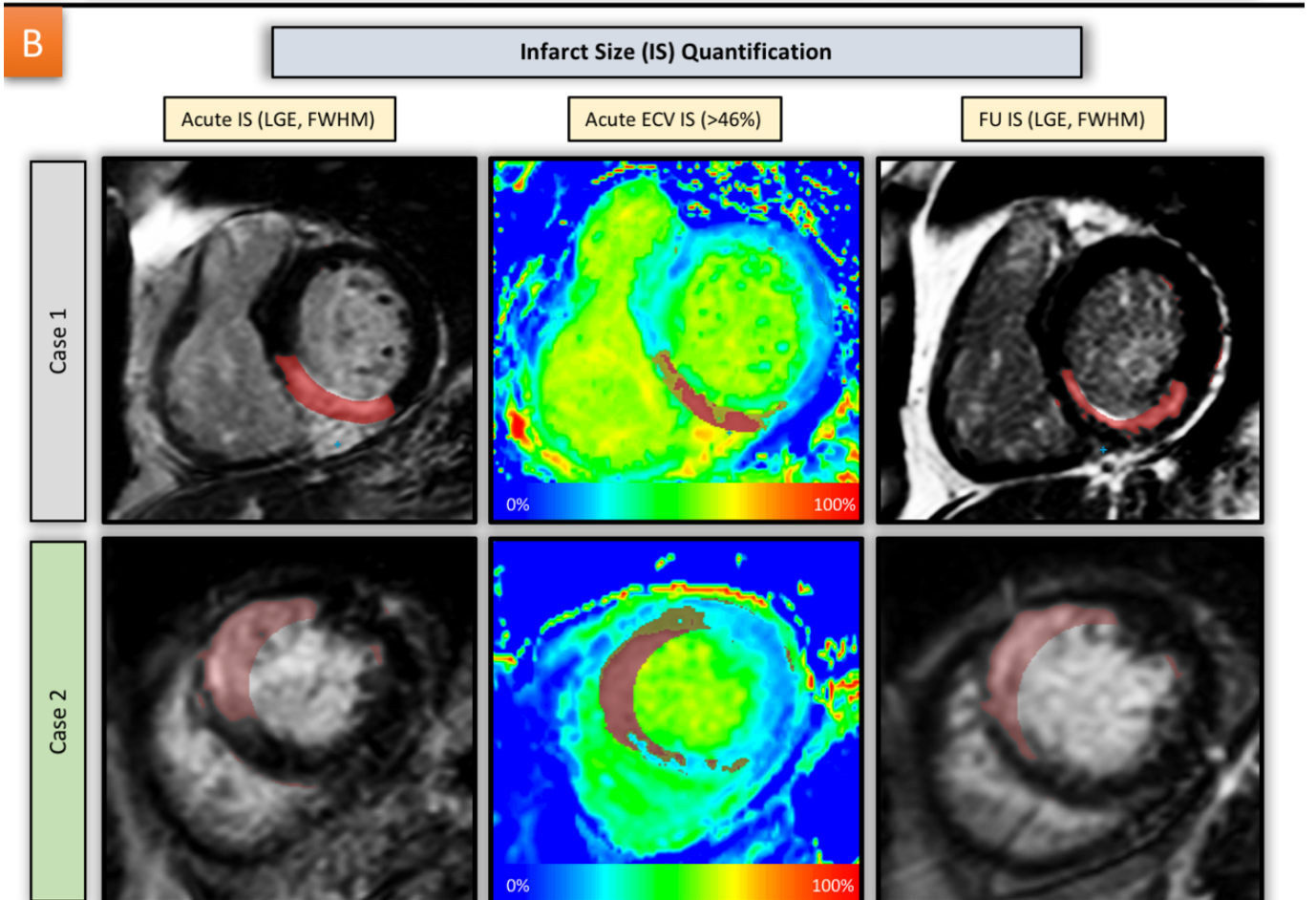
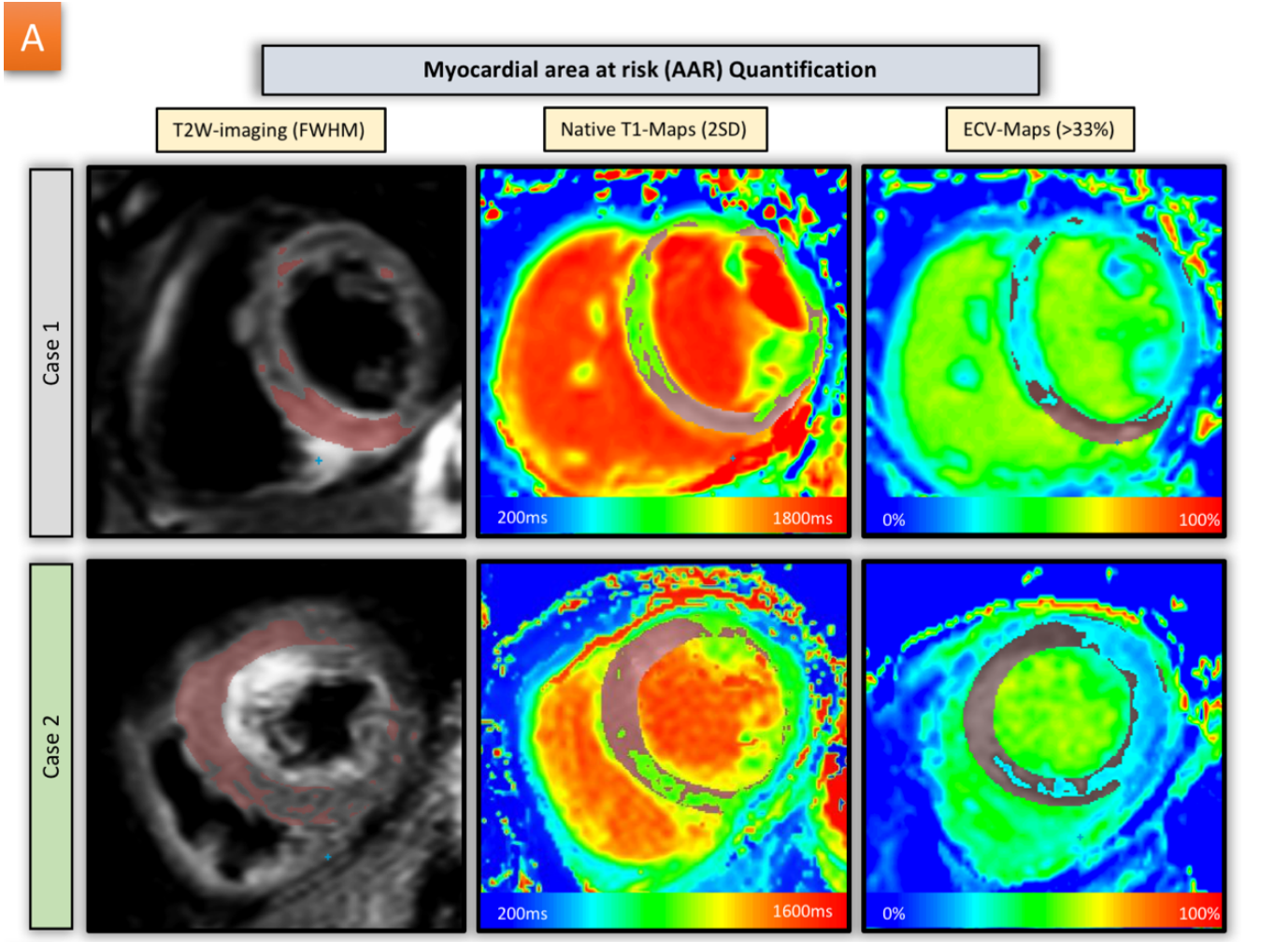


*Figure 6.1 AAR and IS quantification by multiple methods.*

*Panel A: 2 cases of AAR quantification. Case 1: Inferior AMI and Case 2: Anterior AMI by T2W-imaging (applying FWHM thresholding), native T1-maps (applying 2SD thresholding) and ECV-maps (applying greater than 33% threshold). The AAR quantified by all three methods is comparable. IS quantification (Panel B): Demonstrates two cases of IS quantification. In case 1, acute IS by LGE-imaging appears to be transmural whereas acute ECV-maps demonstrate less transmural (red-zone is above 46%) and follow-up LGE-imaging confirms viability in the inferior segments (<50% transmural). Case 2 demonstrate transmural infarct acutely on LGE-imaging and ECV-maps and also on follow-up LGE-imaging.*

### **6.3.6 Follow-up scans**

Follow-up scans were planned at 3-months following the index event. Patients were scanned at 3-months at the same field strength as the baseline scan. IS was estimated using the most validated method to estimate chronic infarct size: the FWHM method (Flett et al., 2011). Segmental infarction using a 16-segment model (Cerqueira et al., 2002) was assessed from LGE images and a greater than 75% volume of infarction per-segment was considered transmural and the segment classified as 'non-viable' (Choi et al., 2001). The number of non-viable segments was recorded for each patient.

### **6.3.7 Statistical analysis**

Agreement between the different tests for IS and AAR are expressed as bias according to Bland-Altman analysis. For paired comparison of the IS, non-parametric Wilcoxon test (paired samples) was used. Univariate analysis was performed for each variable separately. Step-wise multivariate linear regression was used for parameters with statistical significance from one-way analysis ( $p < 0.1$ ).

## **6.4 Results**

### **6.4.1 Patient characteristics**

*Seventy patients were considered for inclusion, of which 50 had baseline and follow up CMR (Figure 6.2). Patient demographics are presented in Table 6.1.*

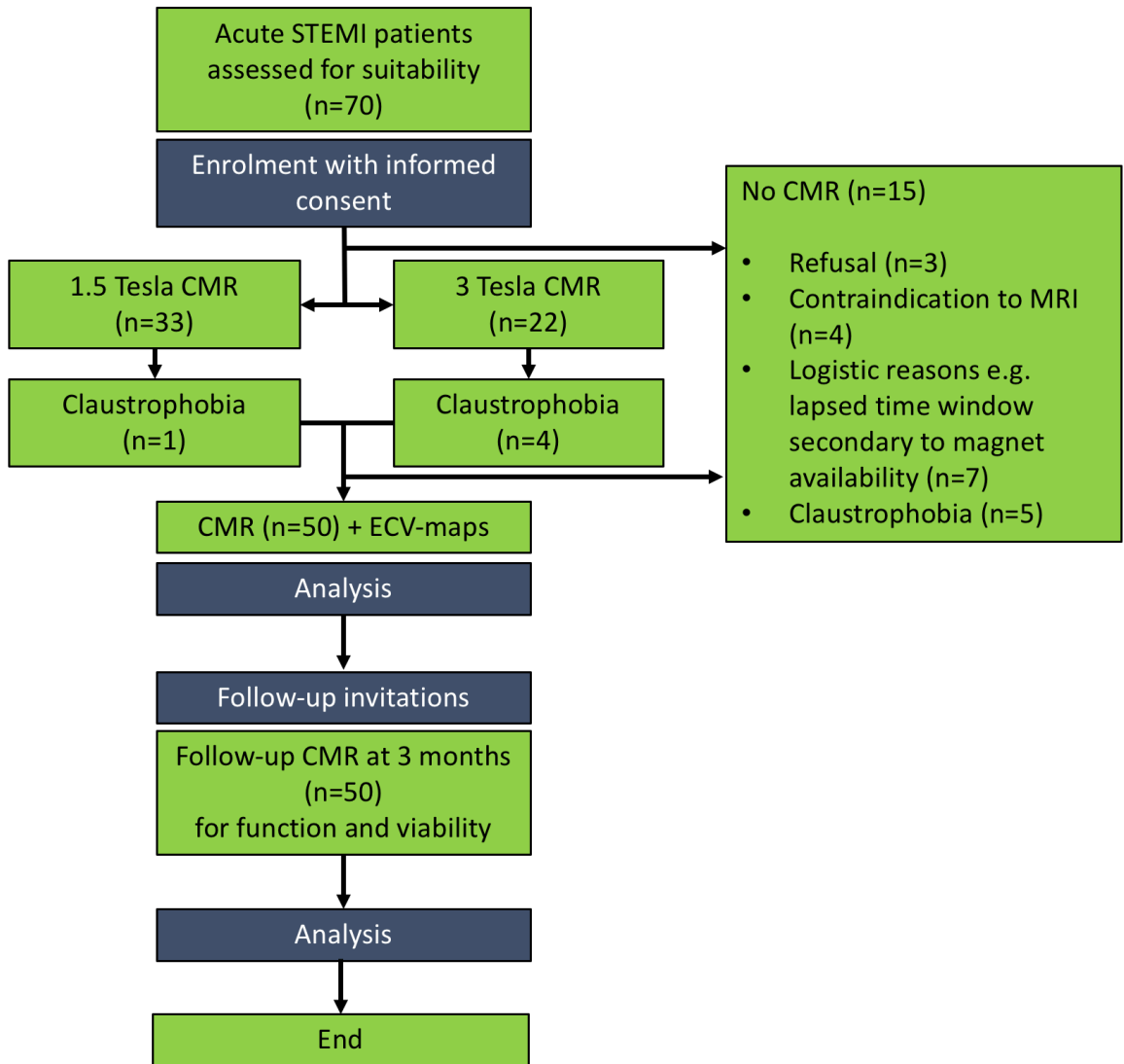


Figure 6.2 Recruitment flowchart.

	All patients (n=50)	1.5 Tesla (n=32)	3 Tesla (n=18)	p- value
Age, yrs	59±11	61±12	57±11	0.27
Male	42	26	16	0.49
BMI, kg/m <sup>2</sup>	28±4	28±4	28±3	0.44
Smoker	30	18	12	0.48
Hypertension	8	6	2	0.49
Hyperlipidaemia	17	10	7	0.59
Diabetes Mellitus	6	4	2	0.89
Family History of Coronary Heart Disease	21	14	7	0.74
<b>Presenting Characteristics</b>				
Systolic Blood Pressure, mmHg	135±31	138±35	130±21	0.41
Heart rate, beats/min	73±15	76±14	68±14	0.06
Time from onset of CP to reperfusion, min	228(155-392)	234(144-383)	222(185-407)	0.68
Heart Failure Killip Class †				
I	46	30	16	0.55
II	3	2	1	0.92
III or IV	1	0	1	0.19
Ventricular fibrillation at presentation	3	2	1	0.92
<b>Angiographic Characteristics</b>				

Number of diseased arteries <sup>ø</sup>				
1	31	18	13	0.27
2	10	8	2	0.25
3	8	5	3	0.93
Left Main Stem	1	1	0	0.46
Culprit Vessel				
Left anterior descending	29	21	8	0.15
Left circumflex	4	3	1	0.64
Right coronary	17	8	9	0.08
TIMI coronary flow pre-PCI				
0-1	44	28	16	0.59
2-3	6	4	2	
TIMI coronary flow post-PCI				
0-1	1	1	0	0.29
2-3	49	31	18	
<b>Laboratory results</b>				
Haemoglobin, grams/litre	146(136-151)	144(135-150)	149(142-155)	0.15
White blood cell, x10 <sup>9</sup> /litre	11(10-13)	11(10-13)	11(10.4-12.5)	0.40
Creatine kinase, U/l	1538(826-2440)	1627(906-2485)	987(553-2120)	0.57
Troponin I, ng/L	41466±16025	44934±12473	34938±19991	0.04
Estimated glomerular filtration rate, ml/min/1.73m <sup>2</sup>	90(77-90)	90(78-90)	83(80-87)	0.99

*Table 6.1 Clinical and angiographic characteristics.*

*Values are mean±SD, n (%), median (IQR). † Killip classification of heart failure after acute myocardial infarction: class I=no heart failure; class II=pulmonary rales or crepitations, a third heart sound, and elevated jugular venous pressure; class III=acute pulmonary edema; and class IV=cardiogenic shock.*

*∅ Multi-vessel coronary artery disease was defined according to the number of stenoses of at least 50% of the reference vessel diameter by visual assessment and whether or not there was left main stem involvement.*

*Abbreviations: BMI, body mass index; CMR, cardiac magnetic resonance; ECV, extracellular volume; IQR, interquartile range; PCI, percutaneous coronary intervention; STEMI, ST-segment elevation myocardial infarction; TIMI, Thrombolysis In Myocardial Infarction.*

#### **6.4.2 Validation of ECV thresholds**

Validation results are presented in Table 6.2. For the quantification of acute AAR, all ECV thresholds (32%, 33% and 34%) were very similar when compared to the reference method of T2W imaging. However, ECV threshold of 33% demonstrated the least absolute error and coefficient of variability (CoV). For the quantification of final IS, ECV thresholds of 46% demonstrate the least absolute error of 10.1% when compared to the final IS on follow-up LGE imaging. Therefore, ECV thresholds of 33% and 46% were used in the prospective analysis to quantify AAR and IS respectively.

	ECV	Acute ECV AAR		T2-W (AAR)		Paired differences				CoV	Absolute Error (%)	
		Mea n	SD	Mean	SD	Mean	SD	95% CI	P <sup>∞</sup>		Median	95% CI
AAR	32	38.7	20.4	37.6	15.1	-1.1	7.2	-6.2 to 4.0	0.64	12.8	12.0%	2.2 to 28.5
	<b>33</b>	35.9	19.7	37.6	15.1	1.7	6.8	-3.2 to 6.5	0.45*	12.8*	11.5%*	3.8 to 28.5
	34	33.3	19.0	37.6	15.1	4.3	6.5	-0.3 to 8.9	0.06	15.0	11.6%	4.8 to 35.9
		Acute ECV IS		LGE IS (Day 90)								
IS	44	15.8	12.6	12.9	9.8	-2.9	4.0	-5.7 to -0.1	0.05	23.6	30.4%	20.7 to 74.4
	45	14.7	12.0	12.9	9.8	-1.7	3.8	-4.4 to 0.9	0.18	20.4	17.0%	12.6 to 74.1
	<b>46</b>	13.2	11.2	12.9	9.8	-0.2	2.9	-2.3 to 1.8	0.80*	15.0*	10.1%*	5.1 to 70.7
	47	12.2	10.4	12.9	9.8	0.8	2.5	-1.0 to 2.5	0.36	14.0	19.8%	3.8 to 56.5
	48	11.2	9.8	12.9	9.8	1.8	2.3	0.1 to 3.4	0.04	16.5	25.5%	8.1 to 41.5
	49	10.1	9.1	12.9	9.8	2.9	2.4	1.1 to 4.6	0.00	22.6	25.9%	9.3 to 49.2
	50	9.1	8.5	12.9	9.8	3.8	2.7	1.8 to 5.7	0.00	29.6	34.6%	9.4 to 56.7
	51	8.2	7.9	12.9	9.8	4.8	3.2	2.6 to 7.0	0.00	37.8	43.4%	19.2 to 64.4
	52	7.3	7.3	12.9	9.8	5.7	3.6	3.2 to 8.3	0.00	46.5	49.9%	28.6 to 72.5

Table 6.2 Validation of ECV thresholding.

<sup>∞</sup> P-values for paired sample T-Test for each thresholding technique.

\* Values on which decision to choose the AAR and IS ECV thresholding values.

### 6.4.3 Myocardial area at risk (AAR) characteristics

AAR characteristics are listed in Table 6.3. The AAR estimated by the FWHM method on T2W imaging demonstrated excellent linear correlation with the AAR estimated by the 2-standard deviation method on the native-T1 maps (R=0.97, 95% CI 0.95-0.98; P<0.0001). Additionally, the AAR estimated by T2W-imaging was not significantly different to the AAR estimated from ECV-maps at a threshold of 33% (47.4±18% versus 47.2±17.4%, P>0.5) and also demonstrated excellent linear correlation to it (R=0.96, 95% CI 0.93-0.98; P<0.0001) (Figure 6.3). On Bland-Altman analysis, the AAR derived from ECV maps demonstrated good agreement with T2W-imaging derived AAR (Bias=0.18, 95% CI -1.6-1.3) and AAR derived from native T1-maps (Bias=1, 95% CI -0.37-2.4) (Figure 6.3).

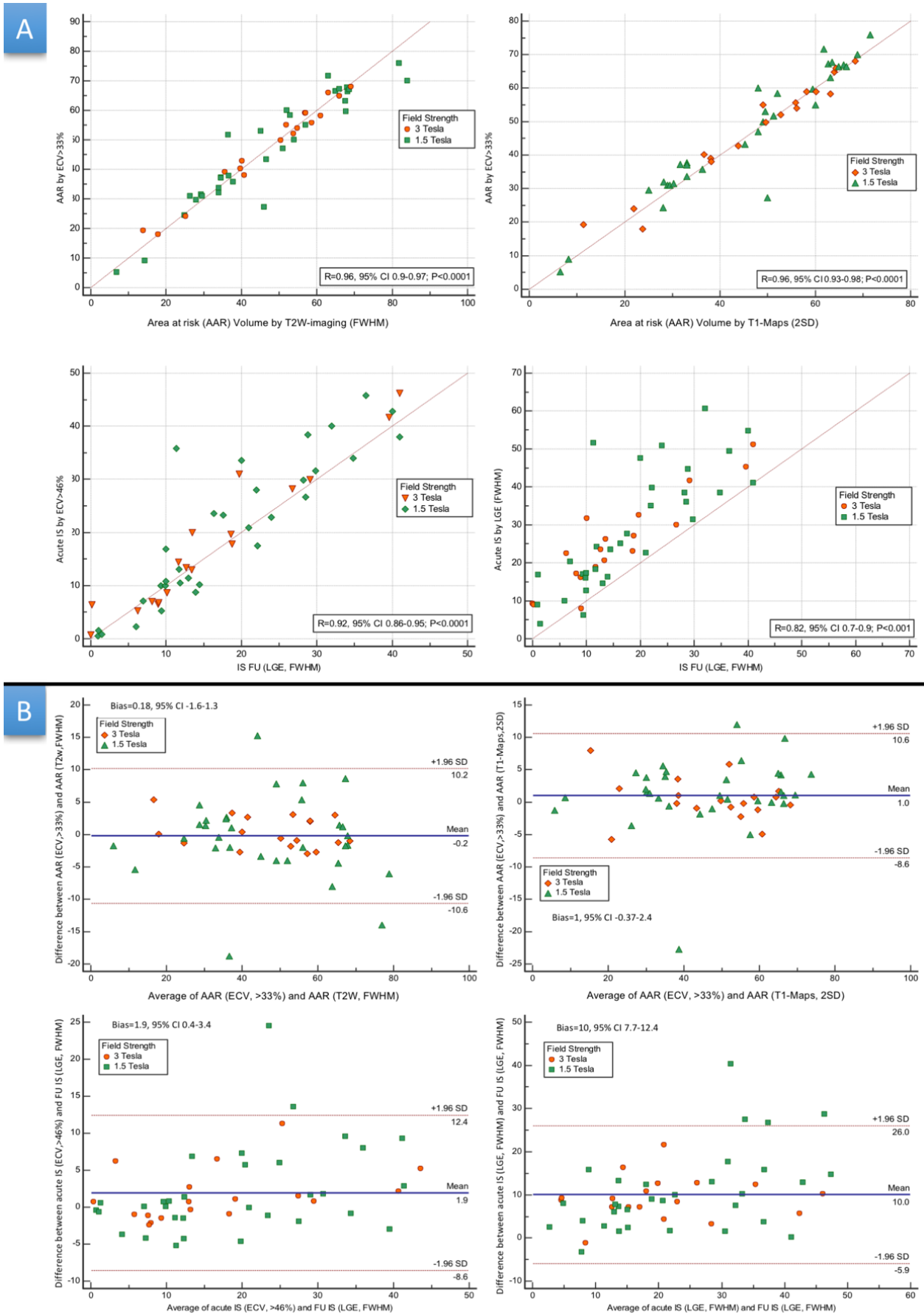


Figure 6.3 Comparison of established quantification methods and ECV-maps.

#### 6.4.4 Infarct Size (IS) characteristics

Baseline infarct characteristics are listed in Table 6.3 and did not differ between the two field strengths. IS estimated from LGE images at the acute scan using the 5SD method overestimated final IS at the follow-up scan ( $P < 0.0001$ ). IS estimated from acute ECV-maps using a 46% threshold did not differ significantly from LGE-defined IS at follow-up ( $P = 0.44$ ). The IS on acute ECV-maps demonstrated excellent linear correlation ( $R = 0.92$ , 95% CI 0.86-0.95;  $P < 0.0001$ ) to the IS at follow-up. IS estimated by acute LGE-imaging (FWHM) also correlated with final infarct size but with a lower  $r$  value than ECV maps ( $R = 0.82$ , 95% CI 0.7-0.9,  $P < 0.01$ ) (Figure 6.3). Moreover, on Bland-Altman analysis, the ECV-maps demonstrated superior agreement to final IS with minimal bias and narrow limits of agreement (Bias=1.9, 95% CI 0.4-3.4) when compared to the acute IS by LGE-imaging (Bias=10, 95% CI 7.7-12.4). Acute IS estimated by the 5-standard deviation method on LGE-imaging demonstrated the lowest linear correlation to IS at follow-up (0.76, 95% CI 0.61-0.86) with worst agreement (Bias=11, 95% CI 7.7-14).

	1.5 TESLA (N=32)	3 TESLA (N=18)	P-VALUE
LVEDVI, ML/M2	82±14.7	79.4±22.6	0.65
LVESVI, ML/M2	45.5±14.5	41.3±8.1	0.27
LVMI, GRAMS	59.4±13.8	55.3±10.8	0.27
EJECTION FRACTION, %	45±11.1	44±7.6	0.72
LGE IS (FWHM), VOLUME IN %	28.8±15.7	25.2±12.2	0.41
LGE IS (5SD), VOLUME IN %	28.1±17	28.6±16.5	0.92
MVO SIZE, VOLUME IN %	4.9±5.4	2.3±3	0.06
AAR, VOLUME IN %	47.3±19.2	47.5±16.2	0.96
ECV >33%, VOLUME IN %	46.8±18.7	47.9±15.5	0.82
ECV >46%, VOLUME IN %	20.4±13.7	17.6±13	0.49
BORDER-ZONE ECV, %	38.2±2.3	39.4±2.5	0.11

Table 6.3 Baseline infarct characteristics at 1.5T and 3T. Values are mean ± SD. LV measurements are indexed to body surface area (BSA), infarct volumes are

*unindexed. LV EDVi Left ventricular end diastolic volume (indexed), LV ESVi Left ventricular end systolic volume (indexed), LVM left ventricular mass (indexed).*

#### **6.4.5 Per segment viability characteristics**

Of the 800 segments 32 (4%) were non-viable on follow-up LGE images. On per patient based analysis, 14 (28%) patients demonstrated loss of viability in at least one segment. There were no statistically significant differences in the area under the curve (AUC) on receiver operator characteristics curve (ROC) analysis for either ECV-maps IS or LGE-imaging IS to predict viability (AUC=0.94, 95% CI 0.88 – 1 versus AUC=0.93, 95% CI 0.86-1; P=0.82). The number of non-viable segments per patient correlated with IS by ECV ( $r=0.70$ ,  $P<0.0001$ ) and LGE-imaging ( $r=0.64$ ,  $P<0.0001$ ) and demonstrated a linear trend of rise of these parameters ( $P<0.0001$ , Figure 6.4).

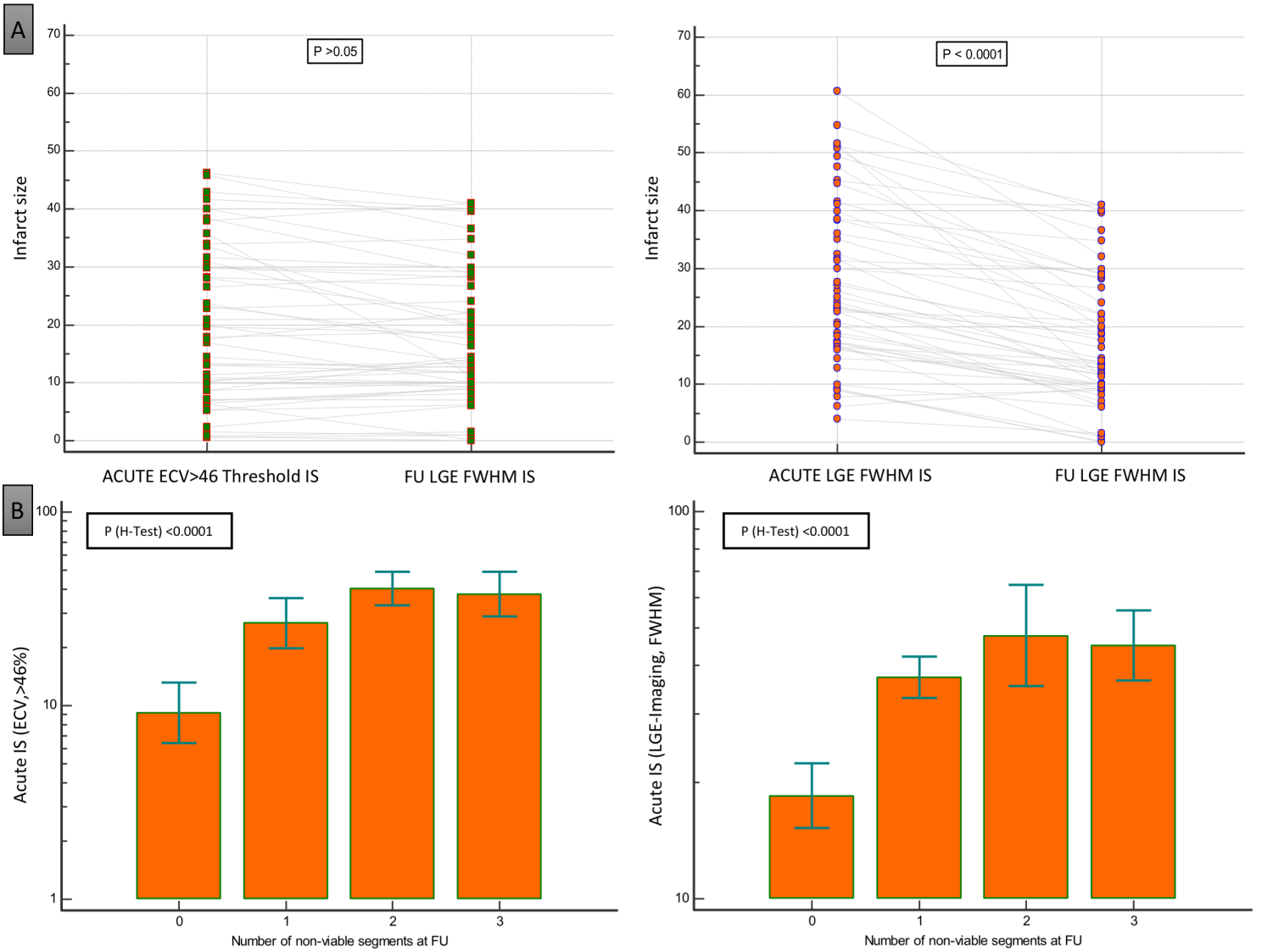


Figure 6.4 Statistical results. Panel A: Dot and line diagram comparing paired IS by acute ECV-maps and LGE-imaging to actual (follow-up) IS on LGE-imaging (FWHM). Panel B: Bar chart demonstrating trend of increase in IS with increase in number of non-viable segments. Even though the trends for both, acute ECV-maps and LGE-imaging, are statistically significant, ECV-maps demonstrate a more homogenous rise than the LGE-imaging.

#### **6.4.6 Regression analysis**

Regression analysis is presented in Table 6.4. On multivariable linear regression analysis, acute IS by ECV-maps was independently associated with follow-up IS (beta 0.92;  $P < 0.0001$ ) and not acute IS by LGE-imaging ( $p = 0.89$ ). Moreover, the number of non-viable segments was independently associated with acute IS by ECV-maps (beta=0.70,  $P < 0.0001$ ) and not with IS by LGE-imaging.

Follow-up Infarct size      Number of non-viable segments

Variable	UV	MV	UV	MV
Age	0.53		0.92	
Gender	0.69		0.24	
Current Smoker	0.03		0.04	0.50
Hypertension	0.98		0.57	
Hypercholesterolemia	0.69		0.66	
Diabetes	0.44		0.53	
Family history of CAD	0.47		0.15	
Systolic BP	0.29		0.96	
Heart Rate	0.22		0.76	
TIMI flow pre-PCI	<0.01	0.37	0.12	
TIMI flow post-PCI	0.96		0.95	
Door to Balloon time	0.20		0.53	
LVEDV	0.01	0.98	0.74	
LVESV	<0.01	0.91	0.04	0.16
LV Mass	0.16		0.89	
Ejection Fraction	<0.01	0.37	<0.01	0.68
MVO	<0.01	0.71	<0.01	0.75
Acute IS (LGE FWHM)	<0.01	0.89	<0.01	0.68
Acute IS (ECV >46%)	<0.01	<b>&lt;0.0001 (0.92)</b>	<0.01	<b>&lt;0.0001 (0.70)</b>

Table 6.4 Predictors of follow-up infarct size and per patient number of non-viable segments in uni-/multi- variable regression analysis.

## **6.5 Discussion**

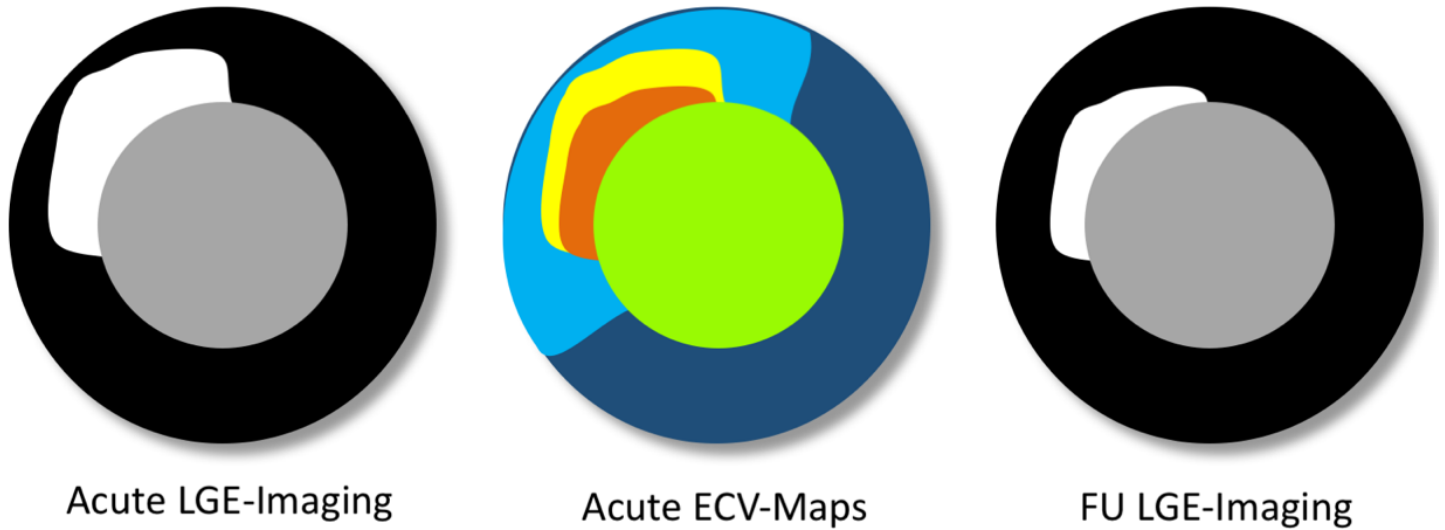
The present study demonstrates that acute ECV-maps offer a robust and reliable alternative to acute T2w-imaging and T1-maps to quantify the AAR (at an ECV threshold of 33%) and to acute LGE-imaging to quantify the final IS at follow-up (at an ECV threshold of 46%). Secondly, ECV-maps are superior to acute LGE-imaging in terms of agreement with final IS. Additionally, IS quantified by ECV maps is strongly associated the number of non-viable segments at 3-months follow-up.

### **6.5.1 Multi-parametric tissue characterisation**

In a previous pilot study, we demonstrated that the signal intensity on LGE-imaging cannot be used to quantify the extent of extracellular matrix expansion (Garg, Kidambi, Ripley, et al., 2015). Native (non-contrast) T1-maps are sensitive, among others, to myocardial oedema, protein deposition and changes in lipid/iron content (Moon et al., 2013); native T1 maps do not inform us however about the intra-/extra-cellular composition of the myocardium. Moreover, even though quantification of native T1 is highly reproducible, it varies between field strengths, vendor platforms and mapping sequences (Dabir et al., 2014). ECV is a measure of extracellular matrix expansion, which is adversely related to mechanical, electrical and vasomotor dysfunction (Moon et al., 2013). Hence, ECV-maps add incremental diagnostic value to quantify global/focal myocardial fibrosis, which is mainly a process in the extracellular matrix. Furthermore, ECV values are independent of the field strength of the CMR scanners.

### **6.5.2 ECV-mapping in acute and chronic myocardial infarction**

Previous studies have explored ECV in both acute and chronic myocardial infarction (Hammer-Hansen et al., 2016; Jablonowski et al., 2015; Ugander, Oki, et al., 2012; White et al., 2013). In a porcine model of acute myocardial infarction, Jablonowski et al demonstrated that LGE-imaging overestimated infarct size by 23% as compared to histopathological findings, and that this overestimation is due to higher ECV in the peri-infarct region, or the border-zone between necrosed and oedematous myocardium (Figure 6.5) (Jablonowski et al., 2015).



- Myocardial area at risk (AAR)  
Area above ECV of 33%
- Border-zone  
Area which is overestimated as infarct by acute LGE-imaging
- Infarct size at follow-up  
Area above ECV of 46%

*Figure 6.5 Short-axis illustration of the LV. This illustration demonstrates acute infarct size is overestimated by acute LGE-imaging. On ECV-maps, it is possible to differentiate three zones in the territory of AMI: the AAR, the border-zone (zone with extensive peri-infarct oedema and possible islets of cell injury, which recovers over-time) and the actual infarcted zone (necrosed myocardial tissue, which does not recover on follow-up).*

They reported that the ECV in this border-zone was significantly different to the ECV in the remainder of the AAR region ( $48.3 \pm 4.4\%$  vs.  $32.4 \pm 3.2\%$ ;  $P < 0.01$ ). The border-zone ECV in the present clinical study ( $38.6 \pm 2.4\%$ ) was lower than in this previous study even though we ran validation tests to define the ECV thresholds informed by their biopsy findings. This can potentially be explained by the fact that pigs were imaged far more acutely than our patient cohort (6hrs versus  $>24$ hrs). ECV in the border-zone drops very rapidly in the first few days post-acute myocardial infarction as oedema regresses (Jablonowski et al., 2015). In a more recent study, Hammer-Hansen and colleagues (Hammer-Hansen et al., 2016) demonstrated that the extent of gadolinium enhancement in acute myocardial infarction patients is modulated by the extracellular space and the contrast kinetics in the injured myocardium and consequently contributes to the over-estimation of IS by LGE-imaging. Another pertinent finding was that the ECV of the infarcted myocardium, computed using the different post-contrast T1-maps at different time points, ranging from 5-20 minutes after the contrast injection, remained similar. This may explain why ECV is more reliable to quantify the IS acutely versus the LGE-imaging, which heavily depends on timing of the acquisition post-contrast delivery.

Ugander et al explored the utility of ECV in chronic infarct patients and demonstrated significantly higher ECV ( $51 \pm 8\%$ ) in the infarct zone (Ugander, Oki, et al., 2012). Another key finding of their study was that remote myocardial ECV, where there was no hyper-enhancement on LGE-imaging, increased concurrently with a decrease in ejection fraction ( $r = -0.50$ ,  $P = 0.02$ ), suggesting that ECV provides insights into sub-clinical myocardial pathology. This study raises the possibility that the pattern of ECV in the infarcted and remote myocardium changes from the acute to the chronic setting.

More recently, in a study which recruited 131 acute STEMI patients, Carberry et al confirmed that remote zone ECV (assessed by ROI) is inversely related to ejection fraction ( $P < 0.001$ ) and delta-ECV of the remote zone was associated left ventricle volume at follow-up. Bulluck et al investigated the utility of automated segmental ECV in acute myocardial infarction and additionally demonstrated that patients with higher remote myocardial ECV on acute presentation were more likely to have adverse remodelling of their left ventricle. Moreover, recent evidence from our

group suggests that the actual expansion in the extracellular matrix of the infarct core quantified by ECV-maps predicts functional recovery better than any other imaging parameter (Kidambi et al., 2015). Therefore, post-acute myocardial infarction, ECV-maps measure the extent of damage within the infarct zone, while AAR and remote-zone predict the likelihood of functional recovery and adverse left ventricular remodelling.

The present study adds to this existing evidence and shows that acute ECV-maps offer a new quantitative thresholding tool to quantify both AAR/ IS reliably and accurately.

### **6.5.3 Limitations**

The present study has limitations. The sample size in the present study is not large, nevertheless is comparable to published research studies in this patient population and also inter-/intra-observer variations are very low for multi-parametric CMR. Of the 70 patients identified at initial recruitment, we managed to recruit 50 patients, possibly introducing a selection bias. Equilibrium contrast ECV estimation may be more exact for high ECV values than a bolus method (White et al., 2013); however, the bolus method used in this study can be more easily integrated into existing clinical protocols. The results from present study cannot be applied in not-acute infarct cases and non-ST elevation MI.

### **6.6 Conclusion**

This study demonstrates that ECV-maps in patients with acute reperfused STEMI permit reliable quantification of AAR and final IS at follow-up. Furthermore, acute IS by ECV-maps are independently associated with the number of non-viable infarcted segments at follow-up. Therefore, acute ECV-maps offer enhanced early tissue characterisation, quantification and clinically relevant prognostic information over standard LGE-imaging.

## **7 Study 5– Comparison of Acceleration Algorithms in Whole-Heart Four-Dimensional Flow for Cardiovascular Applications: Two-centre, 1.5T, Phantom and In-vivo Validation Study.**

### **7.1 Abstract**

#### **7.1.1 Aims**

Validation of four-dimensional (4D) flow CMR accelerated acquisition methods is needed to make it more robust for clinical applications. Our aim was to compare three widely-used acceleration methods in 4D flow CMR: 4D segmented fast-gradient-echo (4D-turbo-field-echo, 4D-TFE), 4D non-segmented gradient-echo with echo-planar imaging (4D-EPI) and 4D-k-t BLAST (Broad-use Linear Acquisition Speed-up Technique) accelerated TFE.

#### **7.1.2 Methods**

CMR was performed in two institutions (Leeds and Leiden) on identical 1.5T systems. Accelerated methods were compared in a phantom and 25 volunteers. In volunteers, the CMR protocol included: cines, 2D phase contrast (PC) at the aortic valve (AV) and mitral valve (MV) and three whole-heart free-breathing (no respiratory motion correction) 4D flow CMR sequences. Field-of-view, slices, phases (30), voxel size and VENC were the same for each subject. In volunteers, net acquisition time for each 4D flow sequence was recorded, as well as a visual grading of image quality on a four-point scale: 0, no artefacts to 3, non-evaluable.

#### **7.1.3 Results**

For the pulsatile phantom experiments, the mean error for 4D-TFE was  $4.9 \pm 1.3\%$ , for 4D-EPI  $7.6 \pm 1.3\%$  and for 4D-k-t BLAST  $4.4 \pm 1.9\%$ . In vivo, acquisition time was shortest for 4D-EPI at  $7\text{min}59\text{s} \pm 2\text{min}30\text{s}$ . 4D-EPI and 4D-k-t BLAST had minimal artefacts. For 4D-TFE, 40% of AV and MV assessments were non-evaluable because of phase dispersion artefacts. Peak velocity assessment using 4D-EPI demonstrated best correlation to 2D PC (AV:  $r=0.78$ ,  $p<0.001$ ; MV:  $r=0.71$ ,  $p<0.001$ ). Coefficient of

variability (CV) for net forward flow (NFF) volume was least for 4D-EPI (7%) (2D PC:11%, 4D-TFE: 29%, 4D-k-t BLAST: 30%, respectively).

#### **7.1.4 Conclusions**

Mean error for all 4D flow CMR sequences with respect to flow volume assessment were within reasonable limits for clinical applications. In vivo, 4D-EPI had the shortest acquisition time, best agreement with 2D PC, best internal consistency between MV and AV NFF and the lowest CV. 4D-k-t BLAST demonstrated significant underestimation of peak velocities, NFF and CV was poor. 4D-TFE was most susceptible to artefacts.

## **7.2 Introduction**

Four-dimensional flow cardiovascular magnetic resonance (4D flow CMR) is increasingly being used in clinical and research applications for complex aortic and intra-cardiac flow assessment. 4D flow CMR is essentially a three-dimensional phase-contrast magnetic resonance imaging (PC MRI) method with three-directional (3D) velocity encoding allowing post-hoc time-resolved 3D visualisation and retrospective quantification of blood flow at any location in a 3D volume. 4D flow CMR enables a wide variety of options for visualization and quantification of intra-cardiac flow, ranging from basic aspects such as flow volume and peak velocity to more complex analyses such as the estimation of hemodynamic effects at the vessel wall and myocardium, as well as visualization of flow pathways in the heart and great vessels (Dyverfeldt et al., 2015). Integrating 4D flow CMR in routine clinical protocols has been challenging in part due to long scan times (acquisition of 3D velocity encoded CMR data along all the three dimensions). Scan times can be reduced with numerous data acceleration methods, including radial under-sampling, k-t Broad Linear Acquisition Speed-up Technique (BLAST) (Philips), k-t Sensitivity encoding (SENSE) (Philips), generalised auto-calibrating partially parallel acquisitions (GRAPPA) (Siemens), echo-planar imaging (EPI), Iterative self-consistent parallel imaging reconstruction (L1-SPIRiT) and 5-point PC-vastly undersampled isotropic voxel radial projection imaging (VIPR) (General Electrics, GE Systems) (Baltes et al., 2005; Moftakhar et al., 2007; Stadlbauer et al., 2010; Lustig et al., 2007; Davis et al., 1994; Debatin et al., 1995; Zaman et al., 2015; Lustig and Pauly, 2010; Johnson and Markl, 2010).

With the use of accelerated acquisition methods free-breathing whole-heart 4D flow CMR can be performed in a total scan time of 5-10 minutes depending on size of the heart and patient habitus (Calkoen, Roest, et al., 2015; Calkoen, de Koning, et al., 2015; Zaman et al., 2015).

### **7.3 Acceleration methods**

For 4D flow CMR, three acceleration methods are widely available on the Philips systems: 4D-TFE, 4D-EPI and 4D-k-t BLAST.

A recently published consensus document recommends the use of fast gradient echo (4D-TFE, turbo field echo) pulse sequences for 4D flow CMR with a segmentation factor of 2 based on the experience of research institutions (Dyverfeldt et al., 2015). Retrospectively-gated, 4D-TFE is currently available as a product on Philips systems for intra-cardiac flow assessment.

Previous research work from our institution has demonstrated that demonstrated the reliability of intra-cardiac flow assessment using the respiratory navigated 4D-k-t BLAST acquisition (Zaman et al., 2015). However, this technique uses prospective ECG gating and does not acquire crucial flow data towards end-diastole.

Restrospectively gated, 4D-EPI has also been used by some research institutions to investigate clinical applications for this novel technique (Elbaz et al., 2014; Westenberg et al., 2008).

However, head-to-head validation of these three accelerated algorithms for whole-heart acquisition in clinical applications is needed for both clinical and research applications. Therefore, the aim of the present study was to 1) validate three commonly applied acceleration methods in 4D flow CMR: 4D turbo-gradient-echo (4D-TFE), 4D echo-planar imaging (4D-EPI) and 4D k-t BLAST (4D-k-t BLAST) in static and pulsatile flow phantoms, and 2) compare these three acceleration methods *in-vivo* in healthy volunteers for quality, consistency and reliability to quantify intra-cardiac flow velocity and volumes.

### **7.4 Methods**

The study was conducted across two centres, in Leeds, UK and Leiden.

#### **7.4.1 Static and pulsatile phantom**

Static and pulsatile flow phantom experiments were carried out at the Leiden University Medical Center using 48 ml diluted gadolinium based contrast agent (Dotarem, Guerbet, Gorinchem, The Netherlands) dissolved in 6 l water. The contrast agent had a concentration of 0.5 mmol/ml and relaxivity of  $3.4 \text{ mmol}^{-1} \cdot \text{l} \cdot \text{s}^{-1}$ ,

resulting in a theoretical T1 of 112 ms (Westenberg et al., 1999). A silicon tube with 1 cm luminal diameter was led through the wall of the MRI room towards the CMR machine. Static or pulsatile flow was applied from outside the MRI room, using a Sarns centrifugal pump which was connected to a Sarns Delphin power supply and a 3M Sarns control module (3M Health care, Borken, Germany) (Figure 7.1A). Approximately 3 meters supplying and 3 meter returning tube was required to led the flow in and out of the MRI room. The tube was placed inside a water tank, submerged under static water and positioned in the iso-center of the CMR gantry. In the static phantom setup, six static flows ranging from 2.52 l/min to 6.50 l/min were applied. Cardiac triggering was physiologically simulated by the scanner software at 120 beats/minute and for all 4D flow CMR and 2D PC CMR sequences, 10 cardiac phases were reconstructed. Next, six pulsatile flow settings were applied, ranging from 2.25 l/min to 5.20 l/min with a frequency of 61 cycles/minute. CMR triggering was realised by an external transistor-transistor-logic TTL trigger signal sent from the pump control unit to the MRI computer. For each acquisition, 30 phases were reconstructed, unless the required amount of data to be collected did not allow reconstruction of this many phases without making changes to the acceleration parameters (i.e. for 4D-k-t BLAST and 4D-TFE acquisition). In those cases, the maximal amount of reconstructed phases was selected and a 2D PC CMR acquisition was repeated with the same number of reconstructed phases.

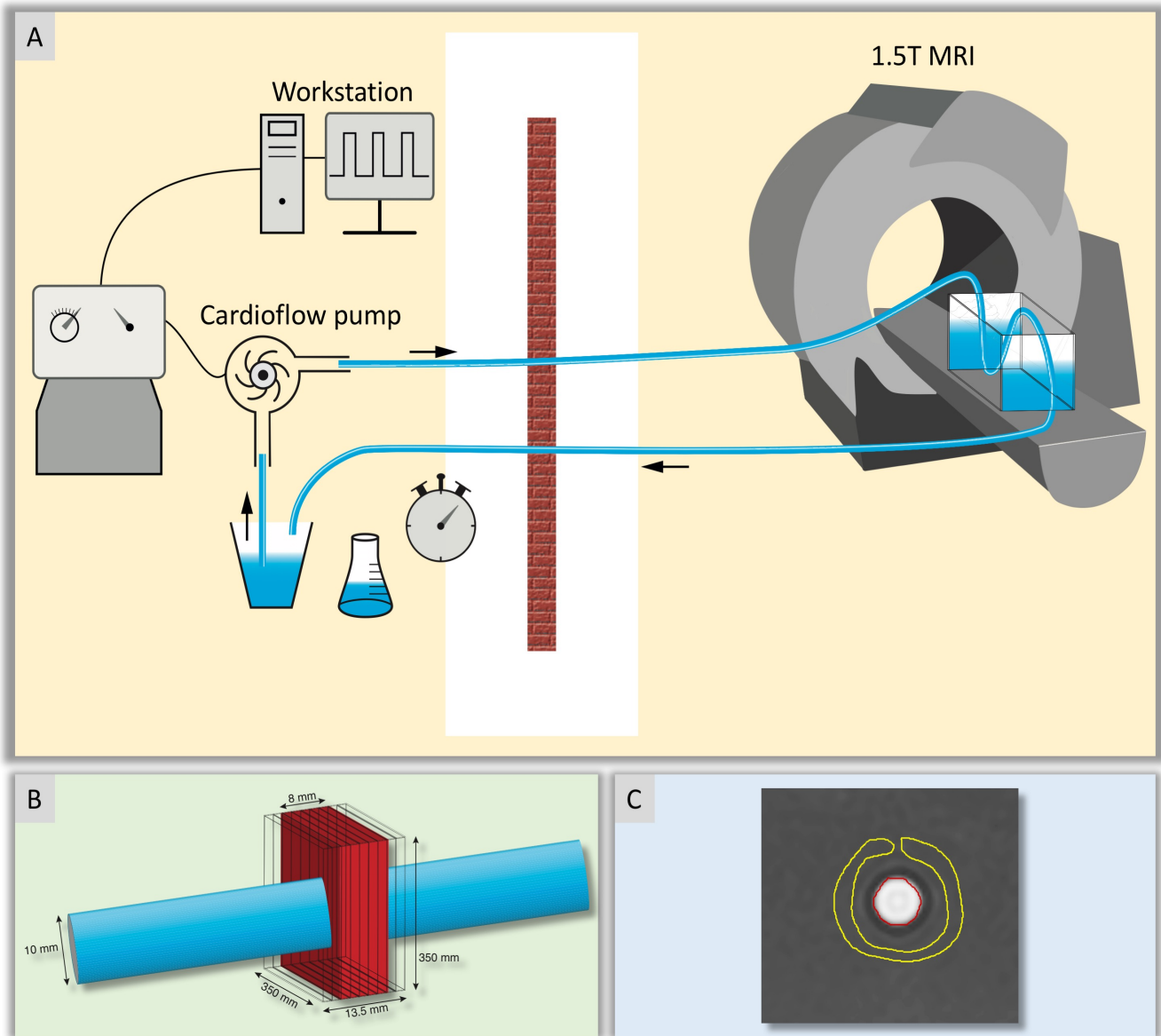


Figure 7.1 Phantom illustrations. Panel A: Illustration to demonstrate static and pulsatile flow phantom setup. Flow of water was applied by a computer controlled pump. For pulsatile flow, ECG triggering was controlled by the pump connected with the CMR computer. Flow of water was led through the wall to the CMR machine. A tank filled with static water was positioned in the iso-center of the magnet. The tube was led through the tank. The returning tube was led out of the CMR room through the wall. Distal to this returning tube, time beaker measurements were performed to calibrate flow volume. Panel B: Illustration to demonstrate the identical 3D volumes of the 4D flow CMR acquisitions covering 1.35 cm (i.e., 9 slices of 1.5 mm thickness each) of the tube. The 2D imaging plane of the 2D PC CMR positioned in the center

*of the 4D flow CMR volume. For all acquisitions, only through-plane flow velocity was analysed. Panel C: Example of contour definition in the velocity encoded images of the phantom. The yellow contour surrounding the cross-sectional lumen of the tube is used for background correction. The red contour segmenting the lumen, is a predefined circular ROI with a fixed 0.79 cm<sup>2</sup> area.*

In-plane resolutions for 2D PC and the three 4D flow sequences for the in-vitro setup were equal (1.5×1.5 mm<sup>2</sup>), and through-plane resolution for 4D flow was also 1.5 mm (i.e., isotropic data), but for 2D PC, slice thickness was 8 mm. Other scan parameters were equal to the in vivo acquisitions (see below). To minimize angulated flow, the tube was positioned straight in the scanner, parallel in feet-head direction with water flowing from feet to head. The 3D volumes of the 4D flow CMR acquisitions were identically planned (Figure 7.1B), covering 1.35 cm (i.e., 9 slices of 1.5 mm thickness each) of the tube, and with the 2D imaging plane of the 2D PC CMR positioned in the center of the 4D flow CMR volume (Figure 7.1B). For all acquisitions, only through-plane flow velocity was analysed.

Before and after each MRI acquisition, a time-beaker measurement was performed distal to the phantom, at the end of the returning tube (Figure 7.1A) where volumetric collection was performed for 30 seconds. The flow rate was determined by averaging both time-beaker measurements.

#### **7.4.2 Cardiac Magnetic Resonance Imaging**

All volunteers underwent CMR imaging on identical 1.5T systems at both sites (Ingenia, Philips, Best, The Netherlands).

The CMR protocol is detailed in Table 7.1.

CMR Protocol		
	Sequences	Details
1.	Survey	
2.	Cine images: 2ch, 3ch, 4ch, short-axis contiguous LV volume stack	
3.	2D PC flow: AV, MV	
4.	4D- k-t BLAST	Once FOV planned at step (4); exactly same used for step (5) and (6)  All three done with M.P.S. reconstruction pre-selected  Free-breathing
5.	4D-TFE	
6.	4D-EPI	
7.	End of CMR scan	Volunteer removed from magnet bore
8.	4D flow data reconstruction	Done on the raw data on scanning workstation
9.	End of protocol	

Table 7.1 CMR Protocol in healthy volunteers

Field of view (FOV), number of slices (35-40), phases (30), voxel size (isotropic;  $3 \times 3 \times 3 \text{mm}^3$ ) and maximum velocity encoding (VENC, 150cm/s) were kept the same for the three 4D pulse sequences for each subject. Flip angle was  $10^\circ$ , echo time (TE) and repetition time (TR) were selected as shortest and number of signal averages was 1. Free breathing was allowed during acquisition and no respiratory motion correction was used. For 4D-TFE and 4D-EPI accelerated techniques, retrospective electrocardiographic (ECG) gating was used and the 4D-k-t BLAST accelerated technique used prospective ECG-triggering. In 4D-TFE, TFE factor of 2 was used and in 4D-EPI, an EPI factor of 5 was used. 4D-k-t BLAST used 5-fold acceleration with 11 lines of training data in both the ky and kz directions. Net acquisition time for each of the 4D flow sequences was recorded during the scans. The 2D PC sequence was a segmented TFE method with 350mm field-of-view, in-plane acquisition resolution

2.5×2.5mm, slice thickness 8mm. TE and TR were shortest, flip angle 10°, number of signal averages was 2. A TFE factor of 4 was used. For both phantom data as well as in vivo data, gradient non-linearity correction and Maxwell correction were compensated by the CMR scanner. Remaining phase background errors (e.g. due to eddy currents) were corrected by background subtraction sampled near the area of interest. For phantom experiments, background correction was performed from a background ROI (indicated by the yellow contour in Figure 7.1C) enclosing the luminal ROI (indicated by the red contour) and for in vivo experiments from ROI positioned in myocardium.

### **7.4.3 Image analysis**

Image analysis of phantom data as well as in vivo cines, 2D PC flow quantification and 4D flow quantification was performed offline using MASS research software (Version 2016EXP, Leiden University Medical Center, Leiden, The Netherlands). For both static as well as pulsatile phantom measurements, an a priori circular-shaped luminal ROI was defined, static for all phases, with an area size imposed by the phantom specifications (i.e. 0.79 cm<sup>2</sup>). This ROI was manually placed on the first phase of a time series and copied to subsequent phases. For all phantom 4D flow data sets, image analysis was performed for the three center slices and measurements were averaged among the three samples.

For each 4D flow CMR sequence, quality checks were performed by J.J.M.W., an experienced researcher in this field of CMR with greater than 15 years' experience. Visual grading of image quality was done on a four-point scale: 0; no artefacts present, 1; good quality but with some blurring artefacts on magnitude images but none on velocity images, 2; moderate quality with substantial blurring on both magnitude and velocity images, 3; severe artefacts with phase dispersion on the velocity images present in the region of interest, leading to non-evaluable data.

In volunteers, valvular stroke volumes (SV) at the mitral valve (MV) and the aortic valve (AV) were calculated using validated techniques including retrospective valve tracking, with measurement planes positioned perpendicular to the inflow direction on 2- and 4-chamber cines (Roes et al., 2009). Contour segmentation was performed manually. Peak velocities at AV (peak systolic) and MV (early filling phase) were

obtained from reformatted planes with identical orientation and position as the static 2D PC MRI planes. Background correction was used from the velocity sampled in the myocardium and phase unwrapping was performed on source images when aliasing occurred in the area of interest.

#### **7.4.4 Statistical analysis**

To investigate linear correlation between two methods, Pearson's correlation statistics was used to derive correlation coefficient ( $r$ ) and its significance. Agreement between two methods was expressed as bias according to Bland-Altman analysis. All statistical tests were 2-tailed;  $p$  values  $<0.05$  were considered significant.

### **7.5 Results**

#### **7.5.1 Phantom Experiments**

The mean error in flow volume assessment (compared to time beaker measurements) for the 2D PC sequence was  $-0.8 \pm 1.2\%$  ( $p=0.22$ ) for the static experiments and  $-1.0 \pm 1.1\%$  ( $p=0.001$ ) for the pulsatile experiments. For static experiments, the mean error for 4D-TFE was  $-5.2 \pm 1.1\%$  ( $p=0.003$ ), for 4D-EPI  $-7.1 \pm 1.9\%$  ( $p=0.001$ ) and for 4D-k-t BLAST  $-4.9 \pm 3.8\%$  ( $p=0.03$ ). For the pulsatile experiments, the mean error for 4D-TFE was  $-4.9 \pm 1.3\%$  ( $p=0.002$ ), for 4D-EPI  $-7.6 \pm 1.3\%$  ( $p<0.001$ ) and for 4D-k-t BLAST  $-4.4 \pm 1.9\%$  ( $p=0.008$ ). For these measurements, the mean error (compared to the 2D PC acquisition) in peak velocity assessment for 4D-TFE was  $-3.2 \pm 1.2\%$  ( $p<0.001$ ), for 4D-EPI  $-5.3 \pm 2.2\%$  ( $p=0.01$ ) and for 4D-k-t BLAST  $-8.8 \pm 2.3\%$  ( $p<0.001$ ).

#### **7.5.2 Healthy Volunteers**

Twenty-five ( $n=25$ , 11 at Leeds, 14 at Leiden) healthy volunteers were recruited for the in-vivo study. We recruited only adult volunteers (age greater than 18-years old) for this study.

Baseline volunteer demographics and CMR parameters are detailed in Table 7.2. 17 (68%) of the volunteers were male and the mean age of all volunteers was  $38 \pm 14$  years. There were no significant differences in characteristics between volunteers from Leeds and Leiden.

	All (n=25)	Leiden (n=14)	Leeds (n=11)	p-value
<b>Age, years</b>	37.6±14.5	38±14.7	38.9±14.7	0.61
<b>Male</b>	17(68%)	10 (71%)	7 (64%)	0.69
<b>Weight, kg</b>	76±13	76.6±14	75.5±12	0.83
<b>Height, cm</b>	171±8	173±7	169±8	0.15
<b>Heart rate, bpm</b>	63±9	63±10	63±9	0.94
<b>LVEDV<sub>i</sub>*, ml/m<sup>2</sup></b>	90.4±16.6	90.4±2	90.5±12.3	1
<b>LVESV<sub>i</sub>†, ml/m<sup>2</sup></b>	34.4±11	35.2±13.4	33.3±7.5	0.66
<b>SV<sub>i</sub>, ml/m<sup>2</sup></b>	56±8	55±8	57±8	0.55
<b>LV Mass<sub>i</sub>, g</b>	53.6±10.5	54±12	53±9	0.88
<b>Ejection Fraction, %</b>	63±6	62±6.7	63±5	0.62
<b>Mitral Regurgitation fraction, % (number of volunteers)</b>	1.6±1.4 (18)	2±2 (11)	1±1(7)	0.17
<b>Aortic Regurgitation fraction, % (number of volunteers)</b>	0.6±1 (9)	0.9 (7)	1.1 (2)	0.20

Table 7.2 Demographics and CMR scan parameters. Values are mean ± SD. LV measurements are indexed to body surface area (BSA). \*LV EDV<sub>i</sub>; Left ventricular end diastolic volume (indexed), †LV ESV<sub>i</sub>; Left ventricular end systolic volume (indexed), SV Stroke volume.

### 7.5.3 Acquisition time and image quality assessments

The acquisition time was shortest for 4D-EPI and it was statistically significantly shorter than for 4D-TFE (7min59s±2min30s versus 9min8s±2min46s, p<0.01). Even though the acquisition time for 4D-k-t BLAST was not statistically different to 4D-EPI (7min59s±2min30s versus 8min50s±2min46s; p=0.29), it was on average almost 1-minute longer. Image quality across mitral and aortic flows was similar for 4D-EPI and 4D-k-t BLAST (MV; p=0.43 and AV; p=0.16) (Figure 7.2 and 7.3). However, 4D-TFE acquisition was of inferior quality when compared to 4D-EPI (MV; p<0.001 and AV; p<0.001) and 4d-k-t BLAST (MV; p<0.001 and AV; p<0.001). Additionally, 10

(40%) 4D-TFE mitral and aortic flows were of very poor quality rendering their analysis impossible.

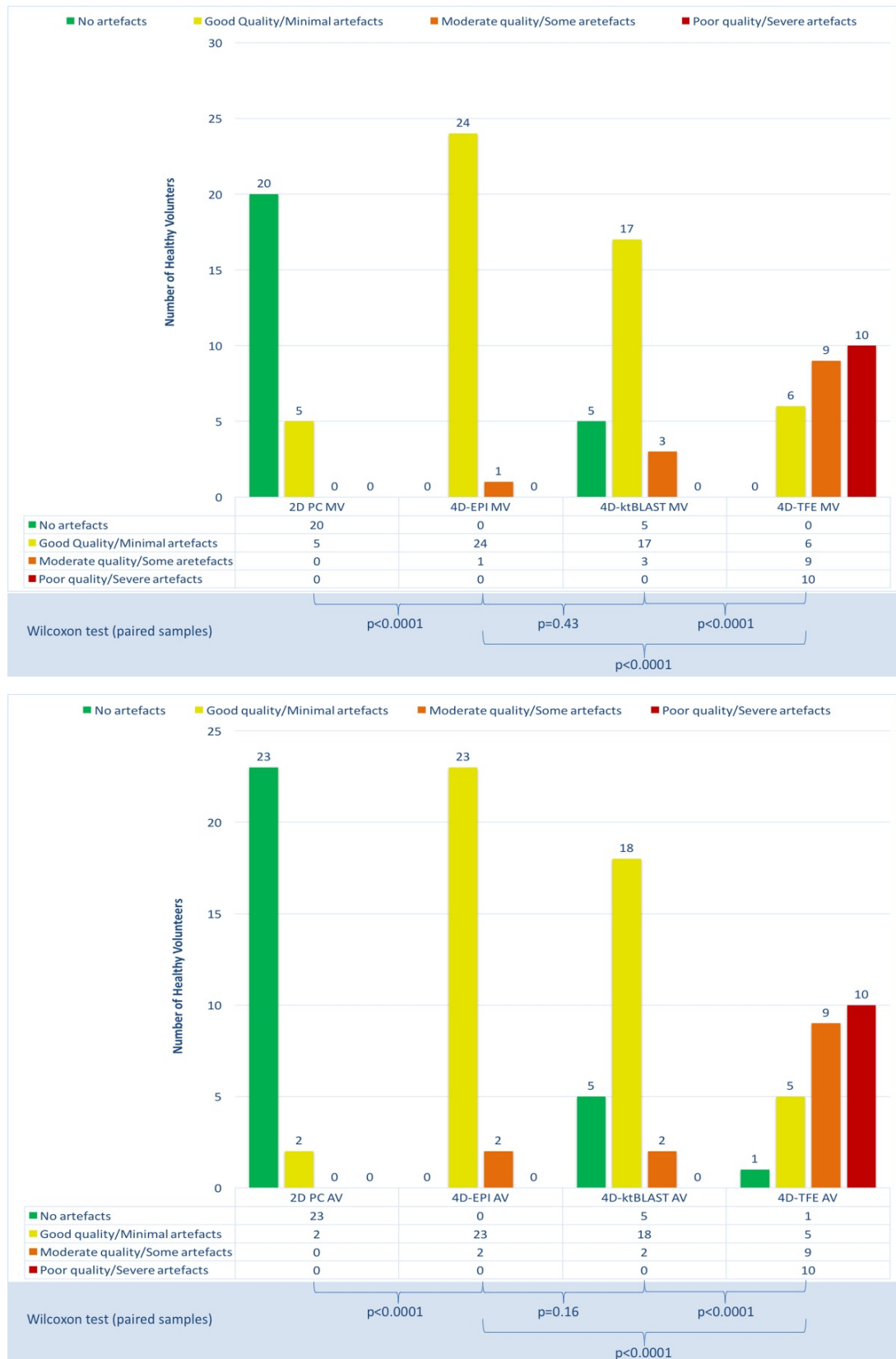


Figure 7.2 Image quality of mitral and aortic valve flow acquisitions.

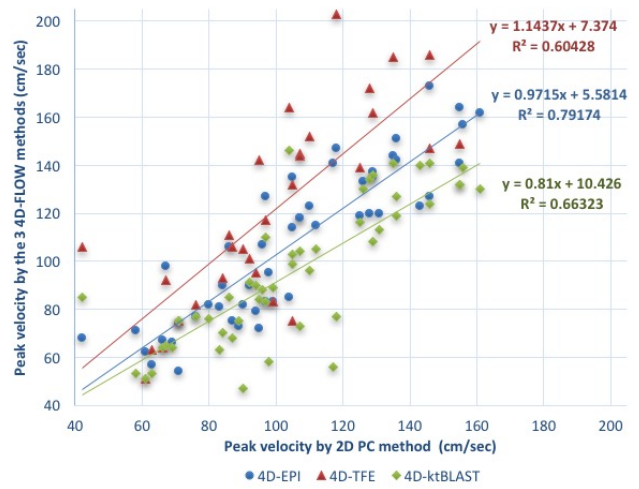
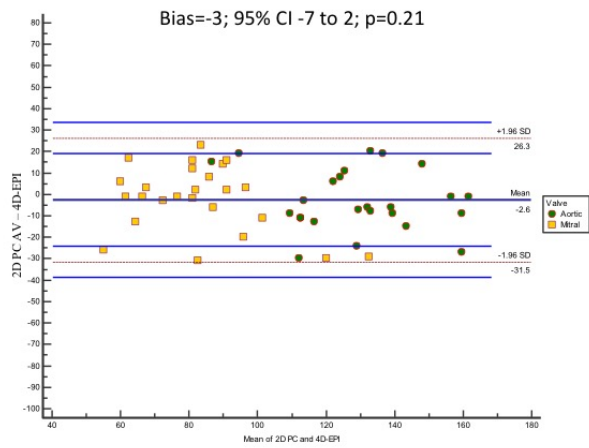
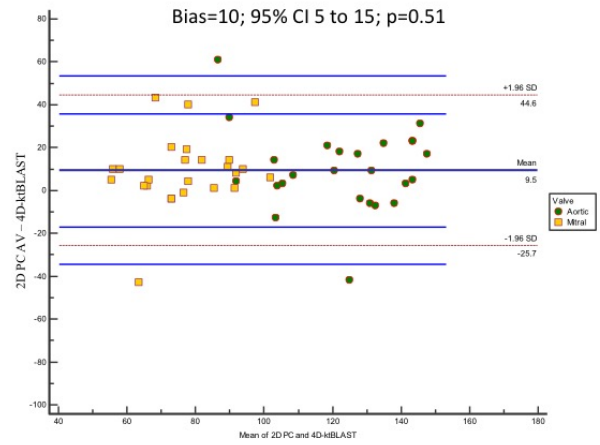
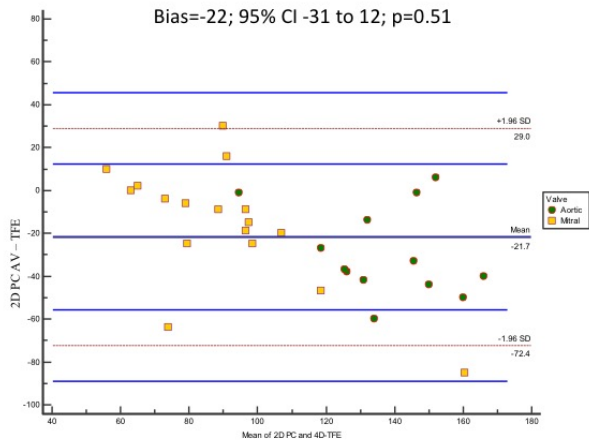


Figure 7.3 Bland Altman and scatter plots analysis for the assessment of peak velocity.

## **7.5.4 Intra-cardiac peak velocity assessment**

### **7.5.4.1 Mitral Valve inflow**

Peak MV early diastolic inflow velocity (E) by 4D-EPI demonstrated good correlation to 2D PC acquisition ( $r=0.71$ ,  $p=0.001$ ) whereas 4D-TFE derived E-velocity had modest correlation ( $r=0.59$ ,  $p=0.01$ ). 4D-k-t BLAST derived E-velocity demonstrated the poorest correlation ( $r=0.42$ ,  $p=0.03$ ).

### **7.5.4.2 Aortic Valve outflow**

Peak systolic AV outflow velocity by 4D-EPI demonstrated best correlation to 2D PC acquisition method ( $r=0.78$ ,  $p<0.001$ ). 4D-TFE and 4D-k-t BLAST demonstrated modest correlation to 2D PC acquisition (4D-TFE:  $r=0.56$ ,  $p=0.04$ ; 4D-k-t BLAST:  $r=0.59$ ,  $p=0.002$ ) (Table 7.3).

Peak velocity assessment for both MV and AV by 4D-EPI demonstrated best correlation to the reference 2D PC acquisition (4D-EPI:  $r=0.89$ ,  $p<0.001$ ; 4D-TFE:  $r=0.78$ ,  $p<0.001$ ; 4D-k-t BLAST:  $r=0.81$ ,  $p<0.001$ ) (Figure 7.3). The overall bias for peak velocity assessment was lowest for 4D-EPI (-2 cm/s, 95% CI -7 to 2 cm/s;  $p=0.21$ ) with a CV of 9.8%. The other acquisition methods demonstrated significant bias and CV (4D-k-t BLAST: bias=10 cm/s, 95% CI 5 to 15 cm/s;  $p<0.001$  and CV 14.3%, 4D-TFE: bias=-22 cm/s, 95% CI -31 to 12 cm/s;  $p<0.001$  and CV 21.4%) (Table 7.3) (Figure 7.3).

	Mean	SD	Pearson's Correlation (r value, p- value)	Bias (95% CI)	Paired Student T-Test (p-value)	CV (%)
<b>Net Forward Flow (ml)</b>						
2D PC AV	95.3	18.0	0.83, p<0.001	-9.16	<0.01	11
2D PC MV	104.5	19.8		(-14 to -4)		
4D-TFE AV	85.5	16.2	0.58, p=0.02	-5	0.28	29
4D-TFE MV	89.2	20.1		(-14 to 4)		
4D-EPI AV	91.0	18.2	0.94, p<0.001	-2	0.14	7
4D-EPI MV	93.0	17.3		(-5 to 1)		
4D-k-t BLAST AV	82.6	15.2	0.57, p=0.003	12	<0.01	20
4D-k-t BLAST MV	70.5	17.6		(6 to 18)		
<b>Peak velocity (cm/s)</b>						
2D PC AV	127.6	19.6	...	...	...	...
2D PC MV	81.7	17.2	...	...	...	...
4D-TFE AV	151.7	23.9	0.56, p=0.04	-22	<0.001	21.4
4D-TFE MV	98.2	35.2	0.59, p=0.01	(-31 to 12)		
4D-EPI AV	130.7	22.1	0.78, p<0.001	-2	0.21	9.8
4D-EPI MV	83.8	22.0	0.71, p<0.001	(-7 to 2)		
4D-k-t BLAST AV	117.8	22.4	0.59, p=0.002	10	<0.001	14.3
4D-k-t BLAST MV	72.6	13.8	0.42, p=0.03	(5 to 15)		

*Table 7.3 Consistency and variability of mitral and aortic flow measurements. Abbreviations: 2D, two-dimensional; 4D-EPI, four-dimensional echo planar imaging; 4D-k-t BLAST, four-dimensional kt-Broad-use Linear Acquisition Speed-up Technique; 4D-TFE, four-dimensional turbo field echo; AV, aortic valve; MV, mitral valve.*

### **7.5.5 Consistency of flow volume assessment**

Net forward flow (NFF) (or effective stroke volume) through the MV and AV correlated best for 4D-EPI with lower correlation for the other 4D acquisition methods and 2D PC (4D-EPI:  $r=0.94$ ,  $p<0.001$  versus 2D PC:  $r=0.83$ ,  $p<0.001$  versus 4D-TFE:  $r=0.58$ ,  $p=0.02$  versus 4D-k-t BLAST:  $r=0.57$ ,  $p=0.003$ ) (Figure 7.4). Bias for NFF between the valves was significant for 2D PC (bias=-9 ml, 95% CI -14 to -4 ml;  $p<0.01$ ) and 4D-k-t BLAST (bias=12 ml, 95% CI 6 to 18 ml;  $p=0.01$ ) acquisitions (Table 7.3). Bias and CV for the NFF were lowest for the 4D-EPI (bias=2 ml, 95% CI -5 to 1 ml;  $p=0.135$ ; CV=7%;). The CVs were very high for the 4D-k-t BLAST (20%) and the 4D-TFE (29%) acquisitions.

	Mean	SD	Paired Student T-Test compared to 2D PC	Paired Student T-Test compared to 4D-EPI
<b>2D Phase Contrast</b>				
E, cm/s	81.7	17.2	...	...
A, cm/s	48.8	9.6	...	...
E volume, ml	77.8	17.8	...	...
A volume, ml	25.00	6.7	...	...
E/A	1.8	0.6	...	...
PEFR, ml/s	602.7	150.9	...	...
PLFR, ml/s	300.8	77.2	...	...
<b>4D-TFE</b>				
E, cm/sec	112.3	26.4	0.000	<0.001
A, cm/sec	69.4	24.4	0.003	<0.001
E volume, ml	67.8	16.9	0.004	0.549
A volume, ml	22.3	6.5	0.051	0.321
E/A	1.8	0.5	0.725	0.052
PEFR, ml/s	494.7	127.1	0.000	0.368
PLFR, mL/s	277.5	71.5	0.148	0.253
<b>4D-EPI</b>				
E, cm/s	90.0	21.4	0.035	...
A, cm/s	48.4	11.8	0.861	...
E volume, ml	69.7	15.3	0.012	...
A volume, ml	21.9	6.3	0.012	...
E/A	1.9	0.6	0.057	...
PEFR, ml/sec	508.1	99.5	0.001	...
PLFR, ml/sec	269.6	80.5	0.043	...
<b>4D-k-t BLAST</b>				
E, cm/s	73.1	13.2	0.041	<0.001
E volume, ml	66.6	17.4	0.007	0.366
PEFR, ml/s	414.6	116.6	<0.001	<0.001

*Table 7.4 Diastolic flow assessment using all acceleration methods.*

*2D PC acquisition was assessed in fixed plane and the 4D flow techniques were assessed using retrospective valve tracking for flow quantifications.*

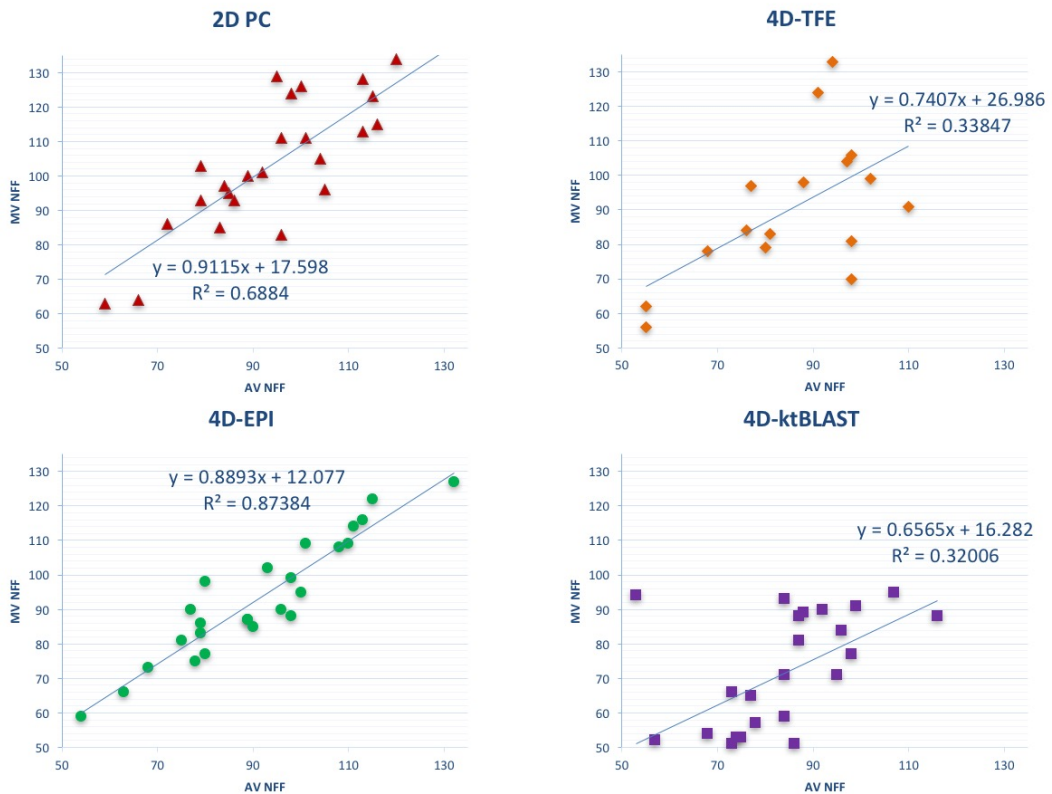


Figure 7.4 Scatter plots of net forward flow (NFF) through the mitral and aortic valve.

### 7.5.6 Diastolic flow assessment

Assessment of diastolic function parameters from the transmitral flow-time curves using 2D PC acquisition with static plane differed significantly to retrospective valve tracking assessment for all the three 4D flow acquisitions (Table 7.4). The mean peak E velocity was significantly higher for 4D-EPI than for 2D PC acquisition ( $90 \pm 21 \text{ cm/s}$  versus  $82 \pm 17 \text{ cm/s}$ ;  $p=0.03$ ). The mean peak E velocity was lowest for 4D-k-t BLAST at  $73 \pm 13 \text{ cm/s}$ .

Overall, there were no significant differences in E/A ratio between different methods (2D PC versus 4D-EPI;  $p=0.06$  and versus 4D-TFE;  $p=0.72$ , 4D-EPI versus 4D-TFE,  $p=0.05$ ). Because of the use of prospective ECG triggering and the consequent lack of data for the full cardiac cycle, 4D-k-t BLAST could not estimate peak late diastolic mitral inflow (A) velocity.

## **7.6 Discussion**

The present study, involving in vitro and in vivo experiments to investigate robustness, accuracy and applicability of accelerated methods of 4D flow CMR for whole-heart imaging and valvular flow assessment demonstrated the following: 1) When comparing three previously used acceleration methods for 4D flow CMR acquisition, 4D-EPI requires the shortest acquisition time versus segmented fast-gradient echo (TFE) and k-t BLAST acceleration, and 4D-EPI results in adequate image quality for analysis. 2) In phantoms, 4D-EPI showed the largest error in in-vitro flow and velocity assessment, but errors were small and within clinically acceptable margins of less than 10%. 4) In-vivo, 4D-EPI demonstrated best correlation and least bias for intra-cardiac peak velocities to the reference method of 2D PC acquisition and 4) 4D-EPI demonstrated the best agreement between aortic valve net forward flow and mitral valve net forward flow and therefore, showed highest internal consistency.

4D flow CMR has evolved in recent years as a clinical application for evaluating intra-cardiac flow. The use of modern data acceleration methods to speed up data acquisition in particular has allowed a wider application of this technique in clinical research studies. Several studies have investigated accelerated methods for flow assessments (Hsiao et al., 2015; Frydrychowicz et al., 2013; Tariq et al., 2013; Westenberg et al., 2008; Roes et al., 2009; Wentland et al., 2013; Hanneman et al., 2014; Nett et al., 2012; Roldán-Alzate et al., 2013; Brix et al., 2009). These studies have not only used different accelerated methods, but also different flow-encoding schemes (symmetric, asymmetric, Hadamard 4-point encoding, 5-point-encoding or multipoint encoding), different field strengths (mainly 1.5T or 3T systems), different scan parameters (FOV, spatio-temporal resolution etc.) and not necessarily with intra-cardiac assessment for quality and consistency of flow. Vendor-specific accelerated algorithms have been investigated by several research groups to investigate consistency and reliability of intra-cardiac flow assessment using 4D flow CMR. One of these studies used GRAPPA (Hanneman et al., 2014), three studies used EPI (Brix et al., 2009; Westenberg et al., 2008; Roes et al., 2009), two studies L1-

SPIRiT (Hsiao et al., 2015; Tariq et al., 2013), two studies compared k-t BLAST acceleration and TFE (SENSE) acceleration (Carlsson et al., 2011; Zaman et al., 2015) and one study used TFE (SENSE) (Kanski et al., 2015). As far as we know, a direct comparison between acceleration algorithms with respect to robustness, reliability and applicability of 4D flow CMR has not been published. The consensus statement recently published recommends the use of segmented fast-gradient echo (TFE) methods combined with 2-fold parallel imaging (SENSE) (Dyverfeldt et al., 2015). We compared this approach with two other acceleration techniques, EPI and k-t BLAST, which have also been widely used in clinical research studies. In vitro validation showed that 2D PC was very accurate with respect to flow volume assessment, presenting an error of 1%. All 4D flow CMR assessments showed a significant underestimation of flow volume, with EPI presenting the highest error (7%) compared to TFE and k-t BLAST (5%). These errors, while being statistically significant, are all within clinically acceptable margins of less than 10%.

Our in-vivo results showed, as expected, substantial bias for internal flow consistency between AV and MV flow 2D PC CMR, as the acquisition plane in this approach remains fixed during the acquisition and MV flow volume is overestimated compared to AV flow. This is in agreement with previously published results (Roes et al., 2009; Westenberg et al., 2008). Furthermore, internal consistency was poor for 4D-k-t BLAST, as this acquisition uses prospective triggering and as a result, part of diastole is missing resulting in an underestimation of MV flow volume. In line with previously published results (Roes et al., 2009; Westenberg et al., 2008), internal consistency was high for 4D-EPI in our in vivo studies. 4D-TFE showed more variation and less correlation, and therefore had a poorer overall performance than 4D-EPI. Also, direct assessment of peak velocity for 4D-EPI was in good agreement with 2D PC, while the other two techniques showed substantial bias, moderate agreement and higher variation.

Initial studies using 4D-k-t BLAST demonstrated underestimation of flow because of time blurring issues with prospective gating (Carlsson et al., 2011). Zaman et al. demonstrated that using contemporary coil systems, this can be mitigated and reliable peak velocity and stroke volume assessment can be made using respiratory navigated 4D-k-t BLAST acquisition (Zaman et al., 2015). However, our study

contradicts this, and again motivates the concern initially raised by Carlsson et al that 4D-k-t BLAST demonstrated underestimation of flow in-vivo (Carlsson et al., 2011). Zaman et al. used respiratory navigation for all their accelerated algorithms, however, the present study did not use respiratory navigation. Hence, the underestimation of flow velocities and poor CV in the present study may be due to the 4D-k-t BLAST acquisition being more susceptible to respiratory artefacts because of under sampling in k-space and temporal window. Additionally, Zaman et al. did not investigate mitral inflow which has an important role for intra-cardiac diastolic and multi-parametric 4D flow assessments. It would be plausible to imply that without respiratory navigation; 4D-k-t BLAST is not suitable for intra-cardiac flow quantification.

Prospectively ECG-triggered GRAPPA and more advanced kt-GRAPPA have been validated for their reliability for the assessment of aortic and pulmonary flows (Hanneman et al., 2014; Schnell et al., 2014). As these are prospectively triggered accelerated methods of acquisition, they also have temporal blurring similar to 4D-k-t BLAST and hence their reliability to quantify intra-cardiac diastolic flow indices may be questionable.

More recently, Petersson et al. demonstrated that retrospectively gated intracardiac 4D flow MRI can be sped up without the use of accelerated algorithms using respiratory navigated spiral trajectories (Petersson et al., 2016). This method does not compromise in spatio-temporal windows and demonstrates reliability and consistency for intracardiac flow quantification including diastolic inflow indices. However, mean scan times for this spiral acquisition in their study were higher ( $13 \pm 3$  minutes) than the most reliable accelerated technique in the present study, 4D-EPI ( $8 \pm 2$  minutes), most likely because Petersson used respiratory navigation. Moreover, the present study, which was done without respiratory navigation, demonstrated similar robust linear correlation between NFF through the mitral and aortic valves (this study:  $r^2=0.87$  versus Petersson study:  $r^2=0.90$ ).

### **7.6.1 Limitations**

The in-vitro validation of the various 2D and 4D flow acquisition techniques was performed using a straight tube with a laminar flow, creating idealized flow

conditions. The use of a more realistic heart phantom model would provide more complex intra-cardiac flow patterns that would probably give more insight in the performance of the various CMR flow acquisition techniques under more physiological conditions.

In this study all healthy volunteers had very stable resting heart rates of  $63\pm 9$  beats per minute (bpm). Additionally, the present study did not investigate the relative performance of the methods in the presence of minor arrhythmias (sinus arrhythmias, isolated ventricular ectopics etc.). Additionally, even though we tried to keep all acquisitions parameters similar for the three 4D flow methods, occasionally, one method would need slight adjustment of the field of view, the number of slices or phases.

## ***7.7 Conclusion***

Of the three 4D flow CMR methods tested, 4D-EPI demonstrated the least susceptibility to artefacts, good image quality, modest agreement with the current reference standard for peak intra-cardiac velocities and the highest consistency of intra-cardiac flow quantifications. We recommend 4D-EPI acceleration method for future clinical and research applications on 1.5 Tesla scanners.

## **8 Final Conclusions**

Multi-parametric tissue characterisation by CMR is a well-established to guide the diagnosis in patients presenting with acute chest pain. There is increasing evidence that CMR can provide accurate quantification of LV longitudinal function and myocardial deformation in both health and disease. Detection of reduced LV longitudinal function has both diagnostic and prognostic potential that has until now primarily been used in research but in the coming years will likely be integrated into clinical practice.

In this thesis, we have used tissue characterisation by T2W, T2\*, T1-mapping, EGE and LGE to detect alterations in myocardial tissue composition and also define how this affects myocardial deformation. We have also developed methods to quantify AAR and IS by acute ECV-maps in STEMI patients. In the last chapter, we aimed to investigate and validate different acceleration methods for 4D flow CMR whole-heart clinical applications. To pursue with research work on this thesis we have carried out CMR studies on a wide range of subjects including patients with acute STEMI, suspected CAD and asymptomatic healthy volunteers.

The main findings were:

### ***8.1 Effect of MVO/ IMH on Myocardial Deformation***

- i. Longitudinal LV function measured by averaged MAPSE on CMR is strongly associated with the presence of MVO and IMH
- ii. The size of MVO adversely affects averaged MAPSE
- iii. Myocardial deformation imaging by CMR reliably detects changes in acute infarct patients versus healthy controls
- iv. The presence of MVO or IMH in acute reperfused STEMI is most strongly associated with GLS
- v. GLS showed modest association with adverse LV remodelling

## **8.2 Effect of Myocardial Hyperaemia on Myocardial deformation**

- i. At peak myocardial hyperaemia GLS is reduced in patients with perfusion defects on simultaneously acquired first-pass perfusion CMR
- ii. Among several strain parameters tested, stress GLS is most strongly associated with the presence of a perfusion defect
- iii. A cut-off value of -19.8% for stress GLS demonstrates 77% sensitivity and 73% specificity for the presence of a perfusion defect

## **8.3 Quantification of AAR and IS by ECV-maps**

- i. Acute ECV-maps offer a robust and reliable alternative to acute T2w-imaging and T1-maps to quantify the AAR (at an ECV threshold of 33%)
- ii. Acute ECV-maps offer a robust and reliable alternative to acute LGE-imaging to quantify the final IS at follow-up (at an ECV threshold of 46%)
- iii. ECV-maps are superior to acute LGE-imaging in terms of agreement with final IS
- iv. IS quantified by ECV-maps is strongly associated the number of non-viable segments at 3-months follow-up

## **8.4 Validation of whole-heart 4D Flow CMR acceleration methods**

- i. 4D-EPI showed the largest error in in-vitro flow and velocity assessment, but errors were small and within clinically acceptable margins of less than 10%
- ii. 4D-EPI requires the shortest acquisition time versus segmented fast-gradient echo (TFE) and k-t BLAST acceleration
- iii. 4D-EPI demonstrated best correlation and least bias for intra-cardiac peak velocities to the reference method of 2D PC acquisition
- iv. 4D-EPI demonstrated the best agreement between aortic valve net forward flow and mitral valve net forward flow and therefore, showed highest internal consistency

## **8.5 Future directions**

The work in this thesis informs potential future studies.

### **8.5.1 Myocardial deformation in coronary artery disease**

In this thesis, we have demonstrated that CMR feature tracking derived longitudinal functional parameters of the left ventricle such as GLS are associated with pathologies predominantly in the sub-endocardium and could be used as a surrogate imaging markers.

Post-STEMI, bedside echocardiography remains the first-line non-invasive imaging modality. Strain imaging packages have become standard plug-ins provided by all vendors and allow rapid bedside assessment of GLS. Data from thesis suggest that post STEMI, GLS can inform on the likelihood of MVO or IMH. These patients can then be offered CMR to clarify the diagnosis. Importantly, even though both MVO and IMH are poor prognostic markers specific target treatments are still lacking and future research should be directed at this clinical problem.

In patients with suspected CAD, rest-GLS and stress-GLS offer an additional tool to identify patients with significant coronary disease. Future studies, with angiographic fractional flow reserve as the reference standard are needed to investigate the incremental value of strain imaging over first-pass perfusion CMR and whether it can improve the sensitivity and specificity for the diagnosis of CAD. We speculate that if this was proven, it would further enhance the diagnostic accuracy of equivocal first-pass perfusion cases.

### **8.5.2 ECV-maps in acute myocardial infarction**

In this thesis, we have demonstrated that using semi-automated thresholding applied to ECV-maps can be used to quantify AAR and IS. ECV thresholds of 33% and 46% proved to be accurate post-acute infarction for AAR and final infarct size. Furthermore, there is a growing body of literature that ECV maps add incremental diagnostic benefit in acute chest pain syndromes (Haaf et al., 2016). In this thesis, we only investigated functional recovery as an outcome measure. Future studies investigating incremental benefit of using ECV maps in infarct patients should

explore additional clinical outcomes including adverse LV remodelling and hard clinical end-points including short-term and long-term cardiovascular mortality.

### **8.5.3 Whole heart 4D flow**

Current two-dimensional methods of blood flow quantification cannot fully assess the complex, three-dimensional and multi-directional nature of intra-cardiac flow. Examining these intricate fluid dynamics has the potential to further our understanding of the principles of cardiovascular health and disease.

In this thesis, we demonstrated that 4D flow using EPI is the most robust and reliable acceleration method for whole-heart flow assessment using a free-breathing sequence with scanning times of 5-8 minutes, suggesting potential for clinical application in both stable and more acute scenarios. Whole heart 4D flow has several advantages over echocardiography or even 2D PC acquisitions. These primarily include: both right and left ventricular flow can be investigated for 'same averaged cardiac cycles', using retrospective valve tracking, accurate stroke volume and regurgitation volumes can be computed and it allows for 3D flow visualisation including vortex formation within cardiac chambers. While this thesis demonstrated feasibility of the method, larger, hypothesis driven clinical studies using 4D flow parameters against standard flow parameters are warranted.

We speculate that 4D flow derived quantitative flow parameters will provide very accurate and precise quantification of intra-cardiac flow indices in routine clinical practice in the near future.

## References

- Abdel-Aty, H., Cocker, M., Meek, C., Tyberg, J. V and Friedrich, M.G. 2009. Edema as a very early marker for acute myocardial ischemia: a cardiovascular magnetic resonance study. *Journal of the American College of Cardiology*. **53**(14),pp.1194–201.
- Abdel-Aty, H., Katus, H.A., Lehrke, S. and Steen, H. 2012. CMR derived MAPSE and TAPSE Measurements in hypertrophic cardiomyopathy: comparison to healthy volunteers. *Journal of Cardiovascular Magnetic Resonance*. **14**(Suppl 1),p.P168.
- Abdel-Aty, H., Zagrosek, A., Schulz-Menger, J., Taylor, A.J., Messroghli, D., Kumar, A., Gross, M., Dietz, R. and Friedrich, M.G. 2004. Delayed enhancement and T2-weighted cardiovascular magnetic resonance imaging differentiate acute from chronic myocardial infarction. *Circulation*. **109**(20),pp.2411–6.
- Afonso, L., Kondur, A., Simegn, M., Niraj, A., Hari, P., Kaur, R., Ramappa, P., Pradhan, J., Bhandare, D., Williams, K.A., Zalawadiya, S., Pinheiro, A. and Abraham, T.P. 2012. Two-dimensional strain profiles in patients with physiological and pathological hypertrophy and preserved left ventricular systolic function : a comparative analyses. *BMJ*. **2**(4),pp.1–9.
- El Aidi, H., Adams, A., Moons, K.G.M., Den Ruijter, H.M., Mali, W.P.T.M., Doevendans, P.A., Nagel, E., Schalla, S., Bots, M.L. and Leiner, T. 2014. Cardiac magnetic resonance imaging findings and the risk of cardiovascular events in patients with recent myocardial infarction or suspected or known coronary artery disease: a systematic review of prognostic studies. *Journal of the American College of Cardiology*. **63**(11),pp.1031–45.
- Aletras, A.H., Tilak, G.S., Natanzon, A., Hsu, L.-Y., Gonzalez, F.M., Hoyt, R.F. and Arai, A.E. 2006. Retrospective determination of the area at risk for reperfused acute myocardial infarction with T2-weighted cardiac magnetic resonance imaging: histopathological and displacement encoding with stimulated echoes (DENSE) functional validations. *Circulation*. **113**(15),pp.1865–70.
- Algranati, D., Kassab, G.S. and Lanir, Y. 2011. Why is the subendocardium more vulnerable to ischemia? A new paradigm. *American journal of physiology. Heart and circulatory physiology*. **300**(3),pp.H1090-100.

- Almutairi, H., Zemrak, F., Treibel, T., Sado, D., Boubertakh, R., Miquel, M. and Petersen, S. 2015. A comparison of cardiac motion analysis software packages: application to left ventricular deformation analysis in hypertensive patients. *Journal of Cardiovascular Magnetic Resonance*. **17**(Suppl 1),p.P57.
- Amado, L.C., Gerber, B.L., Gupta, S.N., Rettmann, D.W., Szarf, G., Schock, R., Nasir, K., Kraitchman, D.L. and Lima, J.A.C. 2004. Accurate and objective infarct sizing by contrast-enhanced magnetic resonance imaging in a canine myocardial infarction model. *Journal of the American College of Cardiology*. **44**(12),pp.2383–9.
- Ambrosio, G., Weisman, H.F., Mannisi, J.A. and Becker, L.C. 1989. Progressive impairment of regional myocardial perfusion after initial restoration of postischemic blood flow. *Circulation*. **80**(6),pp.1846–61.
- Andre, F., Lossnitzer, D., Buss, S. and Steen, H. 2012. Reference values of mitral and tricuspid annular plane systolic excursion for the evaluation of left and right ventricular performance. *Journal of Cardiovascular Magnetic Resonance*. **14**(Suppl 1),p.M3.
- Anon 1985. The Thrombolysis in Myocardial Infarction (TIMI) trial. Phase I findings. TIMI Study Group. *The New England journal of medicine*. **312**(14),pp.932–6.
- Baltes, C., Kozerke, S., Hansen, M.S., Pruessmann, K.P., Tsao, J. and Boesiger, P. 2005. Accelerating cine phase-contrast flow measurements using k-t BLAST and k-t SENSE. *Magnetic resonance in medicine*. **54**(6),pp.1430–8.
- Basso, C. and Thiene, G. 2006. The pathophysiology of myocardial reperfusion: a pathologist's perspective. *Heart (British Cardiac Society)*. **92**(11),pp.1559–62.
- Di Bella, G., Siciliano, V., Aquaro, G.D., Molinaro, S., Lombardi, M., Carerj, S., Landi, P., Rovai, D. and Pingitore, A. 2013. Scar extent, left ventricular end-diastolic volume, and wall motion abnormalities identify high-risk patients with previous myocardial infarction: a multiparametric approach for prognostic stratification. *European heart journal*. **34**(2),pp.104–11.
- Bellenger, N.G., Davies, L.C., Francis, J.M., Coats, A.J. and Pennell, D.J. 2000. Reduction in sample size for studies of remodeling in heart failure by the use of cardiovascular magnetic resonance. *Journal of cardiovascular magnetic resonance: official journal of the Society for Cardiovascular Magnetic*

*Resonance*. **2**(4),pp.271–8.

- Bergerot, C., Mewton, N., Lacote-Roiron, C., Ernande, L., Ovize, M., Croisille, P., Thibault, H. and Derumeaux, G. 2014. Influence of Microvascular Obstruction on Regional Myocardial Deformation in the Acute Phase of Myocardial Infarction: A Speckle-Tracking Echocardiography Study. *Journal of the American Society of Echocardiography*. **27**(1),pp.93–100.
- Betgem, R.P., de Waard, G.A., Nijveldt, R., Beek, A.M., Escaned, J. and van Royen, N. 2015. Intramyocardial haemorrhage after acute myocardial infarction. *Nature reviews. Cardiology*. **12**(3),pp.156–67.
- Bière, L., Donal, E., Terrien, G., Kervio, G., Willoteaux, S., Furber, A. and Prunier, F. 2014. Longitudinal Strain Is a Marker of Microvascular Obstruction and Infarct Size in Patients with Acute ST-Segment Elevation Myocardial Infarction V. Lionetti, ed. *PLoS ONE*. **9**(1),p.e86959.
- Birkeland, S., Westby, J., Hessevik, I., Grong, K., Hexeberg, E. and Lekven, J. 1992. Compensatory subendocardial hyperkinesis in the cat is abolished during coronary insufficiency outside an acutely ischaemic region. *Cardiovascular research*. **26**(3),pp.285–91.
- Bochenek, T., Wita, K., Tabor, Z., Grabka, M., Krzych, Ł., Wróbel, W., Berger-Kucza, A., Elźbieciak, M., Doruchowska, A. and Gluza, M.T. 2011. Value of speckle-tracking echocardiography for prediction of left ventricular remodeling in patients with ST-elevation myocardial infarction treated by primary percutaneous intervention. *Journal of the American Society of Echocardiography: official publication of the American Society of Echocardiography*. **24**(12),pp.1342–8.
- Bondarenko, O., Beek, A.M., Hofman, M.B.M., Kühl, H.P., Twisk, J.W.R., van Dockum, W.G., Visser, C.A. and van Rossum, A.C. 2005. Standardizing the definition of hyperenhancement in the quantitative assessment of infarct size and myocardial viability using delayed contrast-enhanced CMR. *Journal of cardiovascular magnetic resonance: official journal of the Society for Cardiovascular Magnetic Resonance*. **7**(2),pp.481–5.
- Brand, B., Rydberg, E., Ericsson, G., Gudmundsson, P. and Willenheimer, R. 2002. Prognostication and risk stratification by assessment of left atrioventricular

- plane displacement in patients with myocardial infarction. *International Journal of Cardiology*. **83**,pp.35–41.
- Brix, L., Ringgaard, S., Rasmusson, A., Sørensen, T.S. and Kim, W.Y. 2009. Three dimensional three component whole heart cardiovascular magnetic resonance velocity mapping: comparison of flow measurements from 3D and 2D acquisitions. *Journal of cardiovascular magnetic resonance : official journal of the Society for Cardiovascular Magnetic Resonance*. **11**(1),p.3.
- Bulluck, H., Ngamkasem, H., Sado, D., Treibel, T.A., Fontana, M., Maestrini, V., Moon, J., Hausenloy, D.J., Herrey, A.S. and White, S.K. 2014. A simple technique to measure TAPSE and MAPSE on CMR and normal values. *Journal of Cardiovascular Magnetic Resonance*. **16**(Suppl 1),p.P22.
- Bulluck, H., Rosmini, S., Abdel-Gadir, A., White, S.K., Bhuvu, A.N., Treibel, T.A., Fontana, M., Gonzalez-Lopez, E., Reant, P., Ramlall, M., Hamarneh, A., Sirker, A., Herrey, A.S., Manisty, C., Yellon, D.M., Kellman, P., Moon, J.C. and Hausenloy, D.J. 2016. Automated Extracellular Volume Fraction Mapping Provides Insights Into the Pathophysiology of Left Ventricular Remodeling Post-Reperused ST-Elevation Myocardial Infarction. *Journal of the American Heart Association*. **5**(7),p.e003555.
- Burns, R.J., Gibbons, R.J., Yi, Q., Roberts, R.S., Miller, T.D., Schaer, G.L., Anderson, J.L. and Yusuf, S. 2002. The relationships of left ventricular ejection fraction, end-systolic volume index and infarct size to six-month mortality after hospital discharge following myocardial infarction treated by thrombolysis. *Journal of the American College of Cardiology*. **39**(1),pp.30–6.
- Buss, S.J., Krautz, B., Hofmann, N., Sander, Y., Rust, L., Giusca, S., Galuschky, C., Seitz, S., Giannitsis, E., Pleger, S., Raake, P., Most, P., Katus, H.A. and Korosoglou, G. 2015. Prediction of functional recovery by cardiac magnetic resonance feature tracking imaging in first time ST-elevation myocardial infarction. Comparison to infarct size and transmural by late gadolinium enhancement. *International journal of cardiology*. **183**,pp.162–170.
- Calkoen, E.E., de Koning, P.J.H., Blom, N.A., Kroft, L.J.M., de Roos, A., Wolterbeek, R., Roest, A.A.W. and Westenberg, J.J.M. 2015. Disturbed Intracardiac Flow Organization After Atrioventricular Septal Defect Correction as Assessed With

4D Flow Magnetic Resonance Imaging and Quantitative Particle Tracing. *Investigative radiology*. **50**(12),pp.850–7.

- Calkoen, E.E., Roest, A.A.W., Kroft, L.J.M., van der Geest, R.J., Jongbloed, M.R.M., van den Boogaard, P.J., Blom, N.A., Hazekamp, M.G., de Roos, A. and Westenberg, J.J.M. 2015. Characterization and improved quantification of left ventricular inflow using streamline visualization with 4DFlow MRI in healthy controls and patients after atrioventricular septal defect correction. *Journal of magnetic resonance imaging : JMRI*. **41**(6),pp.1512–20.
- Carberry, J., Carrick, D., Haig, C., Rauhalammi, S.M., Ahmed, N., Mordi, I., McEntegart, M., Petrie, M.C., Eteiba, H., Hood, S., Watkins, S., Lindsay, M., Davie, A., Mahrous, A., Ford, I., Sattar, N., Welsh, P., Radjenovic, A., Oldroyd, K.G. and Berry, C. 2016. Remote Zone Extracellular Volume and Left Ventricular Remodeling in Survivors of ST-Elevation Myocardial Infarction. *Hypertension (Dallas, Tex. : 1979)*. **68**(2),pp.385–91.
- Carlsson, M., Töger, J., Kanski, M., Bloch, K., Ståhlberg, F., Heiberg, E., Arheden, H., Thomsen, C., Cortsen, M., Sondergaard, L., Henriksen, O., Stahlberg, F., Kramer, C., Barkhausen, J., Flamm, S., Kim, R., Nagel, E., Arheden, H., Holmqvist, C., Thilen, U., Hanseus, K., Bjorkhem, G., Pahlm, O., Laurin, S., Stahlberg, F., Carlsson, M., Ugander, M., Heiberg, E., Arheden, H., Gatehouse, P., Rolf, M., Graves, M., Hofman, M., Totman, J., Werner, B., Quest, R., Liu, Y., Spiczak, J. von, Dieringer, M., Rolf, M., Hofman, M., Gatehouse, P., Bloch, K.M., Heymans, M., Ebberts, T., Graves, M., Totman, J., Werner, B., Rossum, A., Markl, M., Kilner, P., Ebberts, T., Tsao, J., Boesiger, P., Pruessmann, K., Baltes, C., Kozerke, S., Hansen, M., Pruessmann, K., Tsao, J., Boesiger, P., Stadlbauer, A., Riet, W. van der, Globits, S., Crelier, G., Salomonowitz, E., Marshall, I., Stadlbauer, A., Riet, W. van der, Crelier, G., Salomonowitz, E., Westenberg, J., Roes, S., Marsan, N.A., Binnendijk, N., Doornbos, J., Bax, J., Reiber, J., Roos, A. de, Geest, R. van der, Lotz, J., Doker, R., Noeske, R., Schuttert, M., Felix, R., Galanski, M., Gutberlet, M., Meyer, G., Dyverfeldt, P., Kvitting, J., Sigfridsson, A., Engvall, J., Bolger, A., Ebberts, T., Heiberg, E., Sjogren, J., Ugander, M., Carlsson, M., Engblom, H., Arheden, H., Reeder, S., Wintersperger, B., Dietrich, O., Lanz, T., Greiser, A., Reiser, M., Glazer, G., Schoenberg, S., Eriksson, J., Carlhall, C., Dyverfeldt, P.,

Engvall, J., Bolger, A., Ebbers, T., Markl, M., Chan, F., Alley, M., Wedding, K., Draney, M., Elkins, C., Parker, D., Wicker, R., Taylor, C., Herfkens, R., Pelc, N., Markl, M., Draney, M., Hope, M., Levin, J., Chan, F., Alley, M., Pelc, N., Herfkens, R., Stalder, A., Russe, M., Frydrychowicz, A., Bock, J., Hennig, J., Markl, M., Hulst, A. van der, Westenberg, J., Kroft, L., Bax, J., Blom, N., Roos, A. de, Roest, A., Brix, L., Ringgaard, S., Rasmusson, A., Sorensen, T., Kim, W., Johnson, K., Lum, D., Turski, P., Block, W., Mistretta, C., Wieben, O., Chang, W., Landgraf, B., Johnson, K., Kecskemeti, S., Wu, Y., Velikina, J., Rowley, H., Wieben, O., Mistretta, C., Turski, P., Hope, M., Hope, T., Meadows, A., Ordovas, K., Urbania, T., Alley, M., Higgins, C., Harloff, A., Simon, J., Brendecke, S., Assefa, D., Helbing, T., Frydrychowicz, A., Weber, J., Olschewski, M., Strecker, C., Hennig, J., Brandts, A., Bertini, M., Dijk, E. van, Delgado, V., Marsan, N., Geest, R. van der, Siebelink, H., Roos, A. de, Bax, J., Westenberg, J., Bolger, A., Heiberg, E., Karlsson, M., Wigstrom, L., Engvall, J., Sigfridsson, A., Ebbers, T., Kvitting, J., Carlhall, C., Wranne, B., Eriksson, J., Dyverfeldt, P., Engvall, J., Bolger, A., Ebbers, T., Carlhall, C., Kellman, P., McVeigh, E., Plein, S., Ryf, S., Schwitter, J., Radjenovic, A., Boesiger, P., Kozerke, S., Hansen, M., Baltes, C., Tsao, J., Kozerke, S., Pruessmann, K., Eggers, H., Madore, B., Hoge, W., Chao, T., Zientara, G. and Chu, R. 2011. Quantification and visualization of cardiovascular 4D velocity mapping accelerated with parallel imaging or k-t BLAST: head to head comparison and validation at 1.5 T and 3 T. *Journal of Cardiovascular Magnetic Resonance*. **13**(1),p.55.

Carrick, D., Haig, C., Rauhalampi, S., Ahmed, N., Mordi, I., McEntegart, M., Petrie, M.C., Eteiba, H., Lindsay, M., Watkins, S., Hood, S., Davie, A., Mahrous, A., Sattar, N., Welsh, P., Tzemos, N., Radjenovic, A., Ford, I., Oldroyd, K.G. and Berry, C. 2015. Pathophysiology of LV Remodeling in Survivors of STEMI: Inflammation, Remote Myocardium, and Prognosis. *JACC. Cardiovascular imaging*. **8**(7),pp.779–89.

Cerqueira, M.D., Weissman, N.J., Dilsizian, V., Jacobs, A.K., Kaul, S., Laskey, W.K., Pennell, D.J., Rumberger, J.A., Ryan, T. and Verani, M.S. 2002. Standardized myocardial segmentation and nomenclature for tomographic imaging of the heart. A statement for healthcare professionals from the Cardiac Imaging

- Committee of the Council on Clinical Cardiology of the American Heart Association. *Circulation*. **105**(4),pp.539–42.
- Chiribiri, A., Hautvast, G.L.T.F., Lockie, T., Schuster, A., Bigalke, B., Olivotti, L., Redwood, S.R., Breeuwer, M., Plein, S. and Nagel, E. 2013. Assessment of Coronary Artery Stenosis Severity and Location: Quantitative Analysis of Transmural Perfusion Gradients by High-Resolution MRI Versus FFR. *JACC: Cardiovascular Imaging*. **6**(5),pp.600–609.
- Choi, K.M., Kim, R.J., Gubernikoff, G., Vargas, J.D., Parker, M. and Judd, R.M. 2001. Transmural extent of acute myocardial infarction predicts long-term improvement in contractile function. *Circulation*. **104**(10),pp.1101–7.
- Chow, B.J.W., Abraham, A., Wells, G.A., Chen, L., Ruddy, T.D., Yam, Y., Govas, N., Galbraith, P.D., Dennie, C. and Beanlands, R.S. 2009. Diagnostic Accuracy and Impact of Computed Tomographic Coronary Angiography on Utilization of Invasive Coronary Angiography. *Circulation. Cardiovascular imaging*. **2**(1),pp.16–23.
- Cury, R.C., Shash, K., Nagurney, J.T., Rosito, G., Shapiro, M.D., Nomura, C.H., Abbara, S., Bamberg, F., Ferencik, M., Schmidt, E.J., Brown, D.F., Hoffmann, U. and Brady, T.J. 2008. Cardiac magnetic resonance with T2-weighted imaging improves detection of patients with acute coronary syndrome in the emergency department. *Circulation*. **118**(8),pp.837–44.
- Dabir, D., Child, N., Kalra, A., Rogers, T., Gebker, R., Jabbour, A., Plein, S., Yu, C.-Y., Otton, J., Kidambi, A., McDiarmid, A., Broadbent, D., Higgins, D.M., Schnackenburg, B., Foote, L., Cummins, C., Nagel, E. and Puntmann, V.O. 2014. Reference values for healthy human myocardium using a T1 mapping methodology: results from the International T1 Multicenter cardiovascular magnetic resonance study. *Journal of cardiovascular magnetic resonance : official journal of the Society for Cardiovascular Magnetic Resonance*. **16**(1),p.69.
- Dall'Armellina, E., Karia, N., Lindsay, A.C., Karamitsos, T.D., Ferreira, V., Robson, M.D., Kellman, P., Francis, J.M., Forfar, C., Prendergast, B.D., Banning, A.P., Channon, K.M., Kharbada, R.K., Neubauer, S. and Choudhury, R.P. 2011. Dynamic changes of edema and late gadolinium enhancement after acute

myocardial infarction and their relationship to functional recovery and salvage index. *Circulation. Cardiovascular imaging*. **4**(3),pp.228–36.

Dall'Armellina, E., Piechnik, S.K., Ferreira, V.M., Si, Q. Le, Robson, M.D., Francis, J.M., Cuculi, F., Kharbanda, R.K., Banning, A.P., Choudhury, R.P., Karamitsos, T.D. and Neubauer, S. 2012. Cardiovascular magnetic resonance by non contrast T1-mapping allows assessment of severity of injury in acute myocardial infarction. *Journal of cardiovascular magnetic resonance : official journal of the Society for Cardiovascular Magnetic Resonance*. **14**(1),p.15.

Davis, C.P., McKinnon, G.C., Debatin, J.F., Wetter, D., Eichenberger, A.C., Duewell, S. and von Schulthess, G.K. 1994. Normal heart: evaluation with echo-planar MR imaging. *Radiology*. **191**(3),pp.691–6.

Debatin, J.F., Davis, C.P., Felblinger, J. and McKinnon, G.C. 1995. Evaluation of ultrafast phase-contrast imaging in the thoracic aorta. *Magma (New York, N.Y.)*. **3**(2),pp.59–66.

Delewi, R., Zijlstra, F. and Piek, J.J. 2012. Left ventricular thrombus formation after acute myocardial infarction. *Heart (British Cardiac Society)*. **98**(23),pp.1743–9.

Desch, S., Eitel, I., de Waha, S., Fuernau, G., Lurz, P., Gutberlet, M., Schuler, G., Thiele, H., Kim, R., Fieno, D., Parrish, T., Harris, K., Chen, E., Simonetti, O., Bundy, J., Finn, J., Klocke, F., Judd, R., Wagner, A., Mahrholdt, H., Holly, T., Elliott, M., Regenfus, M., Parker, M., Klocke, F., Bonow, R., Kim, R., Judd, R., Engblom, H., Hedstrom, E., Heiberg, E., Wagner, G., Pahlm, O., Arheden, H., Ibrahim, T., Hackl, T., Nekolla, S., Breuer, M., Feldmair, M., Schomig, A., Schwaiger, M., Kramer, C., Barkhausen, J., Flamm, S., Kim, R., Nagel, E., Kellman, P., Arai, A., McVeigh, E., Aletras, A., Geiser, E., Bove, K., Bondarenko, O., Beek, A., Hofman, M., Kühl, H., Twisk, J., Dockum, W. van, Visser, C., Rossum, A. van, Kim, H., Klem, I., Shah, D., Wu, E., Meyers, S., Parker, M., Crowley, A., Bonow, R., Judd, R., Kim, R., Thiele, H., Kappl, M., Conradi, S., Niebauer, J., Hambrecht, R., Schuler, G., Kim, H., Farzaneh-Far, A., Kim, R., Fieno, D., Kim, R., Chen, E., Lomasney, J., Klocke, F., Judd, R., Amado, L., Gerber, B., Gupta, S., Rettmann, D., Szarf, G., Schock, R., Nasir, K., Kraitichman, D., Lima, J., Flett, A., Hasleton, J., Cook, C., Hausenloy, D., Quarta, G., Ariti, C., Muthurangu, V., Moon, J., Heiberg, E., Ugander, M., Engblom, H., Gotberg, M., Olivecrona, G., Erlinge, D., Arheden,

H., Hsu, L., Ingkanisorn, W., Kellman, P., Aletras, A., Arai, A., Hsu, L., Natanzon, A., Kellman, P., Hirsch, G., Aletras, A., Arai, A., Choi, K., Kim, R., Gubernikoff, G., Vargas, J., Parker, M., Judd, R., Larose, E., Rodes-Cabau, J., Pibarot, P., Rinfret, S., Proulx, G., Nguyen, C., Dery, J., Gleeton, O., Roy, L., Noel, B., Wu, E., Ortiz, J., Tejedor, P., Lee, D., Bucciarelli-Ducci, C., Kansal, P., Carr, J., Holly, T., Lloyd-Jones, D., Klocke, F., Bonow, R., Thiele, H., Schindler, K., Friedenberger, J., Eitel, I., Furnau, G., Grebe, E., Erbs, S., Linke, A., Mobius-Winkler, S., Kivelitz, D., Schuler, G., Thiele, H., Wohrle, J., Neuhaus, P., Brosteanu, O., Sick, P., Prondzinsky, R., Birkemeyer, R., Wiemer, M., Kerber, S., Schuehlen, H., Ibrahim, T., Bulow, H., Hackl, T., Hornke, M., Nekolla, S., Breuer, M., Schomig, A., Schwaiger, M., Miller, T., Christian, T., Hopfenspirger, M., Hodge, D., Gersh, B., Gibbons, R., Ibrahim, T., Nekolla, S., Hornke, M., Bulow, H., Dirschinger, J., Schomig, A., Schwaiger, M., Gibbons, R., Valeti, U., Araoz, P., Jaffe, A., Aletras, A., Tilak, G., Natanzon, A., Hsu, L.-Y., Gonzalez, F., Hoyt, R., Arai, A., Friedrich, M., Abdel-Aty, H., Taylor, A., Schulz-Menger, J., Messroghli, D., Dietz, R., Reimer, K., Jennings, R., Cobb, F., Murdock, R., Greenfield, J., Becker, L., Bulkley, B., Hutchins, G., Schwartz, R., Bailey, K., Lowe, J., Reimer, K., Jennings, R., Abdel-Aty, H., Simonetti, O., Friedrich, M., Kellman, P., Aletras, A., Mancini, C., McVeigh, E., Arai, A., Aletras, A., Kellman, P., Derbyshire, J., Arai, A., Giri, S., Chung, Y., Merchant, A., Mihai, G., Rajagopalan, S., Raman, S., Simonetti, O., Abdel-Aty, H., Cocker, M., Meek, C., Tyberg, J., Friedrich, M., Carlsson, M., Ubachs, J., Hedstrom, E., Heiberg, E., Jovinge, S., Arheden, H., Schulz-Menger, J., Gross, M., Messroghli, D., Uhlich, F., Dietz, R., Friedrich, M., Nilsson, J., Nielsen, G., Groenning, B., Fritz-Hansen, T., Sondergaard, L., Jensen, G., Larsson, H., Ripa, R., Nilsson, J., Wang, Y., Sondergaard, L., Jorgensen, E., Kastrup, J., Kastrati, A., Mehilli, J., Dirschinger, J., Schricke, U., Neverve, J., Pache, J., Martinoff, S., Neumann, F., Nekolla, S., Blasini, R., Milavetz, J., Giebel, D., Christian, T., Schwartz, R., Holmes, D., Gibbons, R., Schomig, A., Kastrati, A., Dirschinger, J., Mehilli, J., Schricke, U., Pache, J., Martinoff, S., Neumann, F., Schwaiger, M., Lonborg, J., Kelbaek, H., Vejlstrup, N., Jorgensen, E., Helqvist, S., Saunamaki, K., Clemmensen, P., Holmvang, L., Treiman, M., Jensen, J., Engstrom, T., Thiele, H., Hildebrand, L., Schirdewahn, C., Eitel, I., Adams, V.,

Fuernau, G., Erbs, S., Linke, A., Diederich, K., Nowak, M., Eitel, I., Desch, S., Fuernau, G., Hildebrand, L., Gutberlet, M., Schuler, G., Thiele, H., Ndrepepa, G., Mehilli, J., Schwaiger, M., Schuhlen, H., Nekolla, S., Martinoff, S., Schmitt, C., Dirschinger, J., Schomig, A., Kastrati, A., Desch, S., Engelhardt, H., Meissner, J., Eitel, I., Sareban, M., Fuernau, G., Waha, S. de, Grothoff, M., Gutberlet, M., Schuler, G., Thiele, H., Werf, F. Van de, Bax, J., Betriu, A., Blomstrom-Lundqvist, C., Crea, F., Falk, V., Filippatos, G., Fox, K., Huber, K., Kastrati, A., Mather, A., Lockie, T., Nagel, E., Marber, M., Perera, D., Redwood, S., Radjenovic, A., Saha, A., Greenwood, J., Plein, S., Waha, S. de, Desch, S., Eitel, I., Fuernau, G., Zachrau, J., Leuschner, A., Gutberlet, M., Schuler, G., Thiele, H., Bekkers, S., Yazdani, S., Virmani, R., Waltenberger, J., Hombach, V., Grebe, O., Merkle, N., Waldenmaier, S., Hoher, M., Kochs, M., Wohrle, J., Kestler, H., Wu, K., Zerhouni, E., Judd, R., Lugo-Olivieri, C., Barouch, L., Schulman, S., Blumenthal, R., Lima, J., Nijveldt, R., Beek, A., Hirsch, A., Stoel, M., Hofman, M., Umans, V., Algra, P., Twisk, J., Rossum, A. van, Vicente, J., Mewton, N., Croisille, P., Staat, P., Bonnefoy-Cudraz, E., Ovize, M., Revel, D., Ambrosio, G., Weisman, H., Mannisi, J., Becker, L., White, H., Norris, R., Brown, M., Brandt, P., Whitlock, R., Wild, C., Pennell, D., Bellenger, N., Grothues, F., Smith, G., Pennell, D., Ganame, J., Messalli, G., Dymarkowski, S., Rademakers, F., Desmet, W., Werf, F. Van de, Bogaert, J., O'Regan, D., Ahmed, R., Karunanithy, N., Neuwirth, C., Tan, Y., Durighel, G., Hajnal, J., Nadra, I., Corbett, S., Cook, S., Yan, A., Shayne, A., Brown, K., Gupta, S., Chan, C., Luu, T., Carli, M. Di, Reynolds, H., Stevenson, W., Kwong, R., Schmidt, A., Azevedo, C., Cheng, A., Gupta, S., Bluemke, D., Foo, T., Gerstenblith, G., Weiss, R., Marban, E., Tomaselli, G., Kribben, A., Witzke, O., Hillen, U., Barkhausen, J., Daul, A., Erbel, R., Abbate, A., Kontos, M., Grizzard, J., Biondi-Zoccai, G., Tassell, B. Van, Robati, R., Roach, L., Arena, R., Roberts, C., Varma, A., Wohrle, J., Merkle, N., Mailander, V., Nusser, T., Schauwecker, P., Scheidt, F. von, Schwarz, K., Bommer, M., Wiesneth, M., Schrezenmeier, H., Hombach, V., Haeck, J., Kuijt, W., Koch, K., Bilodeau, L., Henriques, J., Rohling, W., Baan, J., Vis, M., Nijveldt, R., Geloven, N. van, Patel, M., Worthley, S., Stebbins, A., Dill, T., Rademakers, F., Velletti, U., Barsness, G., Werf, F. Van de, Hamm, C., Armstrong, P., Weir, R., Mark, P., Petrie, C., Clements, S., Steedman,

T., Ford, I., Ng, L., Squire, I., Wagner, G., McMurray, J., Dargie, H., Tendera, M., Wojakowski, W., Ruzyllo, W., Chojnowska, L., Kepka, C., Tracz, W., Musialek, P., Piwowarska, W., Nessler, J., Buszman, P., Song, Y., Hahn, J., Gwon, H., Kim, J., Lee, S., Choe, Y., Choi, S., Choi, J., Lee, S., Dill, T., Schachinger, V., Rolf, A., Mollmann, S., Thiele, H., Tillmanns, H., Assmus, B., Dimmeler, S., Zeiher, A., Hamm, C., Atar, D., Petzelbauer, P., Schwitter, J., Huber, K., Rensing, B., Kasprzak, J., Butter, C., Grip, L., Hansen, P., Suselbeck, T., Hahn, J., Gwon, H., Choe, Y., Rhee, I., Choi, S., Choi, J., Lee, S., Hong, K., Park, J., Engelmann, M., Theiss, H., Hennig-Theiss, C., Huber, A., Wintersperger, B., Werle-Ruedinger, A., Schoenberg, S., Steinbeck, G., Franz, W., Kang, H., Lee, H., Na, S., Chang, S., Park, K., Kim, H., Kim, S., Chang, H., Lee, W., Kang, W., Ripa, R., Jorgensen, E., Wang, Y., Thune, J., Nilsson, J., Sondergaard, L., Johnsen, H., Kober, L., Grande, P., Kastrup, J., Janssens, S., Dubois, C., Bogaert, J., Theunissen, K., Deroose, C., Desmet, W., Kalantzi, M., Herbots, L., Sinnaeve, P., Dens, J., Thiele, H., Engelmann, L., Elsner, K., Kappl, M., Storch, W., Rahimi, K., Hartmann, A., Pfeiffer, D., Kneissl, G., Schneider, D., Wollert, K., Meyer, G., Lotz, J., Ringes-Lichtenberg, S., Lippolt, P., Breidenbach, C., Fichtner, S., Korte, T., Hornig, B., Messinger, D., Darasz, K., Bayliss, J., Underwood, S., Keegan, J., Poole-Wilson, P. and Sutton, G. 2011. Cardiac magnetic resonance imaging parameters as surrogate endpoints in clinical trials of acute myocardial infarction. *Trials*. **12**(1),p.204.

Dyverfeldt, P., Bissell, M., Barker, A.J., Bolger, A.F., Carlhäll, C.-J., Ebbers, T., Francios, C.J., Frydrychowicz, A., Geiger, J., Giese, D., Hope, M.D., Kilner, P.J., Kozerke, S., Myerson, S., Neubauer, S., Wieben, O. and Markl, M. 2015. 4D flow cardiovascular magnetic resonance consensus statement. *Journal of cardiovascular magnetic resonance : official journal of the Society for Cardiovascular Magnetic Resonance*. **17**(1),p.72.

Elbaz, M.S.M., Calkoen, E.E., Westenber, J.J.M., Lelieveldt, B.P.F., Roest, A.A.W. and van der Geest, R.J. 2014. Vortex flow during early and late left ventricular filling in normal subjects: quantitative characterization using retrospectively-gated 4D flow cardiovascular magnetic resonance and three-dimensional vortex core analysis. *Journal of cardiovascular magnetic resonance : official journal of the*

*Society for Cardiovascular Magnetic Resonance.* **16**,p.78.

- Ferreira, V.M., Piechnik, S.K., Dall'Armellina, E., Karamitsos, T.D., Francis, J.M., Ntusi, N., Holloway, C., Choudhury, R.P., Kardos, A., Robson, M.D., Friedrich, M.G. and Neubauer, S. 2013. T(1) mapping for the diagnosis of acute myocarditis using CMR: comparison to T2-weighted and late gadolinium enhanced imaging. *JACC. Cardiovascular imaging.* **6**(10),pp.1048–58.
- Fishbein, M.C., Maclean, D. and Maroko, P.R. 1978. The histopathologic evolution of myocardial infarction. *Chest.* **73**(6),pp.843–9.
- Flett, A.S., Hasleton, J., Cook, C., Hausenloy, D., Quarta, G., Ariti, C., Muthurangu, V. and Moon, J.C. 2011. Evaluation of techniques for the quantification of myocardial scar of differing etiology using cardiac magnetic resonance. *JACC. Cardiovascular imaging.* **4**(2),pp.150–6.
- Frangogiannis, N.G. 2006. The mechanistic basis of infarct healing. *Antioxidants & redox signaling.* **8**(11–12),pp.1907–39.
- Friedrich, M.G., Sechtem, U., Schulz-Menger, J., Holmvang, G., Alakija, P., Cooper, L.T., White, J.A., Abdel-Aty, H., Gutberlet, M., Prasad, S., Aletras, A., Laissy, J.-P., Paterson, I., Filipchuk, N.G., Kumar, A., Pauschinger, M. and Liu, P. 2009. Cardiovascular magnetic resonance in myocarditis: A JACC White Paper. *Journal of the American College of Cardiology.* **53**(17),pp.1475–87.
- Frydrychowicz, A., Wieben, O., Niespodzany, E., Reeder, S.B., Johnson, K.M. and François, C.J. 2013. Quantification of thoracic blood flow using volumetric magnetic resonance imaging with radial velocity encoding: in vivo validation. *Investigative radiology.* **48**(12),pp.819–25.
- Garg, P., Greenwood, J.P. and Plein, S. 2015. Multiparametric relaxometry by cardiac magnetic resonance imaging in Takotsubo cardiomyopathy. *European heart journal cardiovascular Imaging.* **16**(10),p.1174.
- Garg, P., Greenwood, J.P.J.P. and Plein, S. 2015. Multiparametric relaxometry by cardiac magnetic resonance imaging in Takotsubo cardiomyopathy. *European heart journal cardiovascular Imaging.* **16**(10),p.1174.
- Garg, P., Kidambi, A. and Plein, S. 2015. Relation of circumferential and longitudinal strain to other independent prognostic imaging markers in first time ST-elevation myocardial infarction. *International journal of cardiology.*

**186**,pp.202–3.

- Garg, P., Kidambi, A., Ripley, D.P., Dobson, L.E., Swoboda, P.P., Musa, T.A., McDiarmid, A.K., Erhayiem, B., Greenwood, J.P. and Plein, S. 2015. Is signal intensity of late gadolinium enhancement a substitute for extracellular volume mapping in acute myocardial infarction? *Journal of Cardiovascular Magnetic Resonance*. **17**(Suppl 1),p.P156.
- Gibbons, R.J., Valeti, U.S., Araoz, P.A. and Jaffe, A.S. 2004. The quantification of infarct size. *Journal of the American College of Cardiology*. **44**(8),pp.1533–42.
- Gibson, P.H., Becher, H. and Choy, J.B. 2014. The current state of myocardial contrast echocardiography: what can we read between the lines? *European Heart Journal - Cardiovascular Imaging*. **15**(3).
- Goyal, P. and Weinsaft, J.W. 2013. Cardiovascular magnetic resonance imaging for assessment of cardiac thrombus. *Methodist DeBakey cardiovascular journal*. **9**(3),pp.132–6.
- Gradman, A., Deedwania, P., Cody, R., Massie, B., Packer, M., Pitt, B. and Goldstein, S. 1989. Predictors of total mortality and sudden death in mild to moderate heart failure. Captopril-Digoxin Study Group. *Journal of the American College of Cardiology*. **14**(3),pp.564–70–2.
- Greenbaum, R.A., Ho, S.Y., Gibson, D.G., Becker, A.E. and Anderson, R.H. 1981. Left ventricular fibre architecture in man. *Heart*. **45**(3),pp.248–263.
- Greenwood, J.P., Maredia, N., Younger, J.F., Brown, J.M., Nixon, J., Everett, C.C., Bijsterveld, P., Ridgway, J.P., Radjenovic, A., Dickinson, C.J., Ball, S.G. and Plein, S. 2012. Cardiovascular magnetic resonance and single-photon emission computed tomography for diagnosis of coronary heart disease (CE-MARC): a prospective trial. *Lancet*. **379**(9814),pp.453–460.
- Grothues, F., Smith, G.C., Moon, J.C.C., Bellenger, N.G., Collins, P., Klein, H.U. and Pennell, D.J. 2002. Comparison of interstudy reproducibility of cardiovascular magnetic resonance with two-dimensional echocardiography in normal subjects and in patients with heart failure or left ventricular hypertrophy. *The American journal of cardiology*. **90**(1),pp.29–34.
- h-Ici, D.O., Jeuthe, S., Al-Wakeel, N., Berger, F., Kuehne, T., Kozerke, S. and Messroghli, D.R. 2014. T1 mapping in ischaemic heart disease. *European heart*

*journal cardiovascular Imaging*. **15**(6),pp.597–602.

- Haaf, P., Garg, P., Messroghli, D.R., Broadbent, D.A., Greenwood, J.P. and Plein, S. 2016. Cardiac T1 Mapping and Extracellular Volume (ECV) in clinical practice: a comprehensive review. *Journal of Cardiovascular Magnetic Resonance*. **18**(1),p.89.
- Hamm, C.W., Bassand, J.-P., Agewall, S., Bax, J., Boersma, E., Bueno, H., Caso, P., Dudek, D., Gielen, S., Huber, K., Ohman, M., Petrie, M.C., Sonntag, F., Uva, M.S., Storey, R.F., Wijns, W. and Zahger, D. 2011. ESC Guidelines for the management of acute coronary syndromes in patients presenting without persistent ST-segment elevation: The Task Force for the management of acute coronary syndromes (ACS) in patients presenting without persistent ST-segment elevatio. *European heart journal*. **32**(23),pp.2999–3054.
- Hammer-Hansen, S., Bandettini, W.P., Hsu, L.-Y., Leung, S.W., Shanbhag, S., Mancini, C., Greve, A.M., Køber, L., Thune, J.J., Kellman, P. and Arai, A.E. 2016. Mechanisms for overestimating acute myocardial infarct size with gadolinium-enhanced cardiovascular magnetic resonance imaging in humans: a quantitative and kinetic study. *European heart journal cardiovascular Imaging*. **17**(1),pp.76–84.
- Hanneman, K., Sivagnanam, M., Nguyen, E.T., Wald, R., Greiser, A., Crean, A.M., Ley, S. and Wintersperger, B.J. 2014. Magnetic resonance assessment of pulmonary (QP) to systemic (QS) flows using 4D phase-contrast imaging: pilot study comparison with standard through-plane 2D phase-contrast imaging. *Academic radiology*. **21**(8),pp.1002–8.
- Hartlage, G., Janik, M., Anadiotis, A., Veledar, E., Oshinski, J., Kremastinos, D., Stillman, A. and Lerakis, S. 2012. Prognostic value of adenosine stress cardiovascular magnetic resonance and dobutamine stress echocardiography in patients with low-risk chest pain. *The international journal of cardiovascular imaging*. [Online]. **28**(4),pp.803–12. [Accessed 22 October 2014]. Available from:  
<https://www.google.co.uk/search?q=Prognostic+value+of+adenosine+stress+cardiovascular+magnetic+resonance+and+dobutamine+stress+echocardiography+in+patients+with+low->

risk+chest+pain.&oq=Prognostic+value+of+adenosine+stress+cardiovascular+magnetic+resonance.

- Heiberg, E., Ugander, M., Engblom, H., Götberg, M., Olivecrona, G.K., Erlinge, D. and Arheden, H. 2008. Automated quantification of myocardial infarction from MR images by accounting for partial volume effects: animal, phantom, and human study. *Radiology*. **246**(2),pp.581–8.
- Heimdal, A., Støylen, A., Torp, H., Skjaerpe, T., Mirsky, I., Parmley, W., Mirsky, I., Leuven, S. van, Waldman, L., McCulloch, A., Covell, J., Prinzen, F., Augustijn, C., Allessie, M., Arts, T., Delhaas, T., Reneman, R., Piene, H., Myhre, E., Douglas, A., Rodriguez, E., O'Dell, W., Hunter, W., Hashima, A., Young, A., McCulloch, A., Waldman, L., Fann, J., Sarris, G., Ingels, N., al., et, Azhari, H., Weiss, J., Rogers, W., Siu, C., Zerhouni, E., Shapiro, E., McCulloch, A., Omens, J., Axel, L., Rademakers, F., Rogers, W., Guier, W., al., et, Sonnenblick, E., Weber, K., Janicki, J., Robson, M., Constable, R., Fleming, D., Xia, X., McDicken, W., Sutherland, G., Fenn, L., Uematsu, M., Miyatake, K., Tanaka, N., al., et, Kanai, H., Hasegawa, H., Chubachi, N., Koiwa, Y., Tanaka, M., Miyatake, K., Yamagishi, M., Tanaka, N., al., et, Lundback, S., Jones, C., Raposo, L., Gibson, D., Alam, M., Høglund, C., Thorstrand, C., Simonson, J., Schiller, N., Willenheimer, R., Cline, C., Erhardt, L., Israelsson, B., Zamorano, J., Wallbridge, D., Ge, J., Drozd, J., Nesser, J., Erbel, R. and Fung, Y. 1998. Real-time strain rate imaging of the left ventricle by ultrasound. *Journal of the American Society of Echocardiography : official publication of the American Society of Echocardiography*. **11**(11),pp.1013–9.
- Hendel, R.C., Patel, M.R., Kramer, C.M., Poon, M., Carr, J.C., Gerstad, N.A., Gillam, L.D., Hodgson, J.M., Kim, R.J., Lesser, J.R., Martin, E.T., Messer, J. V, Redberg, R.F., Rubin, G.D., Rumsfeld, J.S., Taylor, A.J., Weigold, W.G., Woodard, P.K., Brindis, R.G., Douglas, P.S., Peterson, E.D., Wolk, M.J. and Allen, J.M. 2006. ACCF/ACR/SCCT/SCMR/ASNC/NASCI/SCAI/SIR 2006 appropriateness criteria for cardiac computed tomography and cardiac magnetic resonance imaging: a report of the American College of Cardiology Foundation Quality Strategic Directions Committee Appropriateness C. *Journal of the American College of Cardiology*. **48**(7),pp.1475–97.

- Hillis, G.S., Møller, J.E., Pellikka, P.A., Gersh, B.J., Wright, R.S., Ommen, S.R., Reeder, G.S. and Oh, J.K. 2004. Noninvasive estimation of left ventricular filling pressure by  $e/e'$  is a powerful predictor of survival after acute myocardial infarction. *Journal of the American College of Cardiology*. **43**(3),pp.360–367.
- Hor, K.N., Baumann, R., Pedrizzetti, G., Tonti, G., Gottliebson, W.M., Taylor, M., Benson, W. and Mazur, W. 2011. Magnetic resonance derived myocardial strain assessment using feature tracking. *Journal of visualized experiments : JoVE*. (48).
- Hozumi, T., Yoshida, K., Mori, I., Akasaka, T., Takagi, T., Kaji, S., Kawamoto, T., Ueda, Y. and Morioka, S. 1999. Noninvasive assessment of hemodynamic subsets in patients with acute myocardial infarction using digital color Doppler velocity profile integration and pulmonary venous flow analysis. *The American journal of cardiology*. **83**(7),pp.1027–32.
- Hsiao, A., Tariq, U., Alley, M.T., Lustig, M. and Vasanawala, S.S. 2015. Inlet and outlet valve flow and regurgitant volume may be directly and reliably quantified with accelerated, volumetric phase-contrast MRI. *Journal of magnetic resonance imaging : JMRI*. **41**(2),pp.376–85.
- Hu, K., Liu, D., Herrmann, S., Niemann, M., Gaudron, P.D., Voelker, W., Ertl, G., Bijns, B. and Weidemann, F. 2013. Clinical implication of mitral annular plane systolic excursion for patients with cardiovascular disease. *European heart journal cardiovascular Imaging*. **14**(3),pp.205–12.
- Ibrahim, E.-S.H. 2011. Myocardial tagging by Cardiovascular Magnetic Resonance: evolution of techniques--pulse sequences, analysis algorithms, and applications. *Journal of Cardiovascular Magnetic Resonance*. **13**(1),p.36.
- Ingkanisorn, W.P., Kwong, R.Y., Bohme, N.S., Geller, N.L., Rhoads, K.L., Dyke, C.K., Paterson, D.I., Syed, M.A., Aletras, A.H. and Arai, A.E. 2006. Prognosis of negative adenosine stress magnetic resonance in patients presenting to an emergency department with chest pain. *Journal of the American College of Cardiology*. **47**(7),pp.1427–32.
- Ismail, T.F., Prasad, S.K. and Pennell, D.J. 2012. Prognostic importance of late gadolinium enhancement cardiovascular magnetic resonance in cardiomyopathy. *Heart*. **98**(6),pp.438–442.

- Iwahashi, N., Kimura, K., Kosuge, M., Tsukahara, K., Hibi, K., Ebina, T., Saito, M. and Umemura, S. 2012. E/e' Two Weeks after Onset Is a Powerful Predictor of Cardiac Death and Heart Failure in Patients with a First-Time ST Elevation Acute Myocardial Infarction. *Journal of the American Society of Echocardiography*. **25**(12),pp.1290–1298.
- Jablonowski, R., Engblom, H., Kanski, M., Nordlund, D., Koul, S., van der Pals, J., Englund, E., Heiberg, E., Erlinge, D., Carlsson, M. and Arheden, H. 2015. Contrast-Enhanced CMR Overestimates Early Myocardial Infarct Size: Mechanistic Insights Using ECV Measurements on Day 1 and Day 7. *JACC Cardiovascular imaging*. **8**(12),pp.1379–89.
- Jaffe, R., Charron, T., Puley, G., Dick, A. and Strauss, B.H. 2008. Microvascular obstruction and the no-reflow phenomenon after percutaneous coronary intervention. *Circulation*. **117**(24),pp.3152–6.
- Johnson, K.M. and Markl, M. 2010. Improved SNR in phase contrast velocimetry with five-point balanced flow encoding. *Magnetic resonance in medicine*. **63**(2),pp.349–55.
- Judd, R.M., Lugo-Olivieri, C.H., Arai, M., Kondo, T., Croisille, P., Lima, J.A., Mohan, V., Becker, L.C. and Zerhouni, E.A. 1995. Physiological basis of myocardial contrast enhancement in fast magnetic resonance images of 2-day-old reperfused canine infarcts. *Circulation*. **92**(7),pp.1902–10.
- Kanski, M., Töger, J., Steding-Ehrenborg, K., Xanthis, C., Bloch, K.M., Heiberg, E., Carlsson, M. and Arheden, H. 2015. Whole-heart four-dimensional flow can be acquired with preserved quality without respiratory gating, facilitating clinical use: a head-to-head comparison. *BMC medical imaging*. **15**(1),p.20.
- Ketchum, E.S. and Levy, W.C. 2011. Establishing Prognosis in Heart Failure: A Multimarker Approach. *Progress in Cardiovascular Diseases*. **54**(2),pp.86–96.
- Khan, J.N., Singh, A., Nazir, S.A., Kanagala, P., Greenwood, J., Gershlick, A.H. and McCann, G.P. 2015. Comparison of cardiovascular magnetic resonance feature tracking and tagging for the assessment of left ventricular systolic strain in acute myocardial infarction. *European journal of radiology*. **17**(5),pp.840–8.
- Kidambi, A., Biglands, J.D., Higgins, D.M., Ripley, D.P., Zaman, A., Broadbent, D.A., McDiarmid, A.K., Swoboda, P.P., Al Musa, T., Erhayiem, B., Greenwood, J.P. and

- Plein, S. 2014. Susceptibility-weighted cardiovascular magnetic resonance in comparison to T2 and T2 star imaging for detection of intramyocardial hemorrhage following acute myocardial infarction at 3 Tesla. *Journal of cardiovascular magnetic resonance : official journal of the Society for Cardiovascular Magnetic Resonance*. **16**(1),p.86.
- Kidambi, A., Mather, A.N., Motwani, M., Swoboda, P., Uddin, A., Greenwood, J.P. and Plein, S. 2013. The effect of microvascular obstruction and intramyocardial hemorrhage on contractile recovery in reperfused myocardial infarction: insights from cardiovascular magnetic resonance. *Journal of cardiovascular magnetic resonance : official journal of the Society for Cardiovascular Magnetic Resonance*. **15**(1),p.58.
- Kidambi, A., Mather, A.N., Swoboda, P., Motwani, M., Fairbairn, T.A., Greenwood, J.P. and Plein, S. 2013. Relationship between Myocardial Edema and Regional Myocardial Function after Reperfused Acute Myocardial Infarction: An MR Imaging Study. *Radiology*. **267**(3),pp.701–708.
- Kidambi, A., Motwani, M., Uddin, A., Ripley, D.P., McDiarmid, A.K., Swoboda, P.P., Broadbent, D.A., Musa, T.A., Erhayiem, B., Leader, J., Greenwood, J.P. and Plein, S. 2015. Myocardial extracellular volume estimation by CMR predicts functional recovery following acute myocardial infarction. *Journal of Cardiovascular Magnetic Resonance*. **17**(Suppl 1),p.Q63.
- Killip, T. and Kimball, J. 1967. Treatment of myocardial infarction in a coronary care unit. A two year experience with 250 patients. *The American journal of cardiology*. **20**(4),pp.457–64.
- Klem, I., Shah, D.J., White, R.D., Pennell, D.J., van Rossum, A.C., Regenfus, M., Sechtem, U., Schwartzman, P.R., Hunold, P., Croisille, P., Parker, M., Judd, R.M. and Kim, R.J. 2011. Prognostic value of routine cardiac magnetic resonance assessment of left ventricular ejection fraction and myocardial damage: an international, multicenter study. *Circulation. Cardiovascular imaging*. **4**(6),pp.610–9.
- Korosoglou, G., Haars, A., Humpert, P.M., Hardt, S., Bekeredjian, R., Giannitsis, E., Kuecherer, H. and Katus, H.A. 2008. Evaluation of myocardial perfusion and deformation in patients with acute myocardial infarction treated with primary

- angioplasty and stent placement. *Coronary artery disease*. **19**(7),pp.497–506.
- Kristen, A. V, Voss, A., Schellberg, D., Zugck, C., Galuschky, C., Giannitsis, E., Hegenbart, U. and Ho, A.D. 2012. Longitudinal Left Ventricular Function for Prediction of Survival in Systemic Light-Chain Amyloidosis Incremental Value Compared With Clinical and Biochemical Markers. *Journal of the American College of Cardiology*. **60**(12),pp.1068–76.
- Kul, S., Ozcelik, H.K., Uyarel, H., Karakus, G., Guvenc, T.S., Yalcinsoy, M., Asoglu, E., Kemik, A.S., Tasal, A., Gungor, S., Karaarslan, E., Kart, L. and Goktekin, O. 2014. Diagnostic value of strain echocardiography, galectin-3, and tenascin-C levels for the identification of patients with pulmonary and cardiac sarcoidosis. *Lung*. **192**(4),pp.533–542.
- Kwon, D.H., Asamoto, L., Popovic, Z.B., Kusunose, K., Robinson, M., Desai, M., Marwick, T.H. and Flamm, S.D. 2014. Infarct Characterization and Quantification by Delayed Enhancement Cardiac Magnetic Resonance Imaging Is a Powerful Independent and Incremental Predictor of Mortality in Patients With Advanced Ischemic Cardiomyopathy. *Circulation: Cardiovascular Imaging*. **7**(5),pp.796–804.
- Kwong, R.Y. and Farzaneh-Far, A. 2011. Measuring myocardial scar by CMR. *JACC. Cardiovascular imaging*. **4**(2),pp.157–60.
- Kwong, R.Y. and Korlakunta, H. 2008. Diagnostic and prognostic value of cardiac magnetic resonance imaging in assessing myocardial viability. *Topics in magnetic resonance imaging : TMRI*. **19**(1),pp.15–24.
- Kwong, R.Y., Schussheim, A.E., Rekhraj, S., Aletras, A.H., Geller, N., Davis, J., Christian, T.F., Balaban, R.S. and Arai, A.E. 2003. Detecting acute coronary syndrome in the emergency department with cardiac magnetic resonance imaging. *Circulation*. **107**(4),pp.531–7.
- Larose, E., Ganz, P., Reynolds, H.G., Dorbala, S., Di Carli, M.F., Brown, K.A. and Kwong, R.Y. 2007. Right ventricular dysfunction assessed by cardiovascular magnetic resonance imaging predicts poor prognosis late after myocardial infarction. *Journal of the American College of Cardiology*. **49**(8),pp.855–62.
- Lerakis, S., McLean, D.S., Anadiotis, A. V, Janik, M., Oshinski, J.N., Alexopoulos, N., Zaragoza-Macias, E., Veledar, E. and Stillman, A.E. 2009. Prognostic value of

- adenosine stress cardiovascular magnetic resonance in patients with low-risk chest pain. *Journal of cardiovascular magnetic resonance : official journal of the Society for Cardiovascular Magnetic Resonance*. **11**(1),p.37.
- Liang, H.-Y., Cauduro, S., Pellikka, P., Wang, J., Urheim, S., Yang, E.H., Rihal, C., Belohlavek, M., Khandheria, B., Miller, F.A. and Abraham, T.P. 2006. Usefulness of two-dimensional speckle strain for evaluation of left ventricular diastolic deformation in patients with coronary artery disease. *The American journal of cardiology*. **98**(12),pp.1581–6.
- Lima, J.A., Judd, R.M., Bazille, A., Schulman, S.P., Atalar, E. and Zerhouni, E.A. 1995. Regional heterogeneity of human myocardial infarcts demonstrated by contrast-enhanced MRI. Potential mechanisms. *Circulation*. **92**(5),pp.1117–25.
- Lockie, T., Nagel, E., Redwood, S. and Plein, S. 2009. Use of cardiovascular magnetic resonance imaging in acute coronary syndromes. *Circulation*. **119**(12),pp.1671–81.
- Lustig, M., Donoho, D. and Pauly, J.M. 2007. Sparse MRI: The application of compressed sensing for rapid MR imaging. *Magnetic resonance in medicine : official journal of the Society of Magnetic Resonance in Medicine / Society of Magnetic Resonance in Medicine*. **58**(6),pp.1182–95.
- Lustig, M. and Pauly, J.M. 2010. SPIRiT: Iterative self-consistent parallel imaging reconstruction from arbitrary k-space. *Magnetic resonance in medicine*. **64**(2),pp.457–71.
- Maciver, D.H. 2012. The relative impact of circumferential and longitudinal shortening on left ventricular ejection fraction and stroke volume. *Experimental and clinical cardiology*. **17**(1),pp.5–11.
- Mather, A.N., Fairbairn, T.A., Ball, S.G., Greenwood, J.P. and Plein, S. 2011. Reperfusion haemorrhage as determined by cardiovascular MRI is a predictor of adverse left ventricular remodelling and markers of late arrhythmic risk. *Heart (British Cardiac Society)*. **97**(6),pp.453–459.
- McAlindon, E., Pufulete, M., Lawton, C., Angelini, G.D. and Bucciarelli-Ducci, C. 2015. Quantification of infarct size and myocardium at risk: evaluation of different techniques and its implications. *European heart journal cardiovascular Imaging*. **16**(7),pp.738–46.

- McDonald, R.J., McDonald, J.S., Kallmes, D.F., Jentoft, M.E., Murray, D.L., Thielen, K.R., Williamson, E.E. and Eckel, L.J. 2015. Intracranial Gadolinium Deposition after Contrast-enhanced MR Imaging. <http://dx.doi.org/10.1148/radiol.15150025>.
- McMurray, J.J. V, Adamopoulos, S., Anker, S.D., Auricchio, A., Böhm, M., Dickstein, K., Falk, V., Filippatos, G., Fonseca, C., Gomez-Sanchez, M.A., Jaarsma, T., Køber, L., Lip, G.Y.H., Maggioni, A. Pietro, Parkhomenko, A., Pieske, B.M., Popescu, B.A., Rønnevik, P.K., Rutten, F.H., Schwitter, J., Seferovic, P., Stepinska, J., Trindade, P.T., Voors, A.A., Zannad, F. and Zeiher, A. 2012. ESC Guidelines for the diagnosis and treatment of acute and chronic heart failure 2012: The Task Force for the Diagnosis and Treatment of Acute and Chronic Heart Failure 2012 of the European Society of Cardiology. Developed in collaboration with the Heart. *European heart journal*. **33**(14),pp.1787–847.
- Messroghli, D.R., Bainbridge, G.J., Alfakih, K., Jones, T.R., Plein, S., Ridgway, J.P. and Sivananthan, M.U. 2005. Assessment of regional left ventricular function: accuracy and reproducibility of positioning standard short-axis sections in cardiac MR imaging. *Radiology*. **235**(1),pp.229–36.
- Messroghli, D.R., Walters, K., Plein, S., Sparrow, P., Friedrich, M.G., Ridgway, J.P. and Sivananthan, M.U. 2007. Myocardial T1 mapping: application to patients with acute and chronic myocardial infarction. *Magnetic resonance in medicine : official journal of the Society of Magnetic Resonance in Medicine / Society of Magnetic Resonance in Medicine*. **58**(1),pp.34–40.
- Miller, C.D., Hwang, W., Case, D., Hoekstra, J.W., Lefebvre, C., Blumstein, H., Hamilton, C.A., Harper, E.N. and Hundley, W.G. 2011. Stress CMR imaging observation unit in the emergency department reduces 1-year medical care costs in patients with acute chest pain: a randomized study for comparison with inpatient care. *JACC. Cardiovascular imaging*. **4**(8),pp.862–70.
- Moens, A.L., Claeys, M.J., Timmermans, J.P. and Vrints, C.J. 2005. Myocardial ischemia/reperfusion-injury, a clinical view on a complex pathophysiological process. *International journal of cardiology*. **100**(2),pp.179–90.
- Moftakhar, R., Aagaard-Kienitz, B., Johnson, K., Turski, P.A., Turk, A.S., Niemann, D.B., Consigny, D., Grinde, J., Wieben, O. and Mistretta, C.A. 2007. Noninvasive

- measurement of intra-aneurysmal pressure and flow pattern using phase contrast with vastly undersampled isotropic projection imaging. *AJNR. American journal of neuroradiology*. **28**(9),pp.1710–4.
- Møller, J.E., Hillis, G.S., Oh, J.K., Reeder, G.S., Gersh, B.J. and Pellikka, P.A. 2006. Wall motion score index and ejection fraction for risk stratification after acute myocardial infarction. *American heart journal*. **151**(2),pp.419–25.
- Mollet, N.R., Dymarkowski, S., Volders, W., Wathiong, J., Herbots, L., Rademakers, F.E. and Bogaert, J. 2002. Visualization of Ventricular Thrombi With Contrast-Enhanced Magnetic Resonance Imaging in Patients With Ischemic Heart Disease. *Circulation*. **106**(23).
- Moon, J.C., Messroghli, D.R., Kellman, P., Piechnik, S.K., Robson, M.D., Ugander, M., Gatehouse, P.D., Arai, A.E., Friedrich, M.G., Neubauer, S., Schulz-Menger, J. and Schelbert, E.B. 2013. Myocardial T1 mapping and extracellular volume quantification: a Society for Cardiovascular Magnetic Resonance (SCMR) and CMR Working Group of the European Society of Cardiology consensus statement. *Journal of cardiovascular magnetic resonance : official journal of the Society for Cardiovascular Magnetic Resonance*. **15**(1),p.92.
- Morishima, I., Sone, T., Okumura, K., Tsuboi, H., Kondo, J., Mukawa, H., Matsui, H., Toki, Y., Ito, T. and Hayakawa, T. 2000. Angiographic no-reflow phenomenon as a predictor of adverse long-term outcome in patients treated with percutaneous transluminal coronary angioplasty for first acute myocardial infarction. *Journal of the American College of Cardiology*. **36**(4),pp.1202–9.
- Muehling, O.M., Jerosch-Herold, M., Panse, P., Zenovich, A., Wilson, B. V, Wilson, R.F. and Wilke, N. 2004. Regional heterogeneity of myocardial perfusion in healthy human myocardium: assessment with magnetic resonance perfusion imaging. *Journal of cardiovascular magnetic resonance : official journal of the Society for Cardiovascular Magnetic Resonance*. **6**(2),pp.499–507.
- Myerson, S.G., Bellenger, N.G. and Pennell, D.J. 2002. Assessment of left ventricular mass by cardiovascular magnetic resonance. *Hypertension*. **39**(3),pp.750–755.
- Nett, E.J., Johnson, K.M., Frydrychowicz, A., Del Rio, A.M., Schrauben, E., Francois, C.J. and Wieben, O. 2012. Four-dimensional phase contrast MRI with accelerated dual velocity encoding. *Journal of magnetic resonance imaging :*

*JMRI*. **35**(6),pp.1462–71.

- Ng, A.C.T., Sitges, M., Pham, P.N., Tran, D.T., Delgado, V., Bertini, M., Nucifora, G., Vidaic, J., Allman, C., Holman, E.R., Bax, J.J. and Leung, D.Y. 2009. Incremental value of 2-dimensional speckle tracking strain imaging to wall motion analysis for detection of coronary artery disease in patients undergoing dobutamine stress echocardiography. *American heart journal*. **158**(5),pp.836–44.
- Onishi, T., Saha, S.K., Delgado-Montero, A., Ludwig, D.R., Onishi, T., Schelbert, E.B., Schwartzman, D. and Gorcsan, J. 2015. Global Longitudinal Strain and Global Circumferential Strain by Speckle-Tracking Echocardiography and Feature-Tracking Cardiac Magnetic Resonance Imaging: Comparison with Left Ventricular Ejection Fraction. *Journal of the American Society of Echocardiography*. **28**(5),pp.587–596.
- Pan, J., Huang, S., Lu, Z., Li, J., Wan, Q., Zhang, J., Gao, C., Yang, X. and Wei, M. 2015. Comparison of Myocardial Transmural Perfusion Gradient by Magnetic Resonance Imaging to Fractional Flow Reserve in Patients With Suspected Coronary Artery Disease. *The American Journal of Cardiology*. **115**(10),pp.1333–1340.
- Panaich, S., Briasoulis, A., Cardozo, S. and Afonso, L. 2016. Incremental Value of Two Dimensional Speckle Tracking Echocardiography in the Functional Assessment and Characterization of Subclinical Left Ventricular Dysfunction. *Current cardiology reviews*.
- Parsai, C., O’Hanlon, R., Prasad, S.K., Mohiaddin, R.H., Dietz, R., Tyberg, J., Friedrich, M., Robson, M., Rimoldi, O., Camici, P., Kochsiek, K., Nagel, E. and Neubauer, S. 2012. Diagnostic and prognostic value of cardiovascular magnetic resonance in non-ischaemic cardiomyopathies. *Journal of Cardiovascular Magnetic Resonance*. **14**(1),p.54.
- Payne, A.R., Casey, M., McClure, J., McGeoch, R., Murphy, A., Woodward, R., Saul, A., Bi, X., Zuehlsdorff, S., Oldroyd, K.G., Tzemos, N. and Berry, C. 2011. Bright-blood T2-weighted MRI has higher diagnostic accuracy than dark-blood short tau inversion recovery MRI for detection of acute myocardial infarction and for assessment of the ischemic area at risk and myocardial salvage. *Circulation. Cardiovascular imaging*. **4**(3),pp.210–9.

Pedrizzetti, G., Claus, P., Kilner, P.J., Nagel, E., Singh, A., Barron, J., Fleet, D., Beauchemin, S., Adrian, R., Willert, C., Gharib, M., Hor, K., Gottliebson, W., Carson, C., Wash, E., Cnota, J., Fleck, R., Bohs, L., Trahey, G., Kaluzynski, K., Chen, X., Emelianov, S., Skovoroda, A., O'Donnell, M., Liang, T., Yung, L., Yu, W., Pirat, B., Khoury, D., Hartley, C., Tiller, L., Rao, L., Schulz, D., Bistoquet, A., Oshinski, J., Skrinjar, O., Bistoquet, A., Oshinski, J., Skrimjar, O., Yue, Y., Clark, J., Khoury, D., Heyde, B., Jasaityte, R., Barbosa, D., Robesyn, V., Bouchez, S., Wouters, P., Pennell, D., Chuang, M., Hibberd, M., Salton, C., Beaudin, R., Riley, M., Parker, R., Thiele, H., Paetsch, I., Schnackenburg, B., Bornstedt, A., Grebe, O., Wellenhofer, E., Claus, P., Omar, A., Pedrizzetti, G., Sengupta, P., Nagel, E., Schuster, A., Hor, K., Kowallick, J., Beerbaum, P., Kutty, S., Malpica, N., Santos, A., Zuluaga, M., Ledesma, M., Pérez, E., García-Fernández, M., Leitman, M., Lysyansky, P., Sidenko, S., Shir, V., Peleg, E., Binenbaum, M., Vannan, M., Pedrizzetti, G., Li, P., Gurudevan, S., Houle, H., Main, J., LeGrice, I., Smaill, B., Chai, L., Edgar, S., Gavin, J., Hunter, P., Hales, P., Schneider, J., Burton, R., Wright, B., Bollensdorff, C., Kohl, P., Crosby, J., Hergum, T., Remme, E., Torp, H., Voigt, J.-U., Pedrizzetti, G., Lysyansky, P., Marwick, T., Houle, H., Baumann, R., Mor-Avi, V., Lang, R., Badano, L., Belohlavek, M., Cardim, N., Derumeaux, G., Langeland, S., Wouters, P., Claus, P., Leather, H., Bijmens, B., Sutherland, G., Saito, K., Okura, H., Watanabe, N., Hayashida, A., Obase, K., Imai, K., Yodwut, C., Weinert, L., Klas, B., Lang, R., Mor-Avi, V., Cheng, S., Larson, M., McCabe, E., Osypiuk, E., Lehman, B., Stanchev, P., Morton, G., Schuster, A., Jogiya, R., Kutty, S., Beerbaum, P., Nagel, E., Schuster, A., Morton, G., Hussain, S., Jogiya, R., Kutty, S., Asress, K., Farsalinos, K., Daraban, A., Ünlü, S., Thomas, J., Badano, L., Voigt, J.-U., Pedrizzetti, G., Mangual, J., Tonti, G., Abraham, T., Nishimura, R., Gorcsan, J., Tanaka, H., Goffinet, C., Chenot, F., Robert, A., Pouleur, A.-C., Waroux, J.-B., Vancrayenest, D., Kowallick, J., Morton, G., Lamata, P., Jogiya, R., Kutty, S., Lotz, J., Green, A., Adkins, J., Moore, C., Lugo-Olivieri, C., McVeigh, E., Zerhouni, E., Hess, A., Zhong, X., Spottiswoode, B., Epstein, F., Meintjes, E., Zhong, X., Spottiswoode, B., Meyer, C., Kramer, C., Epstein, F., Pedrizzetti, G., Kraigher-Krainer, E., Luca, A., Caracciolo, G., Mangual, J., Shah, A., Piras, P., Evangelista, A., Gabriele, S., Nardinocchi, P., Teresi, L., Torromeo, C.,

- Pedrizzetti, G., Sengupta, S., Caracciolo, G., Park, C., Amaki, M., Goliash, G., Onishi, T., Saha, S., Ludwig, D., Onishi, T., Marek, J., Cavalcante, J., Duchateau, N., Craene, M., Piella, G., Frangi, A., Zerhouni, E., Parish, D., Rogers, W., Yang, A., Shapiro, E., Wu, L., Germans, T., Güçlü, A., Heymans, M., Allaart, C., Rossum, A., Osman, N., McVeigh, E., Prince, J., Aletras, A., Ding, S., Balaban, R., Wen, H., Osman, N., Sampath, S., Atalar, E., Prince, J., Amundsen, B., Helle-Valle, T., Edvardsen, T., Torp, H., Crosby, J., Lyseggen, E., Bansal, M., Cho, G., Chan, J., Leano, R., Haluska, B., Marwick, T., Seo, Y., Ishizu, T., Enomoto, Y., Sugimori, H., Yamamoto, M., Machino, T., Kaku, K., Takeuchi, M., Tsang, W., Takigiku, K., Yasukochi, S., Patel, A., Schuster, A., Stahnke, V., Unterberg-Buchwald, C., Kowallick, J., Lamata, P., Steinmetz, M., Ohyama, Y., Ambale-Venkatesh, B., Chamera, E., Shehata, M., Corona-Villalobos, C., Zimmerman, S., Azam, S., Desjardins, C., Schluchter, M., Liner, A., Stelzer, J., Yu, X., Amaki, M., Savino, J., Ain, D., Sanz, J., Pedrizzetti, G., Kulkarni, H., Padiyath, A., Gribben, P., Abraham, J., Li, L., Rangamani, S., Schuster, A., Kempny, A., Fernández-Jiménez, R., Orwat, S., Schuler, P., Bunck, A., Maintz, D., Smiseth, O., Torp, H., Opdahl, A., Haugaa, K., Urheim, S., Russo, C., Jin, Z., Elkind, M., Rundek, T., Homma, S., Sacco, R., Lang, R., Badano, L., Mor-Avi, V., Afilalo, J., Armstrong, A., Ernande, L., Nagueh, S., Smiseth, O., Appleton, C., Byrd, B., Dokainish, H. and Edvardsen, T. 2016. Principles of cardiovascular magnetic resonance feature tracking and echocardiographic speckle tracking for informed clinical use. *Journal of Cardiovascular Magnetic Resonance*. **18**(1),p.51.
- Petersson, S., Sigfridsson, A., Dyverfeldt, P., Carlhäll, C.-J. and Ebbers, T. 2016. Retrospectively gated intracardiac 4D flow MRI using spiral trajectories. *Magnetic Resonance in Medicine*. **75**(1),pp.196–206.
- Pfeffer, M.A. and Braunwald, E. 1990. Ventricular remodeling after myocardial infarction. Experimental observations and clinical implications. *Circulation*. **81**(4),pp.1161–72.
- Plein, S., Greenwood, J.P., Ridgway, J.P., Cranny, G., Ball, S.G. and Sivananthan, M.U. 2004. Assessment of non-ST-segment elevation acute coronary syndromes with cardiac magnetic resonance imaging. *Journal of the American College of Cardiology*. **44**(11),pp.2173–81.

- Plein, S., Kozerke, S., Suerder, D., Luescher, T.F., Greenwood, J.P., Boesiger, P. and Schwitler, J. 2008. High spatial resolution myocardial perfusion cardiac magnetic resonance for the detection of coronary artery disease. *European heart journal*. **29**(17),pp.2148–55.
- Radjenovic, A., Biglands, J.D., Larghat, A., Ridgway, J.P., Ball, S.G., Greenwood, J.P., Jerosch-Herold, M. and Plein, S. 2010. Estimates of systolic and diastolic myocardial blood flow by dynamic contrast-enhanced MRI. *Magnetic Resonance in Medicine*. **64**(6),pp.1696–1703.
- Reant, P., Labrousse, L., Lafitte, S., Bordachar, P., Pillois, X., Tariosse, L., Bonoron-Adele, S., Padois, P., Deville, C., Roudaut, R. and Dos Santos, P. 2008. Experimental validation of circumferential, longitudinal, and radial 2-dimensional strain during dobutamine stress echocardiography in ischemic conditions. *Journal of the American College of Cardiology*. **51**(2),pp.149–57.
- Reimer, K.A. and Jennings, R.B. 1979. The ‘wavefront phenomenon’ of myocardial ischemic cell death. II. Transmural progression of necrosis within the framework of ischemic bed size (myocardium at risk) and collateral flow. *Laboratory investigation; a journal of technical methods and pathology*. **40**(6),pp.633–644.
- Reimer, K.A., Lowe, J.E., Rasmussen, M.M. and Jennings, R.B. 1977. The wavefront phenomenon of ischemic cell death. 1. Myocardial infarct size vs duration of coronary occlusion in dogs. *Circulation*. **56**(5),pp.786–94.
- Rinkevich, D., Kaul, S., Wang, X.-Q., Tong, K.L., Belcik, T., Kalvaitis, S., Lepper, W., Dent, J.M. and Wei, K. 2005. Regional left ventricular perfusion and function in patients presenting to the emergency department with chest pain and no ST-segment elevation. *European heart journal*. **26**(16),pp.1606–11.
- Roberts, C.S., Schoen, F.J. and Kloner, R.A. 1983. Effect of coronary reperfusion on myocardial hemorrhage and infarct healing. *The American journal of cardiology*. **52**(5),pp.610–4.
- Roes, S.D., Hammer, S., van der Geest, R.J., Marsan, N.A., Bax, J.J., Lamb, H.J., Reiber, J.H.C., de Roos, A. and Westenberg, J.J.M. 2009. Flow assessment through four heart valves simultaneously using 3-dimensional 3-directional velocity-encoded magnetic resonance imaging with retrospective valve tracking in healthy volunteers and patients with valvular regurgitation. *Investigative radiology*.

44(10),pp.669–75.

- Roldán-Alzate, A., Frydrychowicz, A., Niespodzany, E., Landgraf, B.R., Johnson, K.M., Wieben, O. and Reeder, S.B. 2013. In vivo validation of 4D flow MRI for assessing the hemodynamics of portal hypertension. *Journal of magnetic resonance imaging : JMRI*. **37**(5),pp.1100–8.
- Ruopp, M.D., Perkins, N.J., Whitcomb, B.W. and Schisterman, E.F. 2008. Youden Index and optimal cut-point estimated from observations affected by a lower limit of detection. *Biometrical journal. Biometrische Zeitschrift*. **50**(3),pp.419–30.
- Saeed, M., Lund, G., Wendland, M.F., Bremerich, J., Weinmann, H. and Higgins, C.B. 2001. Magnetic resonance characterization of the peri-infarction zone of reperfused myocardial infarction with necrosis-specific and extracellular nonspecific contrast media. *Circulation*. **103**(6),pp.871–6.
- Schelbert, E.B., Piehler, K.M., Zareba, K.M., Moon, J.C., Ugander, M., Messroghli, D.R., Valeti, U.S., Chang, C.-C.H., Shroff, S.G., Diez, J., Miller, C.A., Schmitt, M., Kellman, P., Butler, J., Gheorghiade, M. and Wong, T.C. 2015. Myocardial Fibrosis Quantified by Extracellular Volume Is Associated With Subsequent Hospitalization for Heart Failure, Death, or Both Across the Spectrum of Ejection Fraction and Heart Failure Stage. *Journal of the American Heart Association*. **4**(12).
- Schnell, S., Markl, M., Entezari, P., Mahadewia, R.J., Semaan, E., Stankovic, Z., Collins, J., Carr, J. and Jung, B. 2014. k-t GRAPPA accelerated four-dimensional flow MRI in the aorta: effect on scan time, image quality, and quantification of flow and wall shear stress. *Magnetic resonance in medicine*. **72**(2),pp.522–33.
- Schulz-Menger, J., Bluemke, D.A., Bremerich, J., Flamm, S.D.S., Fogel, M.A., Friedrich, M.G.M., Kim, R.R.J., von Knobelsdorff-Brenkenhoff, F., Kramer, C.C.M., Pennell, D.J.D., Plein, S., Nagel, E., Douglas, P., Hendel, R., Cummings, J., Dent, J., Hodgson, J., Hoffmann, U., Horn, R., Hundley, W., Kahn, C., Martin, G., Masoudi, F., Peterson, E., Rosenthal, G., Solomon, H., Stillman, A., Teague, S., Thomas, J., Tilkemeier, P., Weigold, W.G., Hundley, W., Bluemke, D.A., Bogaert, J., Friedrich, M.G.M., Higgins, C., Lawson, M., McConnell, M., Raman, S., Rossum, A. van, Flamm, S.D.S., Kramer, C.C.M., Nagel, E., Neubauer, S., Pennell, D.J.D.,

Sechtem, U., Higgins, C., Manning, W., Pohost, G., Rademakers, F., Rossum, A. van, Shaw, L., Yucel, E., Hendel, R., Patel, M., Kramer, C.C.M., Poon, M., Carr, J., Gerstad, N., Gillam, L., Hodgson, J., Kim, R.R.J., Lesser, J., Martin, E., Messer, J., Redberg, R., Rubin, G., Rumsfeld, J., Taylor, A.A., Weigold, W.G., Woodard, P., Brindis, R., Douglas, P., Peterson, E., Wolk, M., Allen, J., Hundley, W., Bluemke, D.A., Finn, J., Flamm, S.D.S., Fogel, M.A., Friedrich, M.G.M., Ho, V., Jerosch-Herold, M., Kramer, C.C.M., Manning, W., Patel, M., Pohost, G., Stillman, A., White, R., Woodard, P., Kramer, C.C.M., Barkhausen, J., Flamm, S.D.S., Kim, R.R.J., Nagel, E., Cerqueira, M., Weissman, N., Dilsizian, V., Jacobs, A., Kaul, S., Laskey, W., Pennell, D.J.D., Rumberger, J., Ryan, T., Verani, M., Maceira, A., Prasad, S., Khan, M., Pennell, D.J.D., Hudsmith, L., Petersen, S., Francis, J., Robson, M., Neubauer, S., Natori, S., Lai, S., Finn, J., Gomes, A., Hundley, W., Jerosch-Herold, M., Pearson, G., Sinha, S., Arai, A., Lima, J., Bluemke, D.A., Hamdan, A., Kelle, S., Schnackenburg, B., Fleck, E., Nagel, E., Silverman, D., Manning, W., Thiele, H., Paetsch, I., Schnackenburg, B., Bornstedt, A., Grebe, O., Wellnhofer, E., Schuler, G., Fleck, E., Nagel, E., Puntmann, V., Gebker, R., Duckett, S., Mirelis, J., Schnackenburg, B., Graefe, M., Razavi, R., Fleck, E., Nagel, E., Alfakih, K., Plein, S., Thiele, H., Jones, T., Ridgway, J., Sivananthan, M., Alfakih, K., Plein, S., Bloomer, T., Jones, T., Ridgway, J., Sivananthan, M., Clarke, C., Gurka, M., Norton, P., Kramer, C.C.M., Hoyer, A., Bella, E. Di, Parker, D., Sinusas, A., Thomson, L., Fieno, D., Abidov, A., Slomka, P., Hachamovitch, R., Saouaf, R., Friedman, J., Berman, D., Chung, S., Lee, K., Chun, E., Lee, W., Park, E., Chang, H., Choi, S., Stanton, T., Marwick, T., Panting, J., Gatehouse, P., Yang, G., Grothues, F., Firmin, D., Collins, P., Pennell, D.J.D., Pilz, G., Klos, M., Ali, E., Hoefling, B., Scheck, R., Bernhardt, P., Kawecka-Jaszcz, K., Czarnecka, D., Olszanecka, A., Klecha, A., Kwiecien-Sobstel, A., Stolarz-Skrzypek, K., Pennell, D.J.D., Pasowicz, M., Klimeczek, P., Banys, R., Klem, I., Heitner, J., Shah, D., Sketch, M., Behar, V., Weinsaft, J., Cawley, P., Parker, M., Elliott, M., Judd, R., Kim, R.R.J., Karamitsos, T., Ntusi, N., Francis, J., Holloway, C., Myerson, S., Neubauer, S., Jerosch-Herold, M., Schwitler, J., DeMarco, T., Kneifel, S., Schulthess, G. von, Jorg, M., Arheden, H., Ruhm, S., Stumpe, K., Buck, A., Parmley, W., Luscher, T., Higgins, C., Kelle, S., Graf, K., Dreysse, S.,

Schnackenburg, B., Fleck, E., Klein, C., Rieber, J., Huber, A., Erhard, I., Mueller, S., Schweyer, M., Koenig, A., Schiele, T., Theisen, K., Siebert, U., Schoenberg, S., Reiser, M., Klauss, V., Klocke, F., Simonetti, O., Judd, R., Kim, R.R.J., Harris, K., Hedjbeli, S., Fieno, D., Miller, S., Chen, V., Parker, M., Jerosch-Herold, M., Wilke, N., Wang, Y., Gong, G., Mansoor, A., Huang, H., Gurchumelidze, S., Stillman, A., Jerosch-Herold, M., Swingen, C., Seethamraju, R., Kim, R.R.J., Shah, D., Judd, R., McCrohon, J., Moon, J., Prasad, S., McKenna, W., Lorenz, C., Coats, A., Pennell, D.J.D., Mahrholdt, H., Wagner, A., Judd, R., Sechtem, U., Kim, R.R.J., Saremi, F., Grizzard, J., Kim, R.R.J., Kellman, P., Arai, A., McVeigh, E., Aletras, A., Bondarenko, O., Beek, A., Hofman, M., Kuhl, H., Twisk, J., Dockum, W. van, Visser, C., Rossum, A. van, Amado, L., Gerber, B., Gupta, S., Rettmann, D., Szarf, G., Schock, R., Nasir, K., Kraitchman, D., Lima, J., Hsu, L., Natanzon, A., Kellman, P., Hirsch, G., Aletras, A., Arai, A., Flett, A., Hasleton, J., Cook, C., Hausenloy, D., Quarta, G., Ariti, C., Muthurangu, V., Moon, J., Kim, H., Farzaneh-Far, A., Kim, R.R.J., Schmidt, A., Azevedo, C., Cheng, A., Gupta, S., Bluemke, D.A., Foo, T., Gerstenblith, G., Weiss, R., Marban, E., Tomaselli, G., Lima, J., Wu, K., Yan, A., Shayne, A., Brown, K., Gupta, S., Chan, C., Luu, T., Carli, M. Di, Reynolds, H., Stevenson, W., Kwong, R., Messroghli, D., Radjenovic, A., Kozerke, S., Higgins, D., Sivananthan, M., Ridgway, J., Iles, L., Pflugler, H., Phrommintikul, A., Cherayath, J., Aksit, P., Gupta, S., Kaye, D., Taylor, A.A., Jerosch-Herold, M., Sheridan, D., Kushner, J., Nauman, D., Burgess, D., Dutton, D., Alharethi, R., Li, D., Hershberger, R., Flett, A., Hayward, M., Ashworth, M., Hansen, M., Taylor, A.A., Elliott, P., McGregor, C., Moon, J., Friedrich, M.G.M., Sechtem, U., Schulz-Menger, J., Holmvang, G., Alakija, P., Cooper, L., White, J., Abdel-Aty, H., Gutberlet, M., Prasad, S., Aletras, A., Laissy, J., Paterson, I., Filipchuk, N., Kumar, A., Pauschinger, M., Liu, P., Zia, M., Ghugre, N., Connelly, K., Strauss, B., Sparkes, J., Dick, A., Wright, G., He, T., Gatehouse, P., Kirk, P., Mohiaddin, R., Pennell, D.J.D., Firmin, D., He, T., Gatehouse, P., Smith, G., Mohiaddin, R., Pennell, D.J.D., Firmin, D., He, T., Gatehouse, P., Kirk, P., Tanner, M., Smith, G., Keegan, J., Mohiaddin, R., Pennell, D.J.D., Firmin, D., Anderson, L., Holden, S., Davis, B., Prescott, E., Charrier, C., Bunce, N., Firmin, D., Wonke, B., Porter, J., Walker, J., Pennell, D.J.D., Carpenter, J., He, T., Kirk, P., Roughton, M., Anderson, L.,

Noronha, S. de, Sheppard, M., Porter, J., Walker, J., Wood, J., Galanello, R., Forni, G., Catani, G., Matta, G., Fucharoen, S., Fleming, A., House, M., Black, G., Firmin, D., Pierre, T.S., Pennell, D.J.D., Kirk, P., Roughton, M., Porter, J., Walker, J., Tanner, M., Patel, J., Wu, D., Taylor, J., Westwood, M., Anderson, L., Pennell, D.J.D., Mohiaddin, R., Kilner, P., Rees, S., Longmore, D., Mohiaddin, R., Pennell, D.J.D., Rebergen, S., Wall, E. van der, Doornbos, J., Roos, A. de, O'Brien, K., Cowan, B., Jain, M., Stewart, R., Kerr, A., Young, A., Holland, B., Printz, B., Lai, W., Chernobelsky, A., Shubayev, O., Comeau, C., Wolff, S., Gatehouse, P., Rolf, M., Graves, M., Hofman, M., Totman, J., Werner, B., Quest, R., Liu, Y., Spiczak, J. von, Dieringer, M., Firmin, D., Rossum, A. van, Lombardi, M., Schwitter, J., Schulz-Menger, J., Kilner, P., Lotz, J., Meier, C., Leppert, A., Galanski, M., Hiratzka, L., Bakris, G., Beckman, J., Bersin, R., Carr, V., Casey, D., Eagle, K., Hermann, L., Isselbacher, E., Kazerooni, E., Kouchoukos, N., Lytle, B., Milewicz, D., Reich, D., Sen, S., Shinn, J., Svensson, L., Williams, D., Holloway, B., Rosewarne, D., Jones, R., Kalb, B., Sharma, P., Tigges, S., Ray, G., Kitajima, H., Costello, J., Chen, Z., Martin, D., Grosse-Wortmann, L., Al-Otay, A., Goo, H., Macgowan, C., Coles, J., Benson, L., Redington, A. and Yoo, S. 2013. Standardized image interpretation and post processing in cardiovascular magnetic resonance: Society for Cardiovascular Magnetic Resonance (SCMR) board of trustees task force on standardized post processing. *Journal of cardiovascular magnetic resonance: official journal of the Society for Cardiovascular Magnetic Resonance*. **15**(1),p.35.

Schwartz, B.G. and Kloner, R.A. 2012. Coronary no reflow. *Journal of molecular and cellular cardiology*. **52**(4),pp.873–82.

Senior, R., Moreo, A., Gaibazzi, N., Agati, L., Tiemann, K., Shivalkar, B., von Bardeleben, S., Galiuto, L., Lardoux, H., Trocino, G., Carrió, I., Le Guludec, D., Sambuceti, G., Becher, H., Colonna, P., Ten Cate, F., Bramucci, E., Cohen, A., Bezante, G., Aggeli, C. and Kasprzak, J.D. 2013. Comparison of sulfur hexafluoride microbubble (SonoVue)-enhanced myocardial contrast echocardiography with gated single-photon emission computed tomography for detection of significant coronary artery disease: a large European multicenter study. *Journal of the American College of Cardiology*.

62(15),pp.1353–61.

- Seward, J.B. and Casaclang-verzosa, G. 2010. Infiltrative cardiovascular diseases: cardiomyopathies that look alike. *Journal of the American College of Cardiology*. 55(17),pp.1769–1779.
- Shah, A.M. and Solomon, S.D. 2012. Myocardial Deformation Imaging: Current Status and Future Directions. *Circulation*. 125(2),pp.e244–e248.
- Sharifov, O.F., Schiros, C.G., Aban, I., Denney, T.S. and Gupta, H. 2016. Diagnostic Accuracy of Tissue Doppler Index E/e' for Evaluating Left Ventricular Filling Pressure and Diastolic Dysfunction/Heart Failure With Preserved Ejection Fraction: A Systematic Review and Meta-Analysis. *Journal of the American Heart Association*. 5(1),p.e002530.
- Solomon, S.D., Anavekar, N., Skali, H., McMurray, J.J. V, Swedberg, K., Yusuf, S., Granger, C.B., Michelson, E.L., Wang, D., Pocock, S., Pfeffer, M.A. and Candesartan in Heart Failure Reduction in Mortality (CHARM) Investigators 2005. Influence of ejection fraction on cardiovascular outcomes in a broad spectrum of heart failure patients. *Circulation*. 112(24),pp.3738–44.
- Stadlbauer, A., van der Riet, W., Crelier, G. and Salomonowitz, E. 2010. Accelerated time-resolved three-dimensional MR velocity mapping of blood flow patterns in the aorta using SENSE and k-t BLAST. *European journal of radiology*. 75(1),pp.e15-21.
- Steg, P.G., James, S.K., Atar, D., Badano, L.P., Blömstrom-Lundqvist, C., Borger, M.A., Di Mario, C., Dickstein, K., Ducrocq, G., Fernandez-Aviles, F., Gershlick, A.H., Giannuzzi, P., Halvorsen, S., Huber, K., Juni, P., Kastrati, A., Knuuti, J., Lenzen, M.J., Mahaffey, K.W., Valgimigli, M., van 't Hof, A., Widimsky, P. and Zahger, D. 2012. ESC Guidelines for the management of acute myocardial infarction in patients presenting with ST-segment elevation. *European heart journal*. 33(20),pp.2569–619.
- Sutherland, G.R., Stewart, M.J., Groundstroem, K.W., Moran, C.M., Fleming, A., Guell-Peris, F.J., Riemersma, R.A., Fenn, L.N., Fox, K.A. and McDicken, W.N. n.d. Color Doppler myocardial imaging: a new technique for the assessment of myocardial function. *Journal of the American Society of Echocardiography : official publication of the American Society of Echocardiography*. 7(5),pp.441–

58.

Sutton, M.G.S.J. and Sharpe, N. 2000. Left Ventricular Remodeling After Myocardial Infarction. *Circulation*. **101**(25).

Swoboda, P.P., Erhayiem, B., McDiarmid, A.K., Lancaster, R.E., Lyall, G.K., Dobson, L.E., Ripley, D.P., Musa, T.A., Garg, P., Ferguson, C., Greenwood, J.P. and Plein, S. 2016. Relationship between cardiac deformation parameters measured by cardiovascular magnetic resonance and aerobic fitness in endurance athletes. *Journal of cardiovascular magnetic resonance : official journal of the Society for Cardiovascular Magnetic Resonance*. **18**(1),p.48.

Swoboda, P.P., McDiarmid, A.K., Erhayiem, B., Haaf, P., Kidambi, A., Fent, G.J., Dobson, L.E., Musa, T.A., Garg, P., Law, G.R., Kearney, M.T., Barth, J.H., Ajjan, R., Greenwood, J.P. and Plein, S. 2016. A novel and practical screening tool for the detection of silent myocardial infarction in patients with type 2 diabetes. *The Journal of clinical endocrinology and metabolism*.,p.jc20161318.

Tarantini, G., Razzolini, R., Cacciavillani, L., Bilato, C., Sarais, C., Corbetti, F., Marra, M.P., Napodano, M., Ramondo, A. and Iliceto, S. 2006. Influence of transmural, infarct size, and severe microvascular obstruction on left ventricular remodeling and function after primary coronary angioplasty. *The American journal of cardiology*. **98**(8),pp.1033–40.

Tariq, U., Hsiao, A., Alley, M., Zhang, T., Lustig, M. and Vasanawala, S.S. 2013. Venous and arterial flow quantification are equally accurate and precise with parallel imaging compressed sensing 4D phase contrast MRI. *Journal of magnetic resonance imaging : JMRI*. **37**(6),pp.1419–26.

Thomas, J.D. and Badano, L.P. 2013. EACVI-ASE-industry initiative to standardize deformation imaging: a brief update from the co-chairs. *European heart journal cardiovascular Imaging*. **14**(11),pp.1039–40.

Thygesen, K., Alpert, J.S., Jaffe, A.S., Simoons, M.L., Chaitman, B.R., White, H.D., Katus, H.A., Apple, F.S., Lindahl, B., Morrow, D.A., Clemmensen, P.M., Johanson, P., Hod, H., Underwood, R., Bax, J.J., Bonow, J.J., Pinto, F., Gibbons, R.J., Fox, K.A., Atar, D., Newby, L.K., Galvani, M., Hamm, C.W., Uretsky, B.F., Steg, P.G., Wijns, W., Bassand, J.-P., Menasche, P., Ravkilde, J., Ohman, E.M., Antman, E.M., Wallentin, L.C., Armstrong, P.W., Januzzi, J.L., Niemenen, M.S.,

Gheorghide, M., Filippatos, G., Luepker, R. V, Fortmann, S.P., Rosamond, W.D., Levy, D., Wood, D., Smith, S.C., Hu, D., Lopez-Sendon, J.-L., Robertson, R.M., Weaver, D., Tendera, M., Bove, A.A., Parkhomenko, A.N., Vasilieva, E.J., Mendis, S., Baumgartner, H., Ceconi, C., Dean, V., Deaton, C., Fagard, R., Funck-Brentano, C., Hasdai, D., Hoes, A., Kirchhof, P., Knuuti, J., Kolh, P., McDonagh, T., Moulin, C., Popescu, B.A., Reiner, Z., Sechtem, U., Sirnes, P.A., Torbicki, A., Vahanian, A., Windecker, S., Morais, J., Aguiar, C., Almahmeed, W., Arnar, D.O., Barili, F., Bloch, K.D., Bolger, A.F., Botker, H.E., Bozkurt, B., Bugiardini, R., Cannon, C., de Lemos, J., Eberli, F.R., Escobar, E., Hlatky, M., James, S., Kern, K.B., Moliterno, D.J., Mueller, C., Neskovic, A.N., Pieske, B.M., Schulman, S.P., Storey, R.F., Taubert, K.A., Vranckx, P. and Wagner, D.R. 2012. Third universal definition of myocardial infarction. *Journal of the American College of Cardiology*. **60**(16),pp.1581–98.

Thygesen, K., Alpert, J.S., Jaffe, A.S., Simoons, M.L., Chaitman, B.R., White, H.D., Katus, H.A., Apple, F.S., Lindahl, B., Morrow, D.A., Clemmensen, P.M., Johanson, P., Hod, H., Underwood, R., Bax, J.J., Bonow, J.J., Pinto, F., Gibbons, R.J., Fox, K.A., Atar, D., Newby, L.K., Galvani, M., Hamm, C.W., Uretsky, B.F., Steg, P.G., Wijns, W., Bassand, J.-P.P., Menasche, P., Ravkilde, J., Ohman, E.M., Antman, E.M., Wallentin, L.C., Armstrong, P.W., Januzzi, J.L., Nieminen, M.S., Gheorghide, M., Filippatos, G., Luepker, R. V., Fortmann, S.P., Rosamond, W.D., Levy, D., Wood, D., Smith, S.C., Hu, D., Lopez-Sendon, J.L.J.-L.J.L., Robertson, R.M., Weaver, D., Tendera, M., Bove, A.A., Parkhomenko, A.N., Vasilieva, E.J., Mendis, S., Baumgartner, H., Ceconi, C., Dean, V., Deaton, C., Fagard, R., Funck-Brentano, C., Hasdai, D., Hoes, A., Kirchhof, P., Knuuti, J., Kolh, P., McDonagh, T., Moulin, C., Popescu, B.A., Reiner, Z., Sechtem, U., Sirnes, P.A., Torbicki, A., Vahanian, A., Windecker, S., Morais, J., Aguiar, C., Almahmeed, W., Arnar, D.O., Barili, F., Bloch, K.D., Bolger, A.F., Botker, H.E., Bozkurt, B., Bugiardini, R., Cannon, C., de Lemos, J., Eberli, F.R., Escobar, E., Hlatky, M., James, S., Kern, K.B., Moliterno, D.J., Mueller, C., Neskovic, A.N., Pieske, B.M., Schulman, S.P., Storey, R.F., Taubert, K.A., Vranckx, P., Wagner, D.R., Bonow, R.O., Pinto, F., Gibbons, R.J., Fox, K.A., Atar, D., Kristin Newby, L., Galvani, M., Hamm, C.W., Uretsky, B.F., Gabriel Steg, P., Wijns, W., Bassand, J.-P.P.,

Menasché, P., Ravkilde, J., Magnus Ohman, E., Antman, E.M., Wallentin, L.C., Armstrong, P.W., Januzzi, J.L., Nieminen, M.S., Gheorghiade, M., Filippatos, G., Luepker, R. V., Fortmann, S.P., Rosamond, W.D., Levy, D., Wood, D., Smith, S.C., Hu, D., Lopez-Sendon, J.L.J.-L.J.L., Robertson, R.M., Weaver, D., Tendera, M., Bove, A.A., Parkhomenko, A.N., Vasilieva, E.J., Mendis, S., Baumgartner, H., Ceconi, C., Dean, V., Deaton, C., Fagard, R., Funck-Brentano, C., Hasdai, D., Hoes, A., Kirchhof, P., Knuuti, J., Kolh, P., McDonagh, T., Moulin, C., Popescu, B.A., Reiner, Ž., Sechtem, U., Sirnes, P.A., Torbicki, A., Vahanian, A., Windecker, S., Morais, J., Aguiar, C., Almahmeed, W., Arnar, D.O., Barili, F., Bloch, K.D., Bolger, A.F., Botker, H.E., Bozkurt, B., Bugiardini, R., Cannon, C., de Lemos, J., Eberli, F.R., Escobar, E., Hlatky, M., James, S., Kern, K.B., Moliterno, D.J., Mueller, C., Neskovic, A.N., Pieske, B.M., Schulman, S.P., Storey, R.F., Taubert, K.A., Vranckx, P., Wagner, D.R., Bonow, J.J., Pinto, F., Gibbons, R.J., Fox, K.A., Atar, D., Newby, L.K., Galvani, M., Hamm, C.W., Uretsky, B.F., Steg, P.G., Wijns, W., Bassand, J.-P.P., Menasche, P., Ravkilde, J., Ohman, E.M., Antman, E.M., Wallentin, L.C., Armstrong, P.W., Januzzi, J.L., Nieminen, M.S., Gheorghiade, M., Filippatos, G., Luepker, R. V., Fortmann, S.P., Rosamond, W.D., Levy, D., Wood, D., Smith, S.C., Hu, D., Lopez-Sendon, J.L.J.-L.J.L., Robertson, R.M., Weaver, D., Tendera, M., Bove, A.A., Parkhomenko, A.N., Vasilieva, E.J., Mendis, S., Baumgartner, H., Ceconi, C., Dean, V., Deaton, C., Fagard, R., Funck-Brentano, C., Hasdai, D., Hoes, A., Kirchhof, P., Knuuti, J., Kolh, P., McDonagh, T., Moulin, C., Popescu, B.A., Reiner, Z., Sechtem, U., Sirnes, P.A., Torbicki, A., Vahanian, A., Windecker, S., Morais, J., Aguiar, C., Almahmeed, W., Arnar, D.O., Barili, F., Bloch, K.D., Bolger, A.F., Botker, H.E., Bozkurt, B., Bugiardini, R., Cannon, C., de Lemos, J., Eberli, F.R., Escobar, E., Hlatky, M., James, S., Kern, K.B., Moliterno, D.J., Mueller, C., Neskovic, A.N., Pieske, B.M., Schulman, S.P., Storey, R.F., Taubert, K.A., Vranckx, P., Wagner, D.R., Bonow, R.O., Pinto, F., Gibbons, R.J., Fox, K.A., Atar, D., Kristin Newby, L., Galvani, M., Hamm, C.W., Uretsky, B.F., Gabriel Steg, P., Wijns, W., Bassand, J.-P.P., Menasché, P., Ravkilde, J., Magnus Ohman, E., Antman, E.M., Wallentin, L.C., Armstrong, P.W., Januzzi, J.L., Nieminen, M.S., Gheorghiade, M., Filippatos, G., Luepker, R. V., Fortmann, S.P., Rosamond, W.D., Levy, D., Wood, D., Smith, S.C., Hu, D., Lopez-Sendon, J.L.J.-

- L.J.L., Robertson, R.M., Weaver, D., Tendera, M., Bove, A.A., Parkhomenko, A.N., Vasilieva, E.J., Mendis, S., Baumgartner, H., Ceconi, C., Dean, V., Deaton, C., Fagard, R., Funck-Brentano, C., Hasdai, D., Hoes, A., Kirchhof, P., Knuuti, J., Kolh, P., McDonagh, T., Moulin, C., Popescu, B.A., Reiner, Ž., Sechtem, U., Sirnes, P.A., Torbicki, A., Vahanian, A., Windecker, S., Morais, J., Aguiar, C., Almahmeed, W., Arnar, D.O., Barili, F., Bloch, K.D., Bolger, A.F., Botker, H.E., Bozkurt, B., Bugiardini, R., Cannon, C., de Lemos, J., Eberli, F.R., Escobar, E., Hlatky, M., James, S., Kern, K.B., Moliterno, D.J., Mueller, C., Neskovic, A.N., Pieske, B.M., Schulman, S.P., Storey, R.F., Taubert, K.A., Vranckx, P. and Wagner, D.R. 2012. Third universal definition of myocardial infarction. *European Heart Journal*. **33**(16),pp.2551–2567.
- TUKEY, J.W. 1949. Comparing individual means in the analysis of variance. *Biometrics*. **5**(2),pp.99–114.
- Ugander, M., Bagi, P.S., Oki, A.J., Chen, B., Hsu, L.-Y., Aletras, A.H., Shah, S., Greiser, A., Kellman, P. and Arai, A.E. 2012. Myocardial edema as detected by pre-contrast T1 and T2 CMR delineates area at risk associated with acute myocardial infarction. *JACC. Cardiovascular imaging*. **5**(6),pp.596–603.
- Ugander, M., Oki, A.J., Hsu, L.-Y., Kellman, P., Greiser, A., Aletras, A.H., Sibley, C.T., Chen, M.Y., Bandettini, W.P. and Arai, A.E. 2012. Extracellular volume imaging by magnetic resonance imaging provides insights into overt and sub-clinical myocardial pathology. *European Heart Journal*. **33**(10),pp.1268–1278.
- Utz, J., Herfkens, R., Heinsimer, J., Bashore, T., Califf, R., Glover, G., Pelc, N. and Shimakawa, A. 1987. Cine MR determination of left ventricular ejection fraction. *American Journal of Roentgenology*. **148**(5),pp.839–843.
- Valsangiacomo Buechel, E.R. and Mertens, L.L. 2012. Imaging the right heart: the use of integrated multimodality imaging. *European heart journal*. **33**(8),pp.949–60.
- Vartdal, T., Brunvand, H., Pettersen, E., Smith, H.-J., Lyseggen, E., Helle-Valle, T., Skulstad, H., Ihlen, H. and Edvardsen, T. 2007. Early prediction of infarct size by strain Doppler echocardiography after coronary reperfusion. *Journal of the American College of Cardiology*. **49**(16),pp.1715–21.
- Vogel-Claussen, J., Finn, J.P., Gomes, A.S., Hundley, G.W., Jerosch-Herold, M., Pearson, G., Sinha, S., Lima, J.A.C. and Bluemke, D.A. 2006. Left ventricular

- papillary muscle mass: relationship to left ventricular mass and volumes by magnetic resonance imaging. *Journal of computer assisted tomography*. **30**(3),pp.426–432.
- Warren, S.E., Royal, H.D., Markis, J.E., Grossman, W. and McKay, R.G. 1988. Time course of left ventricular dilation after myocardial infarction: influence of infarct-related artery and success of coronary thrombolysis. *Journal of the American College of Cardiology*. **11**(1),pp.12–9.
- Wentland, A.L., Grist, T.M. and Wieben, O. 2013. Repeatability and internal consistency of abdominal 2D and 4D phase contrast MR flow measurements. *Academic radiology*. **20**(6),pp.699–704.
- Westenberg, J.J., Wasser, M.N., van der Geest, R.J., Pattynama, P.M., de Roos, A., Vanderschoot, J. and Reiber, J.H. 1999. Scan optimization of gadolinium contrast-enhanced three-dimensional MRA of peripheral arteries with multiple bolus injections and in vitro validation of stenosis quantification. *Magnetic resonance imaging*. **17**(1),pp.47–57.
- Westenberg, J.J.M., Roes, S.D., Ajmone Marsan, N., Binnendijk, N.M.J., Doornbos, J., Bax, J.J., Reiber, J.H.C., de Roos, A. and van der Geest, R.J. 2008. Mitral valve and tricuspid valve blood flow: accurate quantification with 3D velocity-encoded MR imaging with retrospective valve tracking. *Radiology*. **249**(3),pp.792–800.
- White, S.K., Sado, D.M., Fontana, M., Banypersad, S.M., Maestrini, V., Flett, A.S., Piechnik, S.K., Robson, M.D., Hausenloy, D.J., Sheikh, A.M., Hawkins, P.N. and Moon, J.C. 2013. T1 mapping for myocardial extracellular volume measurement by CMR: bolus only versus primed infusion technique. *JACC. Cardiovascular imaging*. **6**(9),pp.955–62.
- Windecker, S., Kolh, P., Alfonso, F., Collet, J.-P., Cremer, J., Falk, V., Filippatos, G., Hamm, C., Head, S.J., Jüni, P., Kappetein, A.P., Kastrati, A., Knuuti, J., Landmesser, U., Laufer, G., Neumann, F.-J., Richter, D.J., Schauerte, P., Sousa Uva, M., Stefanini, G.G., Taggart, D.P., Torracca, L., Valgimigli, M., Wijns, W. and Witkowski, A. 2014. 2014 ESC/EACTS Guidelines on myocardial revascularization: The Task Force on Myocardial Revascularization of the European Society of Cardiology (ESC) and the European Association for Cardio-

- Thoracic Surgery (EACTS) Developed with the special contribution o. *European heart journal*. **35**(37),pp.2541–619.
- Wolff, S.D., Schwitter, J., Coulden, R., Friedrich, M.G., Bluemke, D.A., Biederman, R.W., Martin, E.T., Lansky, A.J., Kashanian, F., Foo, T.K.F., Licato, P.E. and Comeau, C.R. 2004. Myocardial First-Pass Perfusion Magnetic Resonance Imaging: A Multicenter Dose-Ranging Study. *Circulation*. **110**(6),pp.732–737.
- Wong, D.T.L., Leong, D.P., Weightman, M.J., Richardson, J.D., Dundon, B.K., Psaltis, P.J., Leung, M.C.H., Meredith, I.T., Worthley, M.I. and Worthley, S.G. 2014. Magnetic resonance-derived circumferential strain provides a superior and incremental assessment of improvement in contractile function in patients early after ST-segment elevation myocardial infarction. *European Radiology*. **24**(6),pp.1219–1228.
- Wong, T.C., Piehler, K.M., Kang, I.A., Kadakkal, A., Kellman, P., Schwartzman, D.S., Mulukutla, S.R., Simon, M.A., Shroff, S.G., Kuller, L.H. and Schelbert, E.B. 2014. Myocardial extracellular volume fraction quantified by cardiovascular magnetic resonance is increased in diabetes and associated with mortality and incident heart failure admission. *European heart journal*. **35**(10),pp.657–64.
- Wu, K.C., Zerhouni, E.A., Judd, R.M., Lugo-Olivieri, C.H., Barouch, L.A., Schulman, S.P., Blumenthal, R.S. and Lima, J.A. 1998. Prognostic significance of microvascular obstruction by magnetic resonance imaging in patients with acute myocardial infarction. *Circulation*. **97**(8),pp.765–72.
- Yancy, C.W., Jessup, M., Bozkurt, B., Butler, J., Casey, D.E., Drazner, M.H., Fonarow, G.C., Geraci, S.A., Horwich, T., Januzzi, J.L., Johnson, M.R., Kasper, E.K., Levy, W.C., Masoudi, F.A., McBride, P.E., McMurray, J.J. V, Mitchell, J.E., Peterson, P.N., Riegel, B., Sam, F., Stevenson, L.W., Tang, W.H.W., Tsai, E.J. and Wilkoff, B.L. 2013. 2013 ACCF/AHA guideline for the management of heart failure: executive summary: a report of the American College of Cardiology Foundation/American Heart Association Task Force on practice guidelines. *Circulation*. **128**(16),pp.1810–52.
- Young, A.A., Kramer, C.M., Ferrari, V.A., Axel, L. and Reichek, N. 1994. Three-dimensional left ventricular deformation in hypertrophic cardiomyopathy. *Circulation*. **90**(2),pp.854–67.

Zaman, A., Motwani, M., Oliver, J.J., Crelier, G., Dobson, L.E., Higgins, D.M., Plein, S. and Greenwood, J.P. 2015. 3.0T, time-resolved, 3D flow-sensitive MR in the thoracic aorta: Impact of k-t BLAST acceleration using 8- versus 32-channel coil arrays. *Journal of magnetic resonance imaging : JMRI*. **42**(2),pp.495–504.

## 9 Appendix

### 9.1 Ethical approval for chapter 3, 4 and 6



**Health Research Authority**  
NRES Committee Yorkshire & The Humber - Leeds West  
Room 001, Jarrow Business Centre  
Rolling Mill Road  
Jarrow  
Tyne and Wear  
NE32 3DT

Tel: 0191 4283548

02 March 2015

Petra Bijsterveld  
Senior Research Nurse, CMR Research Group  
Cardiovascular and Diabetes Research  
Sunshine Corridor  
Leeds General Infirmary  
Great George Street  
Leeds  
LS1 3EX

Dear Ms Bijsterveld

**Study title:** QUANTITATIVE EVALUATION OF MYOCARDIAL CHARACTERISTICS IN REPERFUSED ST-ELEVATION MYOCARDIAL INFARCTION – A 3 TESLA CARDIOVASCULAR MAGNETIC RESONANCE STUDY  
**REC reference:** 12/YH/0169  
**Amendment number:** Minor Amendment to PIS/ICF  
**Amendment date:** 13 February 2015  
**IRAS project ID:** 101941

Thank you for your letter of 13 February 2015, notifying the Committee of the above amendment.

The Committee does not consider this to be a "substantial amendment" as defined in the Standard Operating Procedures for Research Ethics Committees. The amendment does not therefore require an ethical opinion from the Committee and may be implemented immediately, provided that it does not affect the approval for the research given by the R&D office for the relevant NHS care organisation.

#### Documents received

The documents received were as follows:

Document	Version	Date
Notice of Minor Amendment	Minor Amendment to PIS/ICF	13 February 2015
Participant information sheet (PIS) [(and consent form)]	1.2	13 February 2015

#### Statement of compliance

The Committee is constituted in accordance with the Governance Arrangements for

Research Ethics Committees and complies fully with the Standard Operating Procedures for Research Ethics Committees in the UK.

<b>12/YH/0169:</b>	<b>Please quote this number on all correspondence</b>
--------------------	---

Yours sincerely



**Miss Christie Ord**  
**REC Assistant**

E-mail: [nrescommittee.yorkandhumber-leedswest@nhs.net](mailto:nrescommittee.yorkandhumber-leedswest@nhs.net)

*Copy to: Anne Gowing, Leeds Teaching Hospitals NHS Trust*  
*Prof Sven Plein, University of Leeds*

## 9.2 Ethical approval for chapter 5 and 7



### Health Research Authority

#### Yorkshire & The Humber - Leeds West Research Ethics Committee

Jarrow Business Centre  
Rolling Mill Road  
Jarrow  
NE32 3DT

Tel: 0207 104 8087

31 August 2016

Ms Petra Bijsterveld  
Senior Research Nurse & MRI MRF manager  
Division of Biomedical Imaging  
LICAMM  
University of Leeds & Leeds Teaching Hospitals NHS Trust  
Leeds  
LS2 9JT

Dear Ms Bijsterveld

**Study title:** CE-MARC 2: Optimization of Image Acquisition and Analysis Methods  
**REC reference:** 12/YH/0551  
**Amendment number:** SA2  
**Amendment date:** 04 August 2016  
**IRAS project ID:** 116093

The above amendment was reviewed by the Sub-Committee in correspondence.

#### Summary of amendment

This amendment was submitted to inform the Committee of the purchase of an MRI-compatible cycle ergometer. As such, the equipment allowed the option to perform physiological stress testing in the MRI environment.

The protocol was updated to reflect that the Leeds site had three scanners instead of two.

#### Ethical opinion

The members of the Committee taking part in the review gave a **favourable** ethical opinion of the amendment on the basis described in the notice of amendment form and supporting documentation.

The Sub-Committee did not raise any ethical issues.

#### Approved documents

The documents reviewed and approved at the meeting were:

<i>Document</i>	<i>Version</i>	<i>Date</i>
Notice of Substantial Amendment (non-CTIMP)	SA2	04 August 2016
Participant information sheet (PIS) [CE-MARC 2 Physics (Healthy Volunteers) PIS & Consent Form - Tracked Changes]	1.2	04 August 2016
Participant information sheet (PIS) [CE-MARC 2 Physics (Patients) PIS & Consent - Tracked Changes]	1.2	04 August 2016
Research protocol or project proposal [Tracked Changes]	1.1	04 August 2016

#### **Membership of the Committee**

The members of the Committee who took part in the review are listed on the attached sheet.

#### **R&D approval**

All investigators and research collaborators in the NHS should notify the R&D office for the relevant NHS care organisation of this amendment and check whether it affects R&D approval of the research.

#### **Statement of compliance**

The Committee is constituted in accordance with the Governance Arrangements for Research Ethics Committees and complies fully with the Standard Operating Procedures for Research Ethics Committees in the UK.

We are pleased to welcome researchers and R & D staff at our NRES committee members' training days – see details at <http://www.hra.nhs.uk/hra-training/>

<b>12/YH/0551:</b>	<b>Please quote this number on all correspondence</b>
--------------------	---

Yours sincerely  
pp



**Dr Vera Neumann**  
Vice-Chair

E-mail: [nrescommittee.yorkandhumber-leedswest@nhs.net](mailto:nrescommittee.yorkandhumber-leedswest@nhs.net)

*Enclosures:* *List of names and professions of members who took part in the review*

*Copy to:* *Mrs Anne Gowing, Leeds Teaching Hospitals NHS Trust*  
*Dr John P Greenwood, University of Leeds*